



2018

PERFORMANCE OF TWO TIEBACK WALLS AND ROCK ANCHORS IN A SHALE STRATUM

Jorge Octavio Romana Giraldo

University of Kentucky, jromanagiraldo@gmail.com

Digital Object Identifier: <https://doi.org/10.13023/etd.2018.387>

[Click here to let us know how access to this document benefits you.](#)

Recommended Citation

Romana Giraldo, Jorge Octavio, "PERFORMANCE OF TWO TIEBACK WALLS AND ROCK ANCHORS IN A SHALE STRATUM" (2018). *Theses and Dissertations--Civil Engineering*. 71.
https://uknowledge.uky.edu/ce_etds/71

This Master's Thesis is brought to you for free and open access by the Civil Engineering at UKnowledge. It has been accepted for inclusion in Theses and Dissertations--Civil Engineering by an authorized administrator of UKnowledge. For more information, please contact UKnowledge@lsv.uky.edu.

STUDENT AGREEMENT:

I represent that my thesis or dissertation and abstract are my original work. Proper attribution has been given to all outside sources. I understand that I am solely responsible for obtaining any needed copyright permissions. I have obtained needed written permission statement(s) from the owner(s) of each third-party copyrighted matter to be included in my work, allowing electronic distribution (if such use is not permitted by the fair use doctrine) which will be submitted to UKnowledge as Additional File.

I hereby grant to The University of Kentucky and its agents the irrevocable, non-exclusive, and royalty-free license to archive and make accessible my work in whole or in part in all forms of media, now or hereafter known. I agree that the document mentioned above may be made available immediately for worldwide access unless an embargo applies.

I retain all other ownership rights to the copyright of my work. I also retain the right to use in future works (such as articles or books) all or part of my work. I understand that I am free to register the copyright to my work.

REVIEW, APPROVAL AND ACCEPTANCE

The document mentioned above has been reviewed and accepted by the student's advisor, on behalf of the advisory committee, and by the Director of Graduate Studies (DGS), on behalf of the program; we verify that this is the final, approved version of the student's thesis including all changes required by the advisory committee. The undersigned agree to abide by the statements above.

Jorge Octavio Romana Giraldo, Student

Dr. Lindsey Sebastian Bryson, Major Professor

Dr. Timothy Taylor, Director of Graduate Studies

PERFORMANCE OF TWO TIEBACK WALLS AND ROCK ANCHORS IN A
SHALE STRATUM

THESIS

A thesis submitted in partial fulfillment of the
requirements for the degree of Master of Science in
Civil Engineering in the College of Engineering at the
University of Kentucky

By

Jorge Octavio Romana Giraldo

Lexington, Kentucky

Director: Dr. L. Sebastian Bryson, Professor of Civil Engineering

Lexington, Kentucky

2018

Copyright © Jorge Octavio Romana Giraldo 2018

ABSTRACT OF THESIS

PERFORMANCE OF TWO TIEBACK WALLS AND ROCK ANCHORS IN A SHALE STRATUM

Tieback walls are typically design based on predetermined pressure distribution; however, these pressures were proposed based on performance of excavations. For retaining walls used in slope remediation, the application of these pressures might not be adequate; the construction procedure; therefore, a different response of the wall is expected. This document, presents the performance of two tieback walls installed in a shale stratum. Monitored responses is correlated with construction activities; these activates implied excavation and backfilling in both of the tieback walls. In addition, this research shows a numerical procedure to evaluate the anchor capacity based on the t- z approach. Finally, this study introduces an empirical method to estimate lateral wall deformation profiles and internal bending moments along a retaining wall installed in a clay stratum.

KEYWORDS: Tieback wall, Ground anchors, Shale, Wall performance, t-z Approach

Jorge Octavio Romana Giraldo

August 13, 2018

PERFORMANCE OF TWO TIEBACK WALLS AND ROCK ANCHORS IN A SHALE
STRATUM

By

Jorge Octavio Romana Giraldo

Dr. Lindsey Sebastian Bryson
Director of Thesis

Dr. Timothy Taylor
Director of Graduate Studies

August 13, 2018

Dedication

I would like to dedicate this work to my family.

ACKNOWLEDGEMENTS

I would like to express my gratitude to my advisor Dr. Sebastian Bryson for his advice, endless support and guidance throughout this process. He pushed me to grow as a student and civil engineer, I am very thankful for that. His knowledge has allowed me improve not only as a researcher, but also as a person.

I would like to thank my family for their support and love. They motivated me every day during this process. I would like to thank the members of my committee, for offer their recommendations and evaluate my research. I want to thank Sheila and Betty for assisting me whenever I needed it. Finally, I would to thank God for giving me more that I could ever imagine.

TABLE OF CONTENTS

| | |
|---|------|
| Acknowledgements | iii |
| List of Tables | vii |
| List of Figures | viii |
| 1 Introduction..... | 1 |
| 1.1 Problem Synopsis..... | 1 |
| 1.2 Research Objectives | 2 |
| 1.3 Relevance of Research | 2 |
| 1.4 Contents of Thesis..... | 4 |
| 2 Site Location and Project Specifics | 6 |
| 2.1 Site Location | 6 |
| 2.2 Site Investigation..... | 7 |
| 2.3 Wall Description | 9 |
| 2.4 Construction Sequence and Installation Procedures | 11 |
| 2.5 Wall Instrumentation..... | 14 |
| 3 Anchor Tests and t-z Approach | 18 |
| 3.1 Introduction | 18 |
| 3.2 Anchor Design Approach..... | 19 |
| 3.3 Load Test Results..... | 23 |
| 3.3.1 Preproduction Tests | 23 |
| 3.3.2 Performance Tests..... | 27 |
| 3.4 Analytical Model..... | 29 |
| 3.4.1 Softening Model 1..... | 31 |
| 3.4.2 Softening Model 2..... | 32 |
| 3.4.3 Algorithm for the Load Transfer Approach..... | 33 |
| 3.5 Analysis and Results | 34 |
| 3.5.1 Preproduction Tests | 34 |
| 3.5.2 Performance Tests..... | 36 |
| 3.6 Strain Gages Monitoring for Short and Long-term..... | 41 |

| | | |
|------------|---|-----|
| 4 | Lateral Movements and Pore Water Variation | 45 |
| 4.1 | Introduction | 45 |
| 4.2 | Analysis and Results | 46 |
| 4.2.1 | Ground Inclinometers | 46 |
| 4.2.2 | Soldier Pile Inclinometers..... | 49 |
| 4.2.3 | Pore Water Pressure Response..... | 52 |
| 5 | Analysis of Axial Loads and Bending Moments | 54 |
| 5.1 | Introduction | 54 |
| 5.2 | Data Reduction Process..... | 55 |
| 5.3 | Performance of the Wall and Ground Anchors..... | 56 |
| 5.3.1 | Bending Moments..... | 56 |
| 5.3.2 | Axial Loads..... | 61 |
| 5.3.3 | Anchor Loads..... | 63 |
| 5.4 | Earth Pressures and Wall Design | 66 |
| 5.4.1 | Bending Moment estimation from inclinometer data. | 71 |
| 6 | Empirical Method to Estimate Lateral Wall Deformation Profiles and Bending Moment in Excavation Retaining Walls..... | 74 |
| 6.1 | Introduction | 74 |
| 6.2 | Development of the Empirical Method..... | 76 |
| 6.3 | Lateral Profile Deformation | 77 |
| 6.4 | Bending Moments | 77 |
| 6.5 | Method Validation..... | 82 |
| 7 | Conclusions..... | 87 |
| Appendix A | Tieback Notes..... | 90 |
| Appendix B | Handouts for the Tieback Notes | 111 |
| Appendix C | Matlab Code for the Numerical Procedure..... | 135 |
| References | | 140 |
| Vita | | 145 |

LIST OF TABLES

| | |
|---|----|
| Table 2-1 Summary of Wall Characteristics..... | 11 |
| Table 2-2 General Construction Sequence | 12 |
| Table 2-3 Location of the Strain Gages | 15 |
| Table 3-1 Anchor Characteristics | 23 |
| Table 3-2 Input Parameters for the Analysis of the Production Test..... | 35 |
| Table 6-1 Excavation Cases after Zapata-Medina (2007) | 76 |
| Table 6-2 Initial and boundary conditions..... | 79 |

LIST OF FIGURES

| | |
|--|----|
| Fig. 2-1. Site Conditions before Construction of the Walls..... | 7 |
| Fig. 2-2. Plan View of the Project..... | 8 |
| Fig. 2-3. Material Properties: (a) Natural Moisture; (b) Blow Counts; (c) Shear Strength | 9 |
| Fig. 2-4. Lateral View of the Walls | 10 |
| Fig. 2-5. Sequence of Installation of the anchors: (a) Lower wall; (b) Upper wall | 14 |
| Fig. 2-6. Strain gages location: (a) Lower wall; (b) Upper wall..... | 16 |
| Fig. 2-7. Locations of the Vibrating Wire Strain Gauges in Bonded Length of the Anchor 31B | 17 |
| Fig. 3-1. Apparent Earth Pressure..... | 20 |
| Fig. 3-2. Anchor Configuration for the Upper Wall Preproduction Test]. | 22 |
| Fig. 3-3. Typical Anchor Installed..... | 22 |
| Fig. 3-4. Preproduction Test Results: (a) PT1; (b) PT2..... | 24 |
| Fig. 3-5. Components of Anchor Movement until 120 percent of design load: (a) PT1; (b) PT2 | 25 |
| Fig. 3-6. Application of the second failure criteria: (a) PT1; (b) PT2 | 25 |
| Fig. 3-7. Suggested Ultimate Load Range and Pullout tests: (a) A1; (b) B1 and (C1)..... | 27 |
| Fig. 3-8. Performance tests in anchors of soldier pile 30: (a) 30B; (b) 30C..... | 28 |
| Fig. 3-9 Performance Test in Anchor 31 B..... | 28 |
| Fig. 3-10 Residual Movement versus Load | 29 |
| Fig. 3-11. Analytical Model of Ground Anchors: (a) Ground anchor; (b) Stress conditions on a differential element | 30 |
| Fig. 3-12. Load Transfer Models Considered..... | 33 |
| Fig. 3-13. Flow chart describing the t-z approach algorithm..... | 34 |
| Fig. 3-14. Load transfer models used in the analysis of the preproduction test | 35 |
| Fig. 3-15. Measured and Calculated Response for the PT2..... | 36 |
| Fig. 3-16. Load-displacement Response for Performance Test in anchors: (a) 30B; (b) 30C; (c) 31B | 38 |
| Fig. 3-17. Model 1 Effect of β on the response: (a) load transfer curve; (b) load displacement response | 39 |

| | |
|---|----|
| Fig. 3-18. Model 1 Effect of z_u on the load-displacement response: (a) Load transfer curve; (b) Load displacement response..... | 40 |
| Fig. 3-19. Model 2 Effect of n on the load-displacement response: (a) Load transfer curve; (b) Load displacement response..... | 41 |
| Fig. 3-20. Bonded Length Deformation of anchor 31B during performance test..... | 42 |
| Fig. 3-21. Estimated Load during Performance Test..... | 43 |
| Fig. 3-22. Long-term Monitoring of Anchor Bonded Length | 44 |
| Fig. 4-1. Lateral Deformation Measured in the Slope: (a) Inclinometer 1; (b) Inclinometer 1 and (c) Inclinometer 3 | 48 |
| Fig. 4-2. Incremental Lateral Deformation: (a) Inclinometer 2; (b) Inclinometer 3..... | 49 |
| Fig. 4-3. Lateral Deformation Measured in the Lower Wall: (a) Pile 11; (b) Pile 12 | 50 |
| Fig. 4-4. Lateral Deformation Measured in the Upper Wall: (a) Pile 30; (b) Pile 31..... | 51 |
| Fig. 5-1. Assumed Distribution of Strains | 55 |
| Fig. 5-2. Measured Bending Moments in the Lower Wall: (a) Pile 11. (b) Pile 12..... | 57 |
| Fig. 5-3 Measured Bending Moments in the Upper Wall: (a) Pile 30. (b) Pile 31 | 59 |
| Fig. 5-4. Variation of Bending Moment; (a) Lower wall; (b) Upper wall..... | 60 |
| Fig. 5-5. Measured Axial Load in the Lower Wall: (a) Pile 11. (b) Pile 12 | 61 |
| Fig. 5-6. Measured Axial Load in the Upper Wall. (a)Pile 30. (b) Pile 31..... | 62 |
| Fig. 5-7. Anchor Load Variation: (a) Lower Wall; (b) Upper Wall | 64 |
| Fig. 5-8. Load Cell versus Strain Gage Load in Soldier Pile 11: (a) Day 154; (b) Day 208 | 65 |
| Fig. 5-9. Load Cell versus Strain Gage Load in Soldier Pile 30: (a) Day 154; (b) Day 208 | 65 |
| Fig. 5-10. Lower Wall Model: (a) FHWA envelope. (b) Peck envelope..... | 66 |
| Fig. 5-11. Upper Wall Model: (a) FHWA envelope. (b) Peck envelope | 67 |
| Fig. 5-12. Moment Distributions in Lower Wall Calculated from: (a) FHWA envelope (b) Peck envelope | 68 |
| Fig. 5-13. Moment Distributions in Upper Wall Calculated from: (a) FHWA envelope (b) Peck envelope | 69 |
| Fig. 5-14. Development of High Positive Moments below the Lowest Anchor..... | 69 |
| Fig. 5-15. Apparent Earth Pressures: (a) Lower Wall; (b) Upper Wall..... | 70 |

| | |
|--|----|
| Fig. 5-16. Inclinator Data: (a) Lower Wall; (b) Upper Wall..... | 72 |
| Fig. 5-17. Estimated Moments from Inclinator Data (a) Lower Wall; (b) Upper Wall... | 73 |
| Fig. 6-1. Normalized Lateral Deformations for Case Histories: (a) Stiff Clay; (b) Medium Clay; and (c) Soft Clay. | 77 |
| Fig. 6-2. Six-Order Polynomial Functions: (a) Stiff Clay; (b) Medium Clay; and (c) Soft Clay..... | 80 |
| Fig. 6-3. Non-dimensional Bending Moment versus Normalized Depth..... | 81 |
| Fig. 6-4. Predicted and Measured Lateral Deformation for: (a) Stiff Clay; (b) Medium Clay; (c) Soft Clay..... | 82 |
| Fig. 6-5. DeepEX Model for Standard Excavation..... | 83 |
| Fig. 6-6. Moment Reduction Factor Versus s_u | 85 |
| Fig. 6-7. Model Bending Moment versus Proposed Bending Moment Distribution: (a) Stiff Clay; (b) Medium Clay; (c) Soft Clay | 86 |

1 Introduction

1.1 Problem Synopsis

Worldwide, tieback walls are used as retaining structures; particularly, they are used commonly in open cuts and bridge abutments. In addition, the adaptability of a tieback wall makes the system an adequate option as a slope stabilization structure. Essentially, tieback walls consists of three elements: support system, anchorage and connection between these two elements. The support system can be sheet piles, wood lagging, secant piles, tangent piles among others; anchorage is formed by concrete grout in a drilled hole. The connection between the support system and the anchorage can be either a bar tendon or a strand composed of several wires.

Current construction techniques make possible to install tieback walls in almost any type of soil or rock. Several standard test have been develop in order to assure the stability of the system; particularly, the load carrying capacity of the ground anchors. In addition, corrosion seals developed over the years make the system more reliable in regards to long-term stability. Compared with other earth retaining systems, tieback walls seem to offer a faster construction; consequently, less costly option in most cases.

In retaining structures, earth pressures acting behind the structure are a function of the structure lateral and vertical movements. These pressures on the backside of the wall are transferred to the ground through the anchorage and the tendon. Furthermore, the distribution of the earth pressures is affected by factors such as ground surcharges, slope of the terrain, and ground water regime. These factors combined with the natural variation of geological settings in a site make the interaction soil-structure complex.

This research will presents a comprehensive study of the performance of two tieback walls used in an unstable slope. In order to extend the knowledge of ground and wall response during construction, the different components of the walls were instrumented and monitored. Additionally, methodologies to evaluate the anchors performance and estimate maximum bending moments in the support system are presented.

1.2 Research Objectives

The following objectives were established for this study:

- Develop a t-z approach that allows engineers the estimation of the load-displacement curve for anchors installed in shale or other type of material. Use the data obtained during proof, performance and preproduction tests to validate the methodology and to presents recommendations.
- Present a descriptive chart that facilitate the application of the proposed numerical algorithm in a common programing software.
- Estimate the response of the two walls to backfilling and excavation activities using the measured deformations along the soldier piles; additionally, analyze the variation of the anchor load after installation and testing.
- Developed numerical models for the two walls to estimate the responses using apparent earth pressure envelopes; use the commercial software DeepEX to create the models.
- Correlate the construction sequence of both walls with the measured response of the slope in terms of ground lateral movements and pore pressures variation.
- Compare the measured wall response in each instrument (strain gages, load cells, inclinometers), identify the sources of agreement or disparity, and analyze how these responses are related to wall construction activities.
- Collect and analyze a database of excavation induced lateral deformations to develop an empirical method to estimate lateral deformation profiles and maximum wall bending moments based on material type.

1.3 Relevance of Research

Traditionally, the design of retaining structures for deep excavations is based on apparent earth pressure envelopes; these are semi-empirical diagrams that were originally developed to provide loadings for conservative design of struts in braced excavations. Among these, the most common pressures envelopes have been proposed by Peck (1969), Tschebotarioff

(1973) and the Federal Highway Administration (Sabatini et al. 1999). Pressure envelopes were based on back calculation of anchor or struts loads in excavations; therefore, for retaining walls that imply activities as backfilling and excavation during the same construction, the validity of these pressures to wall design needs to be addressed.

As previously described, apparent earth pressures were developed based on braced excavations; nonetheless, these pressures are regularly used for the design of retaining walls for slope stabilization. However, construction activities during excavation and during slope stabilization are different; consequently, the use of apparent pressure might not be pertinent in walls to remediate slope stability problems. In order to clarify this issue, it is necessary to measure and to analyze the response of retaining walls for slope stabilization against studies for walls used as excavations support systems.

This study attempts to validate the appropriateness of using these apparent pressures in the design of wall in slope remediation; additionally, it is expected to analyze the influence of backfilling and excavation activities in the wall performance. Data used during the development of this report was presented by Liang (2000) and involve the construction of two tieback walls in a shale stratum.

Other aspect concerning the construction of retaining walls is the wall support system; these are generally ground anchors, steel struts or combination of both. In this study, ground anchors were used as wall support system. Due to the natural uncertainties of soil or rock deposits, after installation, anchors in either soil or rock material must be tested. Although typically values of anchor resistance are given literature, the soil profile variability makes necessary to check anchor capacity. Engineers are continuously searching for alternatives to improve anchor design and installation; in this research, a numerical procedure to estimate anchor load displacement is presented. The method was based on a series of anchor tests conducted in shale stratum before and during construction of the two walls. The numerical procedure can be extended to anchors installed in different condition using results of pullout tests; this alternative may give designers an agile estimation of anchor capacities before construction.

Last aspect treated in this study is the wall and ground movements associated with construction. Preservation of adjacent infrastructure during wall construction is critical;

therefore, it is necessary to monitor the induced displacements and pore water pressure variation in order to evaluate the possible damages in contiguous facilities. The pattern of wall and deformations is highly influenced by the construction sequence; typical patterns and methods to estimated induced movements during excavations have been proposed in the literature (Hsieh and Ou 1998; Finno et al. 2007; Kung et al. 2007; Bryson and Zapata-Medina 2012) . However, these studies were developed for excavations; consequently, it is necessary to extend the analysis of pattern and magnitude of deformations to walls that imply backfilling and excavation activities at the same time. In this matter, construction of the two walls of this study represents an opportunity to expand the knowledge presented by previous studies.

This thesis presents the performance and the analysis of two instrumented tieback walls located in the Cuyahoga Valley National Park in Brecksville, Ohio. The walls were constructed as a solution to stabilize an existing slope in the west front of the Cuyahoga River over the Route 82. A special remark of this project is the opportunity to analyze the behavior of tieback walls in shale. Shale is well known for its unpredictable behavior in presence of water (Terzaghi and Peck 1967). Consequently, the degradation of the anchors in this type of material is important from an engineering standpoint.

1.4 Contents of Thesis

Chapter 2 will introduce the project description, the necessity for the construction of the walls and a general geotechnical description of the site of construction. In addition, plan and lateral views of the walls are presented as well as the general construction sequence.

Chapter 3 will present the results and analysis of the proof, performance and preproduction tests conducted during the completion of the project. Furthermore, this chapter includes the numerical procedure developed within this research; the procedure allows to estimate the load-displacement behavior of ground anchors.

Chapter 4 will detail the measured ground and wall responses in terms of lateral movements and pore water pressures. Results will be associated with the construction activities and compared to typical values reported in the literature for this type of walls

Chapter 5 will analyze the data collected with the strain gages installed in the soldier piles and the load cells in the anchors. Measured values are compared with theoretical values estimated based on typical earth pressure envelopes.

Chapter 6 will show the semi-empirical method developed to the estimation of lateral displacement profile and bending moments along support systems. Database for the method will be presented and the validation of the methodology using the software DeepEX.

Chapter 7 summarizes the results obtained during the research and presents comprehensive conclusions of the performance of both walls and developed methodologies.

2 Site Location and Project Specifics

2.1 Site Location

Both tieback walls are located in the Cuyahoga Valley National Recreation Area (CVNRA) on the western side of the Cuyahoga River under the State Route 82, in Brecksville, Ohio. The slope under consideration was formed by cutting a bench into the toe of the western river valley side to the development of the Valley Railroad.

This area has been identified as prone to slope movements (Hansen 1995; Nandi and Shakoor 2008; Gorsevski et al. 2016). Stability analysis of the area indicated that large portions of the zone were barely stable; i.e., the factor of safety was low against shallow and deep seated earth movements. A well-defined failure surface was difficult to define due to the variability in the subsurface conditions; this difficulty is supported with the site observations that many local movements are occurring throughout the area.

Slumps and block movements were observed throughout the area; in addition, surface erosion was observed near the rail tracks in the lower portion of the area. The extent of movement based on site conditions was determined as 60 m and 120 m to the north and south of the State Route 82 bridge centerline, respectively. Fig. 2-1 shows the site conditions before any major intervention in the area; as seen, remediation of the steep slope was necessary to preserve the bridge foundation. It has been determined that a combination of steep slopes, low shear strength of silty and clayey soils, and undercutting of the toes of slopes causes the landslides in this area.



Fig. 2-1. Site Conditions before Construction of the Walls

2.2 Site Investigation

In the proximity of the State Route 82 and Cuyahoga River valley, the instable slope rose sharply from the valley changing elevation of 12 to 15 m over a horizontal distance of 15 to 18 m. It continued in a moderate slope for an elevation change of 9 to 12 m over a horizontal distance of 30 to 60 m; finally, it rose steeply with a change in elevation of 9 m over a distance of 9 to 18 m.

Fig. 2-2 presents a plan view of the project including the location of the exploratory borings. From the subsurface investigation, three geologic strata were identified at the site. An upper soil layer consisted of brown silty clay or clayey silt combined with loose to medium sand. These deposits combined vertically and horizontally without a consistent pattern throughout the site. A lower soil layer consisted generally of gray clayey silt and silty clay with a consistency that was typically stiff to very stiff. The lowest part of the soil profile consisted of the shale stratum; according to the boring data the shale surface drops sharply to the west with a tendency north-south. Shale was mostly, black, carbonaceous

with numerous scatter thin clay seams. Top of the shale stratum was weathered or severely weathered with the degree of weathering decreasing with depth.

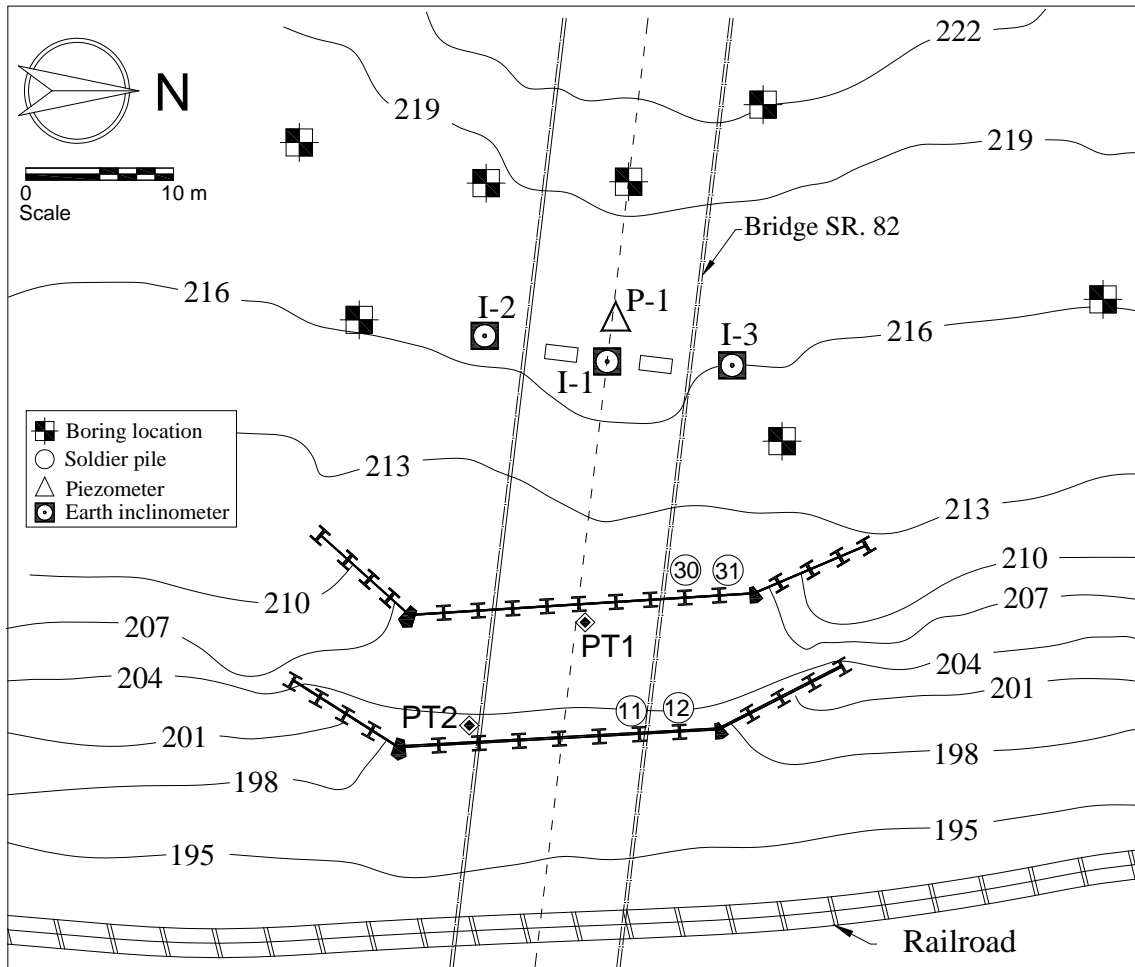


Fig. 2-2. Plan View of the Project

Based on data collected in the boring logs, estimated composite soil characteristics were developed and are presented in Fig. 2-3. The natural moisture content was fairly uniform with depth ranging between 20 and 30 percent. Blow counts showed a similar trend. Undrain shear strength was obtained from unconfined compression tests and appeared to increase as a function of the effective overburden stress, with a considerable increase observed near the shale layer.

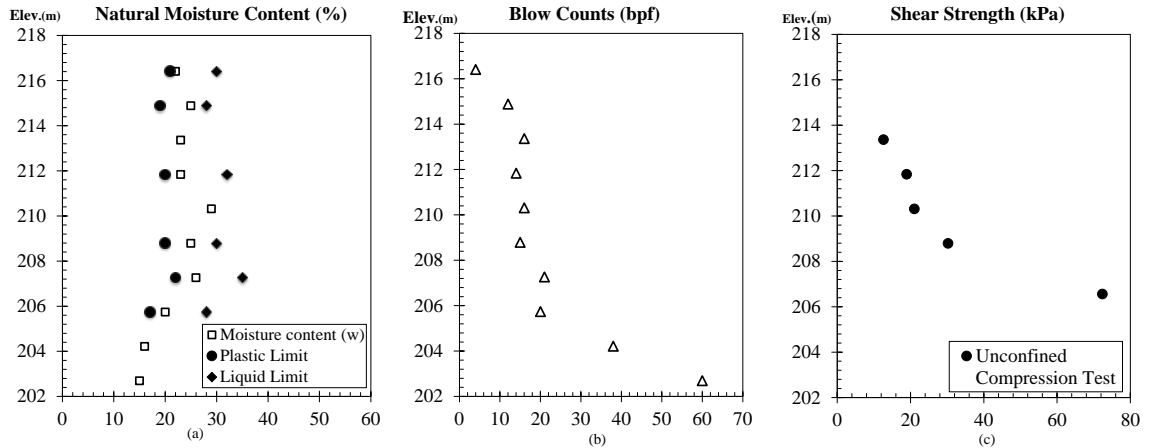


Fig. 2-3. Material Properties: (a) Natural Moisture; (b) Blow Counts; (c) Shear Strength

2.3 Wall Description

Lateral view of both walls shown in Fig. 2-4; the clayey and silty soils behind the walls were excavated and replaced with a granular backfill. The upper wall was 15.2 m height and supported by three rows of anchors; similarly, the lower wall was 14.3 m height with two rows of anchors. Both walls were inclined at their ends; with angles varying between 18.5 and 45 degrees measured with respect to the center of the wall.

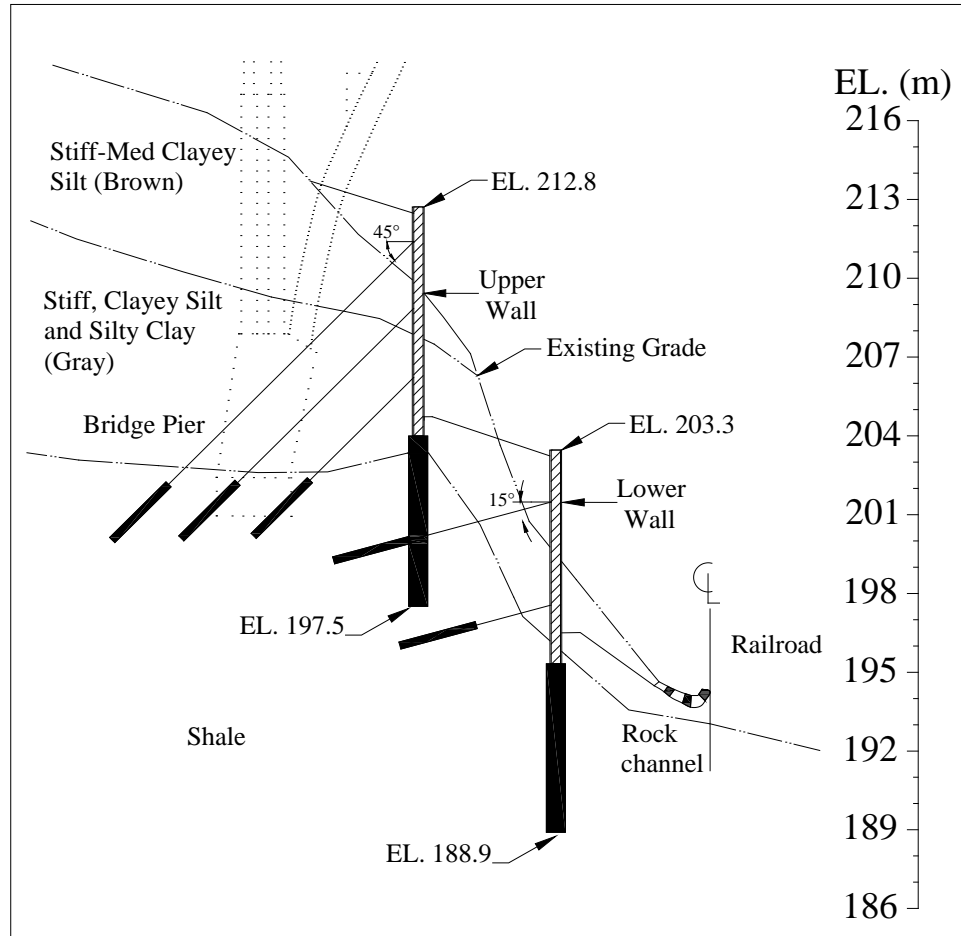


Fig. 2-4. Lateral View of the Walls

Thirty-six soldier piles were installed in the project; seventeen in the lower wall and nineteen in the upper one with their toes embedded in concrete. Precast concrete lagging was installed between the HP14x73 piles. Soldier piles were installed in prebored holes of 0.61 m diameter; however, at wall deflections, channel type sections were used with their toes embedded in drilled holes of 0.8 m of diameter.

Sixty-eight rock anchors were installed. Inclination of the anchor in the lower wall was 15 degrees measured from the horizontal; while for the upper wall this inclination was established as 45 degrees. Anchors installed in the upper rows were cased using steel struts to prevent the boreholes from collapsing and to support the jacking system while testing; steel casing were penetrated to depths ranging from 1.8 to 2.4 m into the shale. The free length of the anchors the free length was extended to the top of the shale stratum, this length

ranged from 5.2 m to 17.1 m. The bonded length of all the anchors was 4.6 m; this length was installed in the shale stratum.

Table 2-1 presents the walls characteristics, free-length of the ground anchors varied according to the row; row A corresponds to the upper row of anchors in both walls.

Table 2-1 Summary of Wall Characteristics

| | Pile No | Row | Design load (kN) | Minimum Free Length (m) | Deflection Angle (Deg) |
|-------------------|----------------|------------|-------------------------|--------------------------------|-------------------------------|
| Lower wall | 1-17 | A | 391-489 | 4.6 | 15 |
| | | B | 489 | 4.6 | 15 |
| Upper Wall | 18-36 | A | 343 | 7.3 | 45 |
| | | B | 343 | 5.5 | 45 |
| | | C | 343 | 4.6 | 45 |

2.4 Construction Sequence and Installation Procedures

A general construction sequence is presented in Table 2-2. The upper soldier piles were installed first; the lower soldier piles were installed after completion of the upper installation. The holes for both the upper and lower soldier piles were drilled 762 mm in diameter and 6.1 m deep in the shale. The piles were lifted by a crane and lowered into place. Then, they were fixed to a supporting frame to maintain alignment; concrete was placed using tremie techniques. Anchors from the lower wall were inclined horizontally to prevent that they intersect the embedded portion of the soldier piles from the upper wall during installation.

The upper two rows (Rows A and B) of the upper wall and the upper (Row A) in the lower wall were installed under “fill” conditions (i.e backfill was later place at these elevations). Lower row of anchors in both walls was installed under “cut” conditions; that is, shale stratum was excavated in from of the soldier piles to install the anchors. During anchor installation, the drill mast was supported by a crane and clamped to the flange of the soldier piles for lateral stability.

Table 2-2 General Construction Sequence of the Project

| Day | Construction activity |
|---------|---|
| 1 | Establishment of upper and lower benches. |
| 20 | Installation of earth inclinometer and piezometers. |
| 28-41 | Installation of soldier piles for upper wall. |
| 41-51 | Installation of soldier piles for lower wall. |
| 50-57 | Upper failure test |
| 36-61 | Lower failure test |
| 72-106 | Installation and testing of anchors in row B in upper wall. |
| 106-115 | Installation and testing of anchors in row B in lower wall. |
| 115-132 | Installation and testing of anchors in row C in upper wall. |
| 132-146 | Installation and testing of anchors in row A in lower wall. |
| 146-177 | Installation and testing of anchors in row A in upper wall. |
| 157 | Concrete lagging installation in lower wall was completed. |
| 157-185 | Final backfilling of the lower wall. |
| 181 | Concrete lagging installation in upper wall was completed. |
| 181-188 | Final backfilling of the upper wall, post-grouting and construction were completed. |
| 226 | Finish set up for long-term monitoring. |

Only one row of anchors was installed at a time in the project. Namely, when installing a row of anchors in a wall, activities as excavation, backfilling and installation of precast concrete panels were conducted in the other wall. Installation of the anchors began in the upper wall with the Row B. Before installation of these anchors, steel casings were penetrated in the shale stratum to avoid the transfer of load to the soldier pile during tensioning of the anchors.

Following the construction of the middle row in the upper wall; for the lower wall, lower row of anchors (Row B) was installed. These anchors were under “cut” conditions; a bench was established at an elevation of 197.2 m, 0.38 m below anchors elevation; then, anchors were installed and tested without using steel casings. After installation of anchors, ground was excavated to an elevation of 196.60 m and precast panels were installed from this elevation towards the top of the wall. Afterwards, the wall was backfilled to an elevation of 200.7 m approximately; notice that the soldier piles acted as a cantilever beam from the row B to the top of the wall. When placing the backfilling material, this unsupported height was 5.72 m.

Continuing with the installation process, the Row C of anchors in the upper wall was installed. These anchors were installed under “cut” conditions; shale was excavated using temporary wood lagging to maintain safety conditions as the excavation proceeds. The excavation was held 0.65 m below the row C; then, anchors were installed and tensioned. Upon completion of the installation, ground in front of the upper wall was excavated to the elevation of 204.7 m; the permanent lagging was installed from this elevation to 210.5 m. Backfilling proceeded to an elevation of 1.5 m above the middle row of anchors approximately. Note that under these conditions, the upper wall had about 3.8 m of cantilever height.

The construction sequence continued with the upper row (Row A) in the lower wall; this row was installed under “fill” conditions. Then steel casings were passed through the backfilling material until reached the specified penetration in the shale stratum. After that, the anchor in this row were installed and tested. Construction was then moved to the upper wall area.

Finally, the Row A of anchors in the upper wall was installed; steel casings were also used to act as a support during installation of this row. Grading behind the wall was elevation at 210.46 m approximately. Upon installation and testing of the ground anchors, backfilling material was place to the designs elevation in both walls. Fig. 2-5 presents a schematic sequence for the anchor installation.

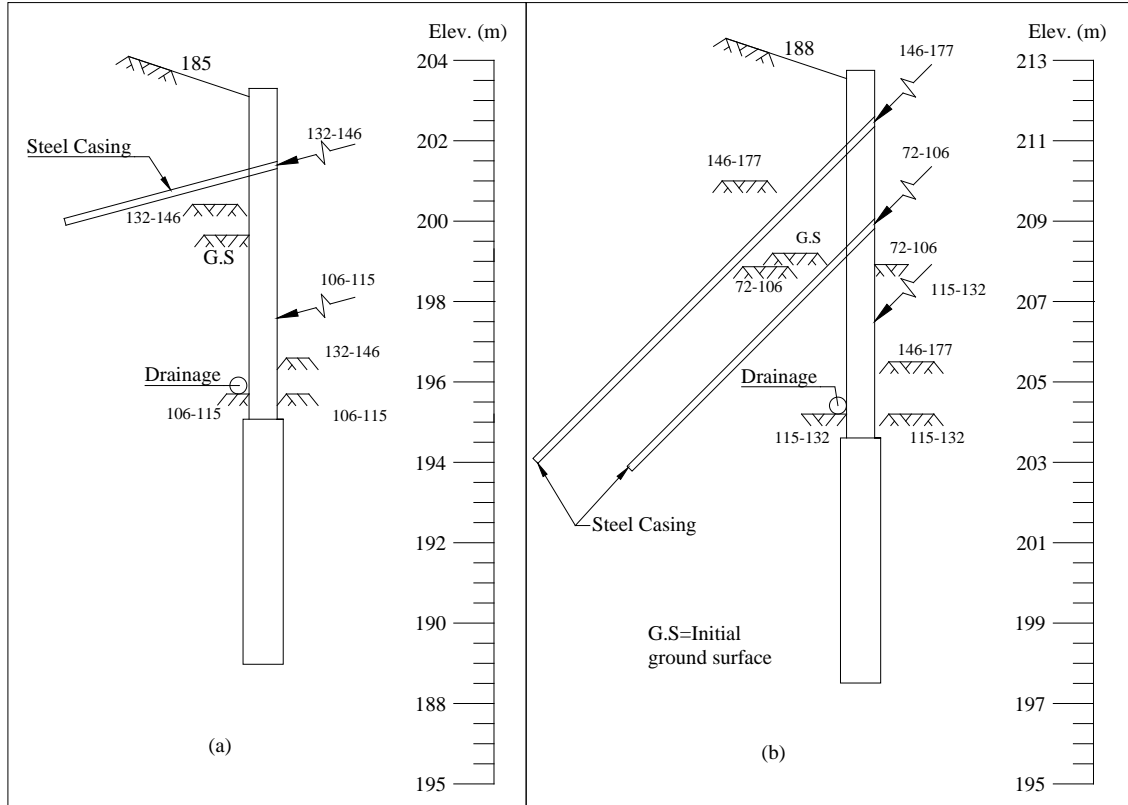


Fig. 2-5. Sequence of Installation of the anchors: (a) Lower wall; (b) Upper wall

2.5 Wall Instrumentation

Several components of both anchor were instrument in order to study the performance of the walls. In order to monitor the movements of the ground and foundation of the bridge, prior to the beginning of the construction of the walls, slope movements were monitored using three inclinometers. The three inclinometers had depths of 29.6 m, 25.3 m and 24.4 m; these were installed near the bridge piers as shown in Fig. 2-1. Additionally, a vibrating wire piezometer was installed in the slope; its location is shown in Fig. 2-1.

Lateral deformation of the upper and lower wall was monitored using inclinometers attached to the soldier piles. A total of four soldier piles were instrumented; two in the upper wall and two in the lower wall. Fig. 2-1 shows the location of the soldier piles with inclinometers. These inclinometers were installed in segments of 3 m during lowering of the soldier piles; the bottom of the inclinometers was extended 4.6 m below the bottom of

the soldier piles to monitor movement at the bottom of the pile. Top of the inclinometers was left 3 m shorter than the soldier piles to protect them from damage during construction. These same four soldier piles were instrumented using vibrating wire strain gages; in the lower wall, soldier piles 11 and 12. Accordingly, in the upper wall soldier piles 30 and 31. Fig. 2-1 shows the location of these soldier piles in the walls. Table 2-3 presents the location of the strain gages with respect to the top of the soldier piles; sixteen vibrating wire strain gages were installed in each pile.

Table 2-3 Location of the Strain Gages

| Strain Gage Row | Depth (m) | |
|--------------------|------------|------------|
| | Lower wall | Upper wall |
| 1 | 1.2 | 1.9 |
| 2 | 3.1 | 2.8 |
| 3 | 4.3 | 4.4 |
| 4 | 6.5 | 5.3 |
| 5 | 8.0 | 6.7 |
| 6 | 9.7 | 8.5 |
| 7 | 11.2 | 10.9 |
| 8 | 12.7 | 13.3 |

Gages were installed in pairs corresponding to eight rows on each soldier pile; a steel protection cover was used in each gage to prevent damage during construction. Fig. 2-6 shows the location of each pair of strain gages in the walls.

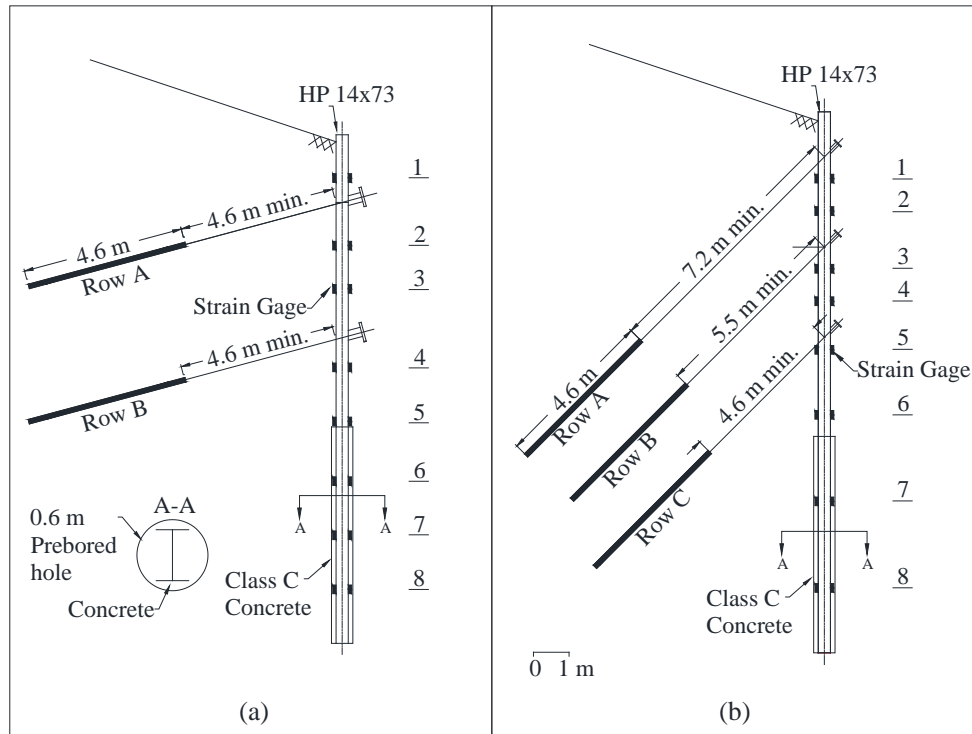


Fig. 2-6. Strain gages location: (a) Lower wall; (b) Upper wall

In order to monitor the load variation in the anchors, load cells were installed at the head of selected anchors in the upper and lower wall. In the upper wall. Load cells were installed in the anchors of the soldier pile 30; similarly, in the lower wall, load cells were installed in pile 11.

Evaluation of the load-transfer mechanism along the bonded length was conducted in anchor 31B through strain gages. Gages were installed at 0.9 m, 2.1 m and 3.4 m from top of the bonded length as shown in Fig. 2-7. Changes in deformation were observed during performance tests and after the tests for a period of 185 days considered herein as the long-term analysis. Strain gages were mounted to the strand and wrapped around to protect them during grout installation.

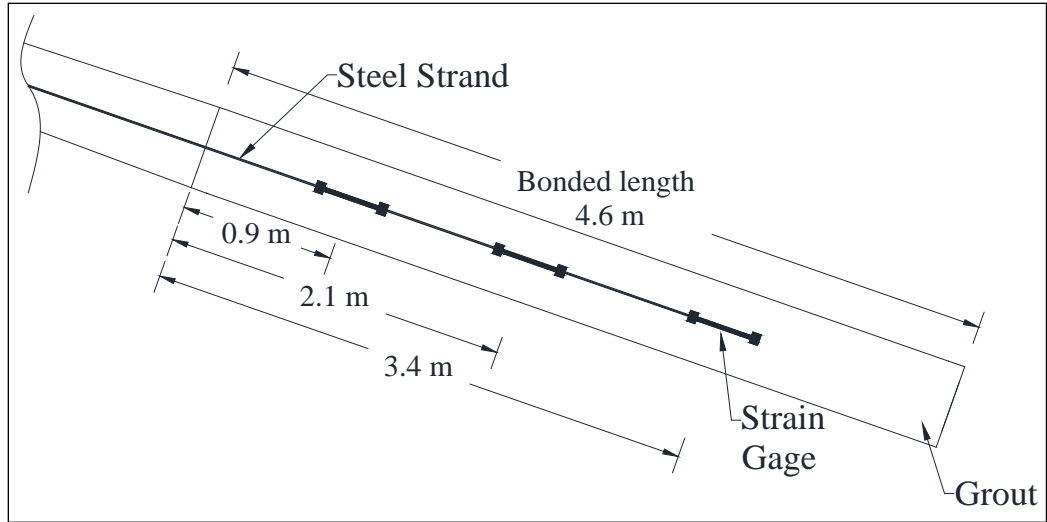


Fig. 2-7. Locations of the Vibrating Wire Strain Gauges in Bonded Length of the Anchor 31B

3 Anchor Tests and t-z Approach

3.1 Introduction

Ground anchors have been widely used to support retaining walls for deep excavations, stabilize natural or man-made slopes, prevent uplifts of submerged structures, and providing support for bulkhead or wharf systems (Littlejohn 1997; Sabatini et al. 1999; Ehrlich and Silva 2015). Although there have been significant advances utilizing new materials to improve the performance of ground anchors, design methods have remained essentially the same over the last decades (Xu and Yin 2016).

Typically, the ultimate load capacity is estimated via a limit equilibrium analysis that utilizes a presumptive ultimate bond stress along the bonded zone of the anchors. The presumptive ultimate bond stress is typically given in various design manuals (Sabatini et al. 1999) or prescribed codes as the Post-Tensioning Institute (PTI) (2014). This approach relies on a uniform bond stress along the bond length. However, it is recognized that this stress distribution is not uniform (Benmokrane et al. 1995; Sabatini et al. 1999; Kim 2003).

The stress distribution might be uniform in weak rock as clay shales, but in more rocks that are competent, the bond stress is mobilized only in the upper portion of the anchor-bonded length (Sabatini et al. 1999). Given the recommended range of presumptive bond strength at the ground/grout interface, selection of the appropriate value is highly subjective to the experience of the designer. According to Hegazy (2003), the use of the maximum recommended bond strength may lead to inadequate designs when factors of safety of 2.0 and 3.0 are applied in soil and rock, respectively.

Several authors have used a non-linear relationship along the ground-grout interface to analyze the behavior of ground anchor subjected to tensile loads. Kim (2003) analyzed the load transfer in tension anchors using a purely elastic-plastic model. The analysis was divided in two parts; one part corresponded to the anchor-soil interface and the other to the strand-grout interface. More recently, Xu et al. (2014) proposed a hyperbolic load–displacement model to study the deformation characteristics in a jet mixing anchor pile support system. Another study reported by Liu et al. (2017) used a broken line model to analyze the distribution of stress transfer along the bonded length of ground anchors. This

model considers softening; the transition between the ultimate skin friction and the residual stress is given by and abrupt change in the load transfer relationship which might be unrealistic.

Models that considered a smoother transition between the ultimate and the residual side resistance tend to be more realistic; two models can be considered among these. First model proposed by Zhang and Zhang (2012); this depends on three parameters, the ultimate skin friction, relative displacement at the ultimate skin friction and the ratio between the residual skin friction and the ultimate skin friction. More recently another model considering softening was proposed by Ni et al. (2017); their model was based on a single parameter, n , to describe the load-transfer function.

These aforementioned studies support the idea of using a more realistic load transfer function along the bonded length of ground anchors as a mean to predict better the ground anchor response. This chapter presents the analysis of the two preproduction tests and the three performance tests conducted during the construction of the two tieback walls. From the data collected, the load transfer mechanism was investigated numerically using load transfer models that include softening behavior. In addition, strain gage data was used to assess the long-term variation of the loads along the bonded length of the anchors.

3.2 Anchor Design Approach

The Peck (1969) apparent earth pressure envelope for granular backfill was used to determine the anchor loads. Because the Peck envelope was intended for horizontal ground surface and the backfill in both walls was inclined, a modified Coulomb active earth pressure coefficient, K_a , was used in the design and is given as

$$K_a = \frac{\cos^2 \phi}{\left[1 + \sqrt{\frac{\sin(\phi) \sin(\phi - w)}{\cos(w)}} \right]^2} \quad (1)$$

Equation 1 corresponds to an active earth pressure coefficient on a vertical wall with no friction and backfill inclination of w . Therefore, the maximum intensity of the apparent

earth pressure was $P_a=0.65 K_a\gamma H$ where γ = unit weight of the backfilling material and H = height of the excavation as shown in Fig. 3-1.

Selection of the unbonded length of the anchors was based on Rankine failure plane and an offset of 1/5 the height of the excavation as recommended by Sabatini et al. (1999). In the lower wall, the anchor unbonded length in both rows of anchors was equal. However, in the upper wall this was selected in such a manner that the bonded length was installed in the shale stratum. In the lower wall, the anchors were inclined slightly in the horizontal direction to avoid any intersection with soldier piles of the upper wall. In addition, some anchors in the upper wall were inclined to avoid intersection with the bridge pier.

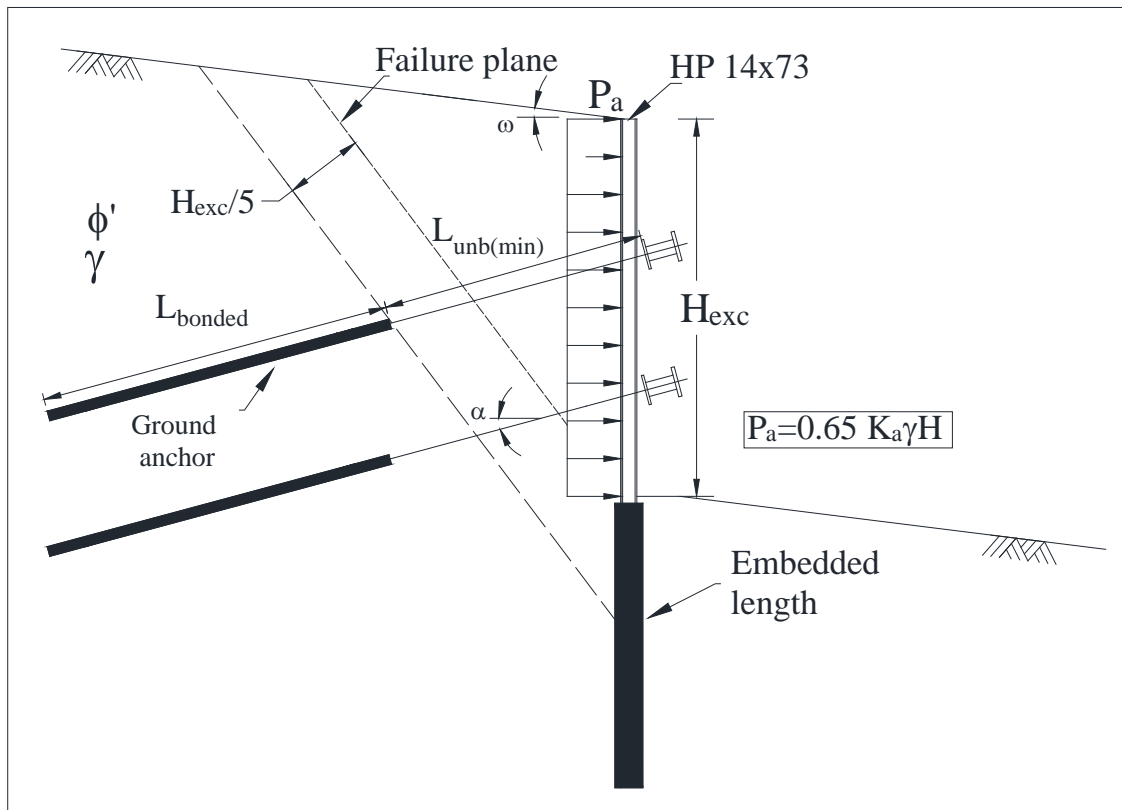


Fig. 3-1. Apparent Earth Pressure

Based on the applied pressured distribution and the tributary area method (Terzaghi and Peck 1967), the design anchor load for the upper wall was 343 kN based on a separation of 2.4 m between soldier piles. Conversely, for the lower wall, anchor design load was 489 kN for a given separation of 3 m.

As registered in the subsurface investigation, soil conditions at the project site were fairly variable horizontally and vertically with respect to soil types and consistency of these materials. This variability made it necessary to conduct preproduction tests prior to the installation of production anchors; tests were intended to study the anchor capacity and load transfer mechanism. One test was performed for the upper wall and one test was performed for the lower wall. The upper wall test anchor (PT1) was installed between soldier piles 26 and 27 and the lower wall test anchor (PT2) was installed between piles 6 and 7. Both load tests were conducted after installation of the soldier piles in both walls. The locations of these tests are shown in Fig. 2-1; they are identified as PT1 and PT2, for the upper and lower wall tests, respectively.

The anchor holes for both upper and lower wall tests had a diameter of 101.6 mm, anchor tendons were composed of seven 7-wire strands. Although both test locations were relatively close, some differences emerged in the testing conditions. The upper wall test had a steel casing in the unbonded length to prevent the anchor hole from collapsing; steel casing was penetrated 1.2 m into the shale stratum and it had 139.7 mm diameter. Additionally, in the lower test, the unbonded and bonded length of the anchor were installed completely in the shale stratum. An illustration of the anchor for the upper wall test is shown in Fig. 3-2. Similar anchor configuration was used in the lower wall test, but without the steel casing. Both load tests were conducted against the ground surface using a bearing plate.

There was concern at the site that the shale stratum would absorb water as a result of infiltration. Consequently, the anchor holes were filled with water after drilling and before installation of the tendons, to study the effect of water in load-carrying capacity. Water remained 7 days for the lower wall test and 9 days for the upper wall test until insertion of the tendon and grouting of the anchor. Test procedures were conducted according to the Post-Tensioning Institute (2014). Specifically, after 1.33 times the design load, load was increased to 1.5, 1.75, 2.0, 2.25, 2.5, 2.75 and 3.0 times this load.

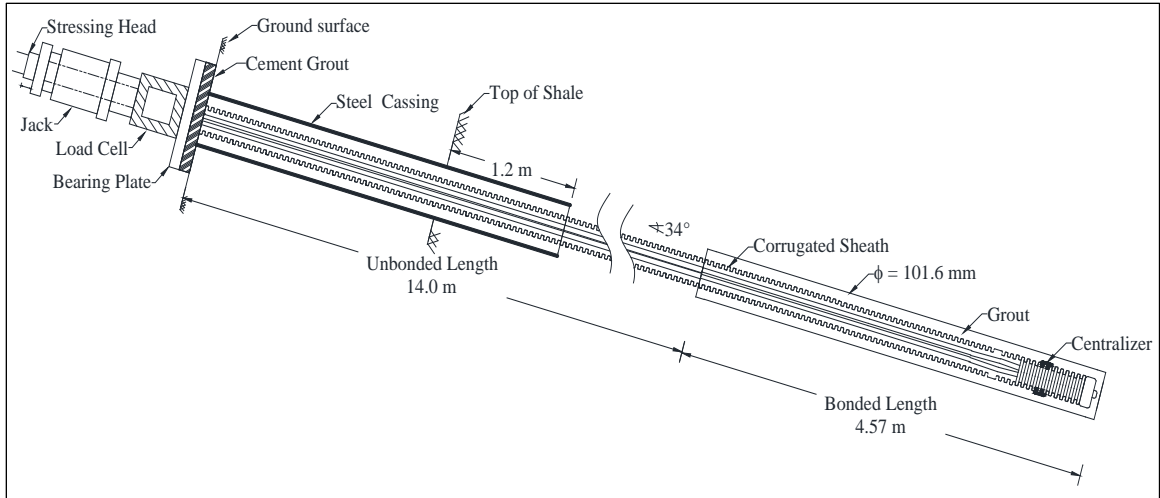


Fig. 3-2. Anchor Configuration for the Upper Wall Preproduction Test.

Table 3-1 shows the characteristics of the tested anchors. In addition to the preproduction load tests, performance test were also conducted in several production anchors. Fig. 3-3 shows a typical production anchor installed in the project; this figure correspond to the anchors installed in the upper wall. Anchors in the lower wall had a similar configuration, but were composed of four tendons.

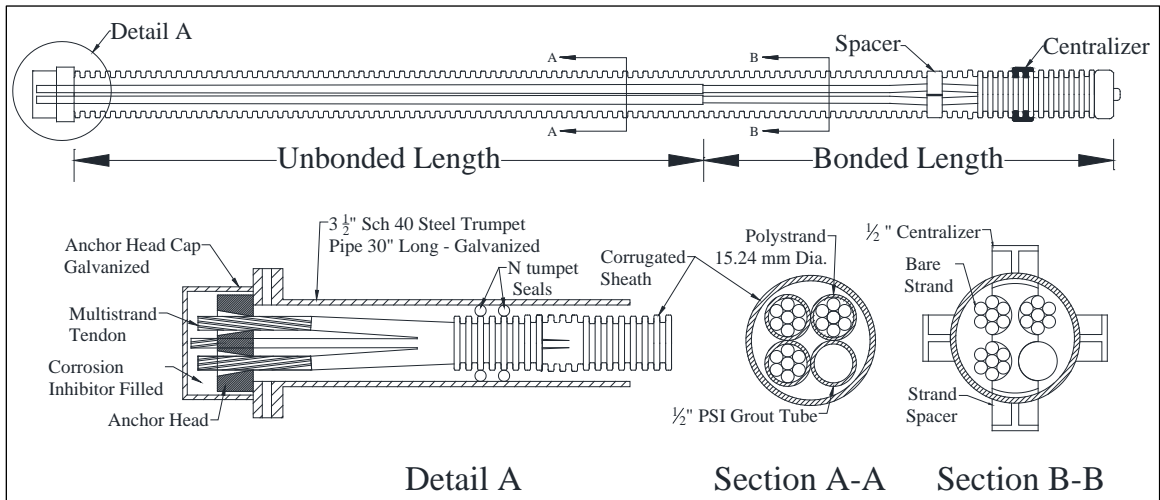


Fig. 3-3. Typical Anchor Installed in the Upper Wall.

Table 3-1 Anchor Characteristics

| Test | Design Load (kN) | Diameter (mm) | Tendon Assembly | Total Length (m) | Bonded Length (m) | Unbonded Length (m) | Incl. (Deg) |
|----------|------------------|---------------|-----------------|------------------|-------------------|---------------------|-------------|
| PT1 * | 343 | 101.6 | 7 | 18.62 | 4.57 | 14.05 | 34 |
| PT2 | 489 | 101.6 | 7 | 12.89 | 4.57 | 8.32 | 15 |
| 30B | 343 | 101.6 | 3 | 10.06 | 4.57 | 5.49** | 45 |
| 30C | 343 | 101.6 | 3 | 9.14 | 4.57 | 4.57** | 45 |
| 31B | 343 | 101.6 | 3 | 10.06 | 4.57 | 5.49** | 45 |

* Steel casing. **Minimum value.

3.3 Load Test Results

3.3.1 Preproduction Tests

The preproduction tests were intended to go to complete pullout of the anchors, causing failure at grout-ground interface and facilitating the investigation of the load transfer characteristics for the anchors in shale. However, for PT1 the applied load was stopped at 2.75 times the design load and for PT2 the applied load was stopped at 3 times the design load. The load-displacement curves for both tests are shown in Fig. 3-4. During the tests, load-unload cycles were applied until 120 percent of the design load, with hold times varying with the load application. At 25 percent of the design load, the hold time was 10 minutes and at 120 percent of the design load, the hold time was 60 minutes.

To ensure a proper alignment of the equipment during the tests, a load of 20 percent the design load, termed the alignment load, was applied at the beginning of the tests. Fig. 3-4 shows that from the beginning of the tests until the maximum applied load, load-displacement curves in both tests did not show a significant degradation in the anchor capacity. Consequently, the load-displacement relationship was approximately linear.

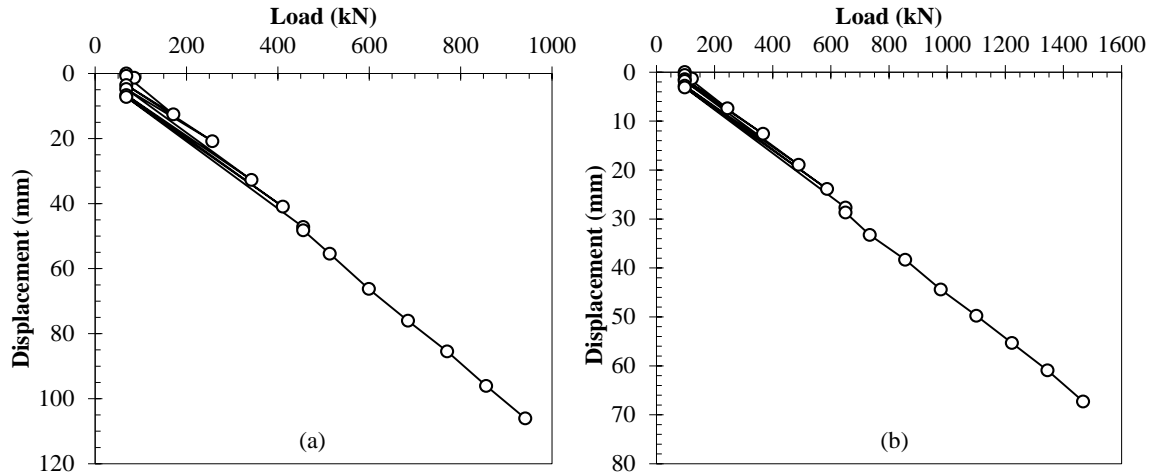


Fig. 3-4. Preproduction Test Results: (a) PT1; (b) PT2

Fig. 3-5 presents the components of anchor movement. The total movement measured included the elastic elongation in the unbonded length of the anchor and the residual movement. Residual movement was define as the non-recoverable movement after the load application.

Analysis of the test results was mostly focus on the preproduction tests (PT1 and PT2) than the performance test. The ultimate anchor load was defined using the Briaud et al. (1998) failure criteria. Failure Criterion 1 considers that the ultimate load is the load at which the residual movement is one-tenth of the anchor diameter ($D/10$) and Failure Criterion 2 considers that the ultimate load is the load at which the total displacement is ($D/10$) plus the elastic elongation of the anchor unbonded length. The residual movements measured until the applied load was 120 percent the design load are presented in Fig. 3-5. Based on the first failure criterion, neither of the anchors failed before this reaching load. However, the residual movement in the PT1 was close to this threshold. The maximum residual movement observed in the PT1 was 7.2 mm, while in PT2 this value was 3.1 mm.

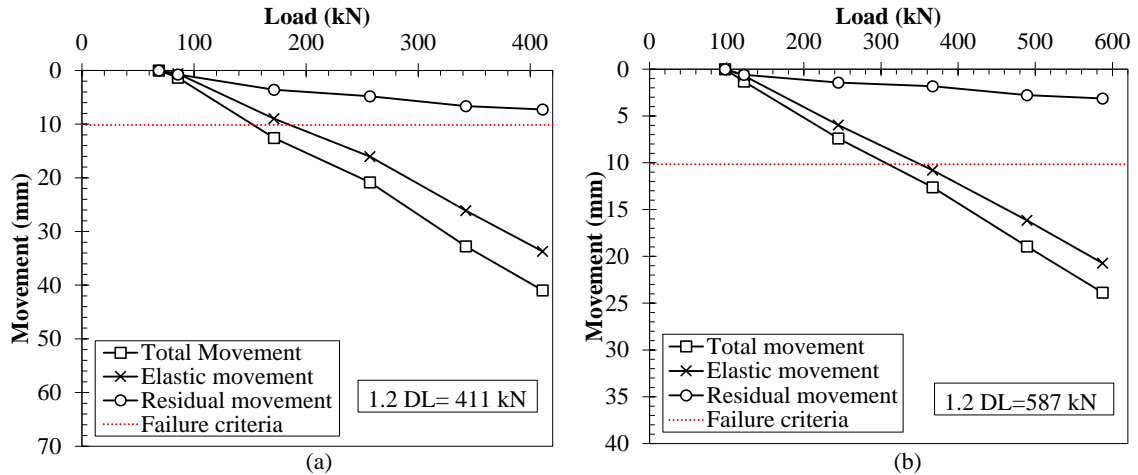


Fig. 3-5. Components of Anchor Movement until 120 percent of design load: (a) PT1; (b) PT2

Fig. 3-6 shows results the second failure criterion applied to the tests; notice that the reloading cycles are not presented in the figure. As seen in the figure, the criterion predicted an ultimate load that was less than the design load for the PT1. Based on these test results, Fig. 3-6a, it was unlikely that the ultimate capacity of the anchor was reached under the range of applied loads because of the nearly linear load-displacement curve. For these criteria, the unbonded length of the anchor is assumed constant; however, because of loading, debonding at the top of the bonded length may occur (Benmokrane et al. 1995). During debonding the free length of the anchor increases and consequently the elastic elongation of the strands that leads to a more linear load-displacement curve.

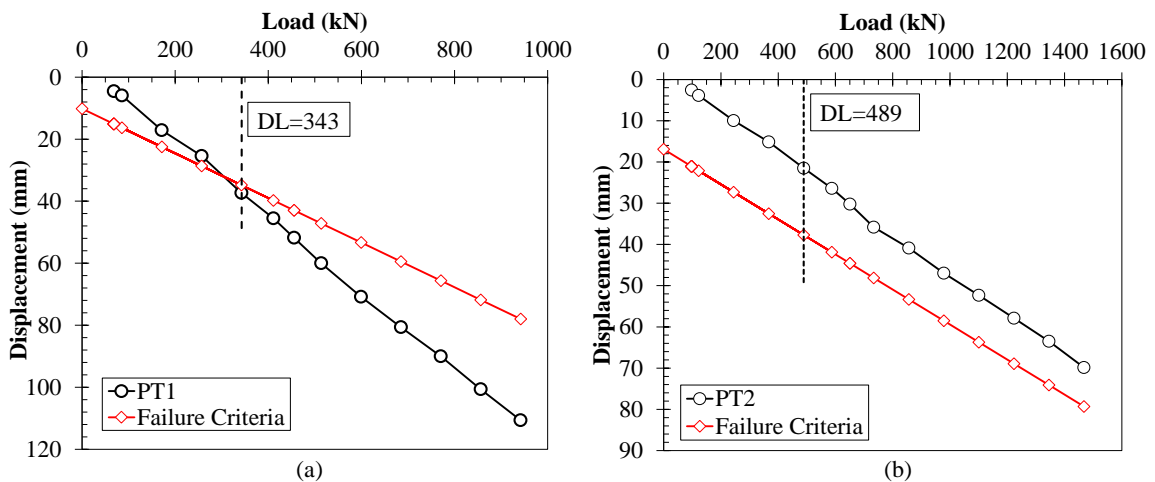


Fig. 3-6. Application of the second failure criteria: (a) PT1; (b) PT2

Additionally, application of the second failure criteria to the PT2 (Fig. 3-6b) shows that the failure load was not reached under the range of loads applied. In this case, it remains uncertain about which load could be considered as the ultimate load. Given that the maximum applied load was about three times the design load in both tests and the anchor movements were considered adequate, the bonded length was assumed to be satisfactory.

As stated by Barley (2005) to determine the ultimate or pullout load, larger displacement than those calculated using the criteria given by Briaud et al. (1998). Liu et al. (2017) presented the results of complete pullout tests in a slightly weathered limestone. The results of two of the anchors tested by Liu et al. are shown in Fig. 3-7 as A1, B1 and C1. In order to compare the results, these tests were normalized with respect to the maximum applied load (P_{max}) and the diameter of the anchor (D). Additionally the second failure criteria proposed by Briaud et al. (1998) is presented in the figure.

Based on the obtained results from the PT2 and results from Liu et al. (2017), it is suggested to define the ultimate load as the load corresponding to the elastic elongation of the free length plus 1/3 to 1/6 the diameter (D) of the anchor. The proposed range of evaluation of the ultimate load is shown also in Fig. 3-7; this range is considered appropriate because more mobilization of shear strength can be accepted. Based on Fig. 3-7 the range is still conservative given that maximum observed load was not included. Suggested range was given only for anchors installed in rock formations, in other ground conditions suggestions might not apply.

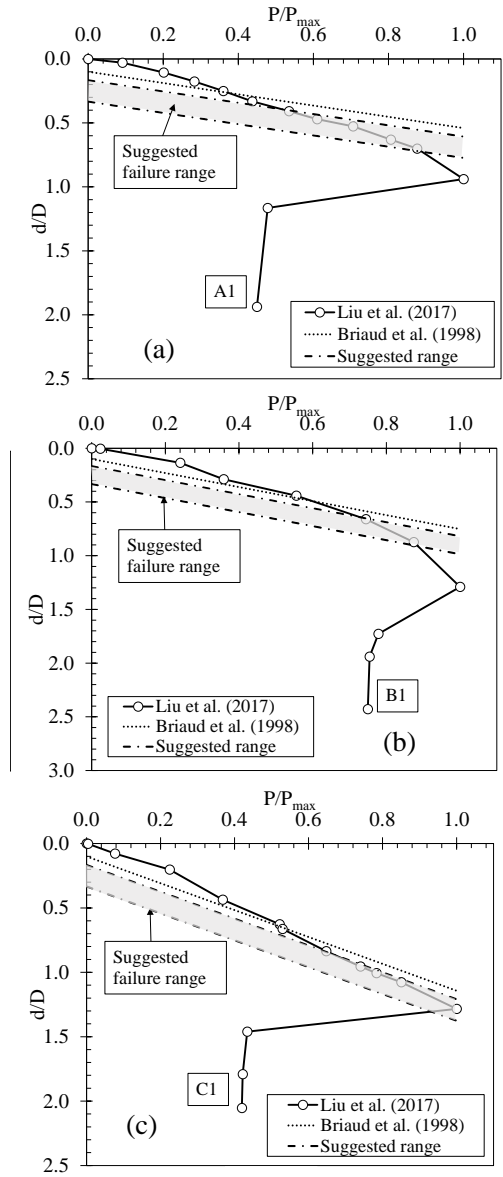


Fig. 3-7. Suggested Ultimate Load Range and Pullout tests: (a) A1; (b) B1 and (C1).

3.3.2 Performance Tests

Performance tests were also conducted at the project site to verify the capacity of the anchors. As with the preproduction tests, these tests were performed in accordance with recommendations given by the Post-Tensioning Institute (PTI) (2014). Results of the performance tests of the anchor installed in Soldier Pile 30 in the middle row (Row B) and lower row (Row C) are presented in Fig. 3-8. In addition, Fig. 3-9 shows the result of the

anchor installed in the middle row of the Soldier Pile 31. The locations of these soldier piles were shown previously in Fig. 2-1.

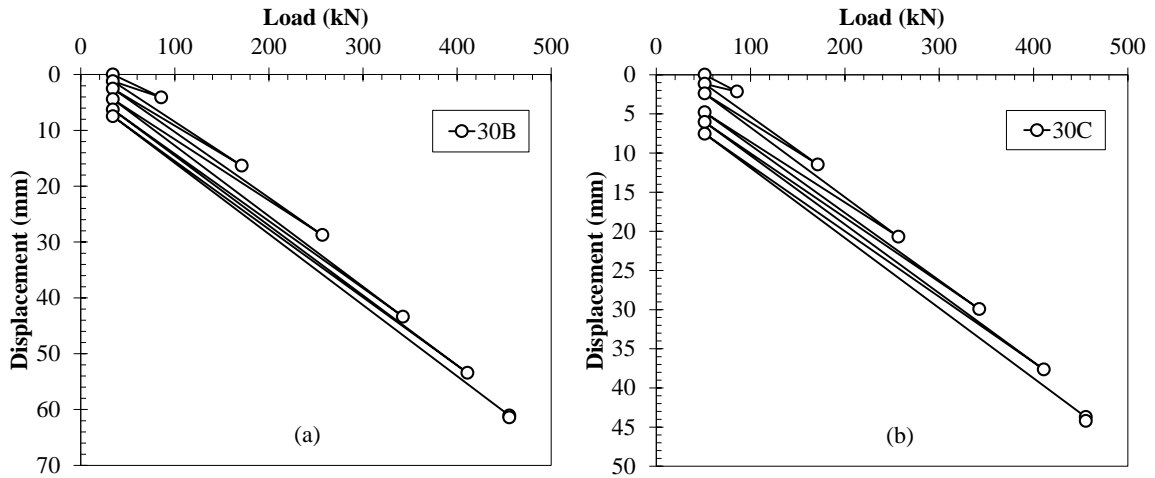


Fig. 3-8. Performance tests in anchors of soldier pile 30: (a) 30B; (b) 30C

The load-displacement response of the three performance tests was similar; maximum displacements were observed in the middle anchors 30B and 31B. Given the same bonded length in all the tests this large displacements in the middle anchors could be attributed to the larger unbonded length with respect to the Row C of anchors.

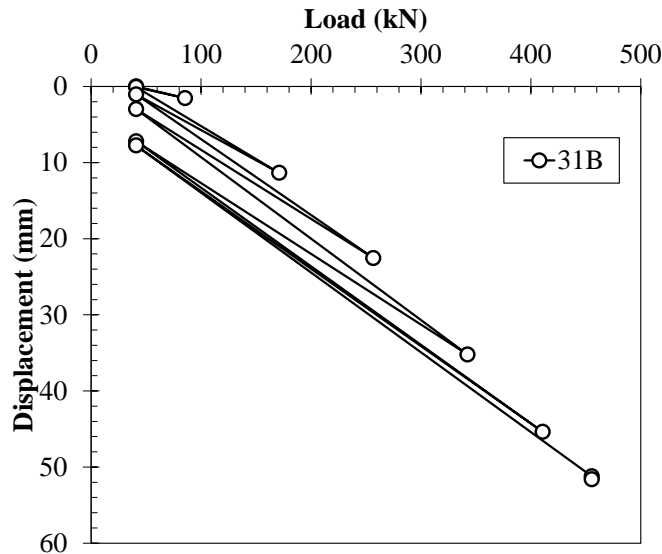


Fig. 3-9 Performance Test in Anchor 31 B

Test load was held ten minutes to investigate the creep characteristics of the anchors according to the Post-tensioning institute procedure. Based on the anchor movements, the

creep acceptability criterion was satisfied; load at the anchor head was consequently reduced to the lock-off load. A rough comparison of the behavior of the bonded length during the three tests can be observed in Fig. 3-10. Residual movement was plotted against the anchor load in the figure. It is noted that the slope of the curves, stiffness of the anchors, was quite similar suggesting that the anchors were successfully installed in the same shale stratum and indicating a similar stress strain response in the bonded length of the anchors.

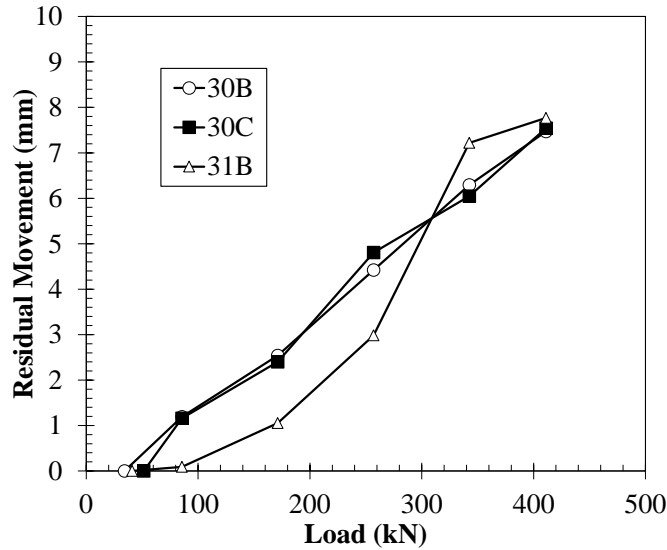


Fig. 3-10 Residual Movement versus Load

3.4 Analytical Model

Based on the results of several pullout test from different authors (Hsu and Chang 2007; Liu et al. 2017), it is observed that during pullout of ground anchors some degree of softening is manifested in the load displacement response. Consequently, analytical models considering softening will be use to analyze the results of the test in the SUM82 project. Although the unbonded length of the anchors is also grouted, it is assumed that load is only transfer in the bonded length of the anchors. Therefore, the load at the top of the bonded length is equal to load at the top of the anchor head.

Considering equilibrium of the segment of length dx shown in Fig. 3-11.

$$\frac{dP(x)}{dx} = 2\pi r_a \tau(x) \quad (2)$$

where $P(x)$ = axial load along the anchor; r_a = is the radius of the anchor and $\tau(x)$ = shear stress along the anchor bonded length. The relation between the axial strain and the axial load can be expressed as:

$$\varepsilon(x) = \frac{dw(x)}{dx} = \frac{P(x)}{AE} \quad (3)$$

where w = displacement at a distance x measured from the bottom of the anchor; A = cross-sectional area of the bonded length E = Elastic modulus of the anchor, which can be calculated based on a composite section.

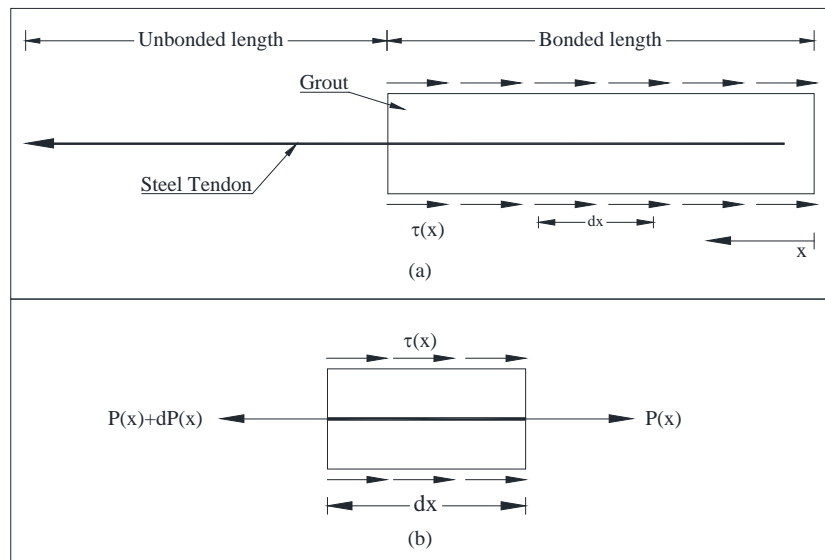


Fig. 3-11. Analytical Model of Ground Anchors: (a) Ground anchor; (b) Stress conditions on a differential element

Now, by taking the derivative of equation (3) and replacing into (2); the basic governing equations for the ground-anchor interaction can be expressed as:

$$\frac{d^2w(x)}{dx^2} = \frac{2\pi r_a}{AE} \tau(w) \quad (4)$$

Equation (4) can be solve using the common t-z technique. In order to solve equation (4) two softening models were considered for the side resistance τ and the relative displacement w .

3.4.1 Softening Model 1.

Zhang and Zhang (2012) proposed a softening model based on three parameters a , b and c . The relationship between the skin friction and relative displacement is given by equation (5)

$$\tau(x) = \frac{w(x)(a + c \cdot w(x))}{(a + b \cdot w(x))^2} \quad (5)$$

The three parameters a , b , and c are expressed as

$$a = \frac{\beta_s - 1 + \sqrt{1 - \beta_s}}{2 \cdot \beta_s} \cdot \frac{w_u}{\tau_u} \quad (5a)$$

$$b = \frac{1 - \sqrt{1 - \beta_s}}{2 \cdot \beta_s} \cdot \frac{1}{\tau_u} \quad (5b)$$

$$c = \frac{2 - \beta_s - 2\sqrt{1 - \beta_s}}{4 \cdot \beta_s} \cdot \frac{1}{\tau_u} \quad (5c)$$

where τ_u = limiting unit skin friction; β_s = ratio between residual skin friction and ultimate skin friction and w_u = relative displacement at limiting friction. Additionally, the reciprocal value of a corresponds to the initial slope, $\lambda = 1/a$, of $\tau(x)$. Oda et al. (1997) proposed that λ can be estimated using equations (5) and (6)

$$\lambda = \frac{\lambda_r \cdot \lambda_g}{\lambda_r + \lambda_g} \quad (6)$$

where λ_r = shear stiffness of the rock and λ_g = shear stiffness of the grout. The parameter λ_g is calculated as

$$\lambda_g = \frac{G}{r_a \cdot \ln\left(1 + \frac{r_a - r_b}{r_b}\right)} \quad (7)$$

where G = shear modulus of the grout; r_a = radius of the grout and r_b = radius of the tendon assembly. In this case where the initial slope is calculated, the value of w_u will be

$$w_u = \frac{a}{b-2c} \quad (8)$$

Consequently, for this model in ground anchors either the value of w_u can be assumed or the initial slope can be estimated based on equations (6) and (7). According to Liu et al. (2017) the shear stiffness of rock vary from 1.5 to 3 GPa/m for soft rock and from 5 to 10 GPa/m for stiff rock.

3.4.2 Softening Model 2

More recently Ni et al. (2017) introduced a softening relationship based on a single parameter, n ($n \geq 0$), to describe the variation of the skin friction with the relative displacement as.

$$\tau(x) = \tau_u \left[(n+1) \left(\frac{w(x)}{w_u} \right)^{n+1} - n \left(\frac{w(x)}{w_u} \right) \right] \quad (9)$$

for $w(x) \leq 2w_u$. For values of $w(x) > 2w_u$, the value of τ at w_u is used. Based on a given ratio β_s between the range 0.65-0.90; the parameter n to use in equation (9) can be approximated as

$$n \approx 0.16\beta_s^{-9.11} \quad (10)$$

Fig. 15 presents both softening models presented above. It can be seen that for the same ratio β_s , the model (1) decreases gradually after the maximum skin friction is achieved. On the other hand, model (2) presents an abrupt change in the load-transfer curve when the relative displacement $w = 2w_u$.

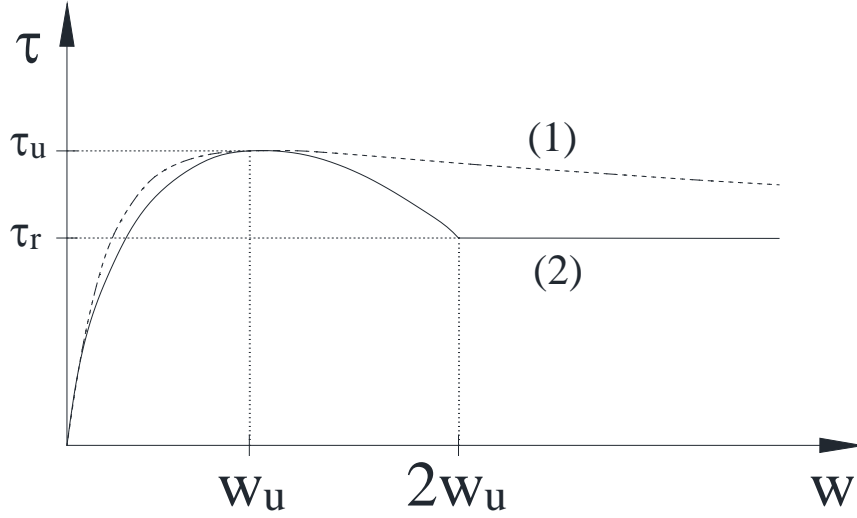


Fig. 3-12. Load Transfer Models Considered

3.4.3 Algorithm for the Load Transfer Approach

A load-displacement curve for an anchor can be estimated using the t-z approach (Coyle and Reese 1966; Knellwolf et al. 2011), calculations can be easily adapted to a spreadsheet. Considering the segment n shown in Fig. 3-11, the displacement at the middle of the segment is giving by:

$$w_{mn} = w_{bn} + \delta_{en} \quad (11)$$

where w_{bn} and w_{mn} = displacements at the bottom and middle of the segment, respectively; δ_{en} = elongation of the half segment. Assuming an average load in the middle segment, δ_{en} is expressed as:

$$\delta_{en} = \left(\frac{P_{bn} + P_{mn}}{2} \right) \cdot \frac{dl/2}{AE} \quad (12)$$

Now, considering equilibrium of the segment

$$P_{mn} = P_{bn} + \frac{dl\pi D}{2} \tau(w_{mn}) \quad (13)$$

where D = diameter of the anchor and $\tau(w_{mn})$ = mobilized skin friction. Replacing equations (12) and (13) into (11), it gives:

$$w_{mn} - w_{bn} - \left(P_{bn} + \frac{dl\pi D}{2} \tau(w_{mn}) \right) \frac{dl/2}{AE} = 0 \quad (14)$$

For a known value of w_{bn} , w_{mn} can be calculated iteratively from equation (14) for a given tolerance. Fig. 3-13 presents a flowchart with the necessary steps to obtain the Load-displacement curve.

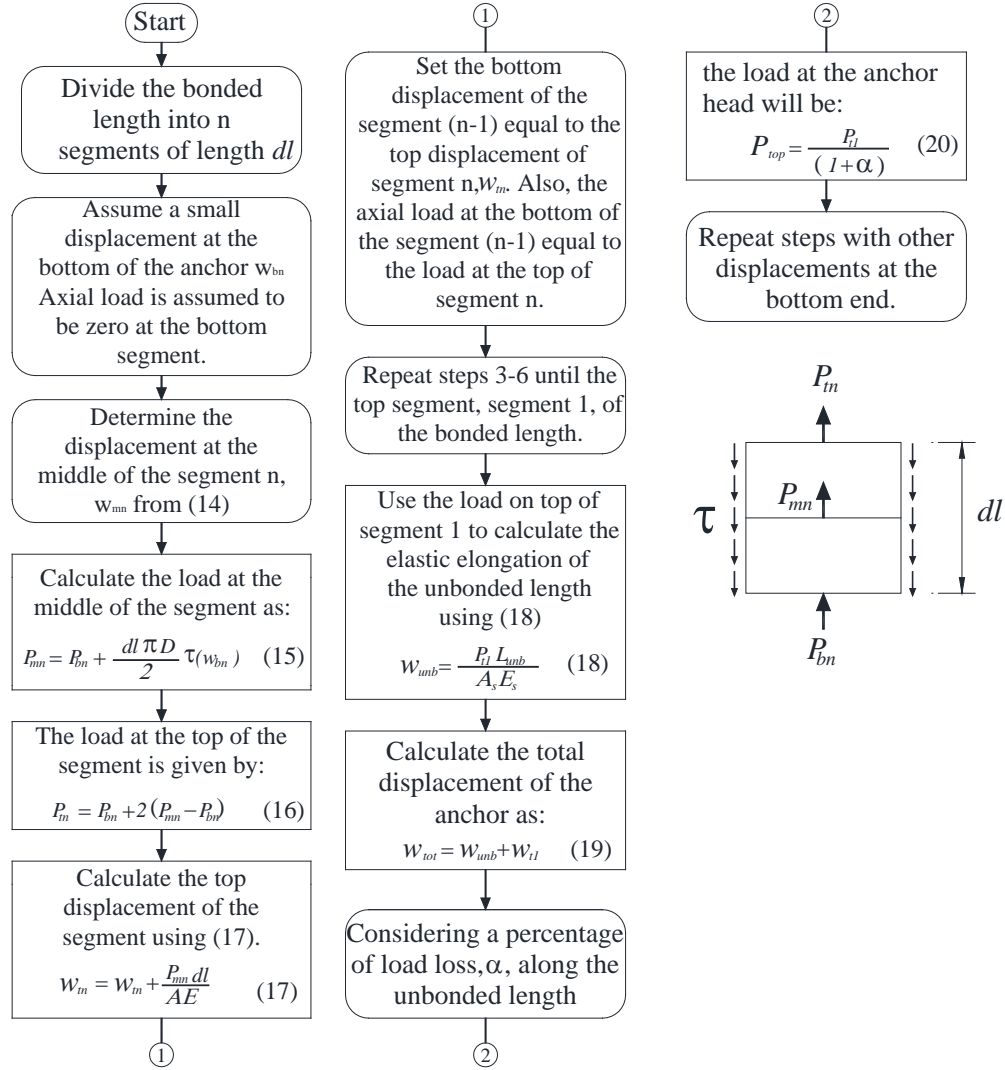


Fig. 3-13. Flow chart describing the t-z approach algorithm

3.5 Analysis and Results

3.5.1 Preproduction Tests

Load-displacement curves for the preproduction and performance tests were determined using the aforementioned procedure. Table 3 presents the input parameters used in the analysis. The ultimate side frictional resistance was limited to 1400 kPa based on the average ultimate bond stress presented by Sabatini et al. (1999) for shales also given in

Xanthakos (1991). However, notice that the ultimate fictional resistance is likely to be greater than the assumed value given that those values reported are average values. Nevertheless, complete pullout was not reached during the tests and only a portion of the load-displacement curve was compared.

Table 3-2 Input Parameters for the Analysis of the Production Test.

| | |
|-----------|----------|
| β_s | 0.7 |
| τ_u | 1400 kPa |
| w_u | 2.5 mm |
| n | 4.12 |
| E_s | 200 GPa |
| E_g | 23GPa |

Load-transfer relationship at the anchor-rock interface is presented in Fig. 3-14 for the two models adopted for the calculations. The value of n in the model 2 was selected based on a β_s value of 0.7 based on results of Liu et al. (2017) which showed considerable softening in the anchor response.

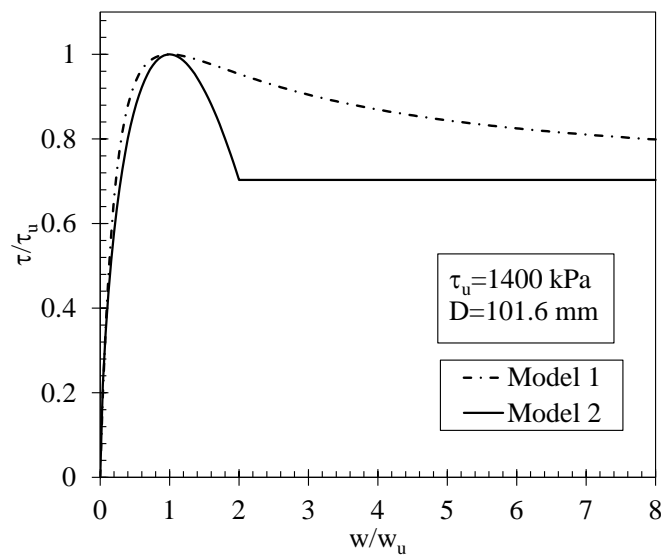


Fig. 3-14. Load transfer models used in the analysis of the preproduction test

Estimated response for the preproduction test 2 is shown in Fig. 3-15. As can be seen the calculated response is similar to the measured during the test. Both models accurately predicted the measured part of the preproduction test. The calculated curves were extrapolated to obtain a representation after the peak load.

As the preproduction test did not reached complete pullout, load-displacement measurements during the test did not display any non-linear behavior, which might develop under ultimate load conditions including any softening. It has to be noted that the predicted response did not consider any cycles of loading during the test; therefore, any progressive degradation of the ground-anchor interface.

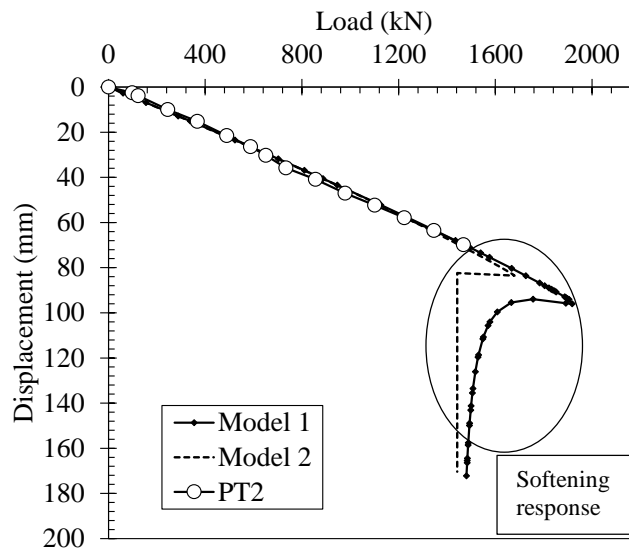


Fig. 3-15. Measured and Calculated Response for the PT2

3.5.2 Performance Tests

For these anchors the minimum requirement unbonded length is presented in Table 3-1 base on Liang (2000) report; actual values of the installed unbonded length for these ground anchors were not reported. Given that the ground anchors were installed according to the recommendations of the Post Tensioning Institute (PTI); the unbonded length can be estimated based on acceptance of the minimum apparent free tendon length criterion. Estimated values of the unbonded length for the anchors 30B, 30C and 31B are 12 m, 9 m and 12 m, respectively.

Calculated load displacement responses for the performance test conducted in the anchors 30B, 30C and 31B are shown in Fig. 3-16 using a friction of $\alpha = 0.05$ in the unbonded length of the anchors. As seen from the figure, results show a satisfactory agreement with the measured response; however, because the applied loads are likely to be far from ultimate load, most displacement observed was corresponding to the elongation of the free length of the anchors. From Fig. 3-16 (a) and (c), it can be observed that the measured response is stiffer than the estimated; this difference may be attributed to more friction developed along the unbonded length of the anchors.

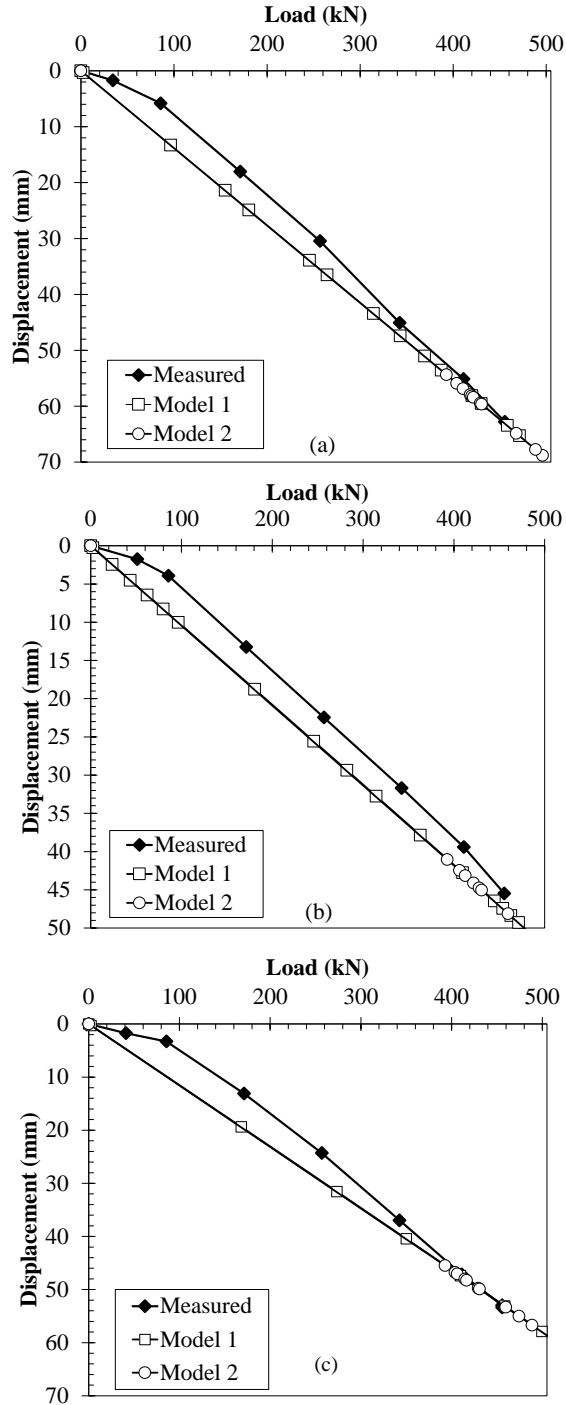


Fig. 3-16. Load-displacement Response for Performance Test in anchors: (a) 30B; (b) 30C; (c) 31B

Because load is transfer from the top of the bonded length towards the bottom, under small load the bottom of the bonded length might not experience any movement; however, to approximate the response used in the presented algorithm, a small value of bottom displacement has to be assumed.

Parametric analyses were conducted to determine the relative implication of the input parameters used in both models. The following anchor characteristics were constant for the analyses: $l_{bon}=5\text{ m}$; $l_{unb}=10\text{ m}$; $d=0.10\text{ m}$; $A_s=4.2 \cdot 10^{-4}\text{ m}^2$ and $E_s = 200\text{ GPa}$. For the first model, results of the analysis varying the ratio β and the displacement to the ultimate load z_u are presented in Fig. 3-17 and Fig. 3-18.

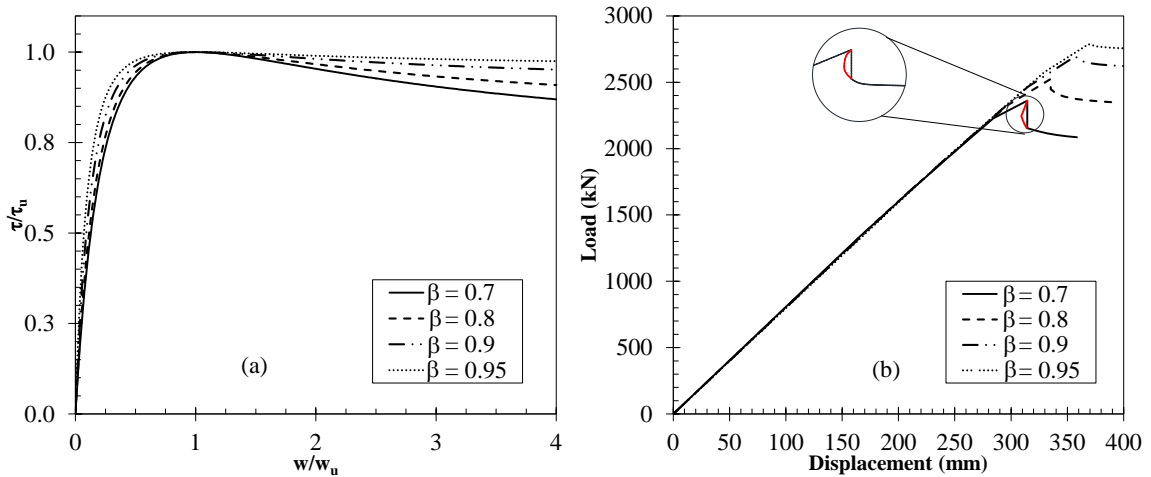


Fig. 3-17. Model 1 Effect of β on the response: (a) load transfer curve; (b) load displacement response

As seen in Fig. 3-17, variation of the parameter β has a noticeable impact in the load deformation curve. As expected, a lower value of β results in a lower ultimate load for the anchors. Also, as β increases the displacement, the displacement at the maximum load increases continuously. The most adequate form to obtain β can be from pullout load tests at construction site.

Because the t-z approach presented here is only valid for monotonic loadings, under certain values of β , as $\beta = 0.7$, the method will result in a decrease in load and displacement for a given bottom displacement. This behavior is physically inadmissible; therefore, the red portion of the curve, shown in Fig. 3-17, was disregarded. Similar behavior was discussed by Ren et al. (2010) and Blanco (2012).

Fig. 3-18 presents the results of load displacement when the displacement at maximum skin friction is varied; for this parameter Kim et al. (2007) assumed a value of 2.5 mm also Liu et al. (2017) obtain values of 1.5 mm and 1.8 mm. From Fig. 3-18, it is seen that

there is minor variation in the maximum load at the anchor head. Only 3.4 percent variation in the maximum load was observed in the range of selected values; consequently the maximum load depends mostly on the ultimate value of the skin friction τ_u and the degree of softening represented by β .

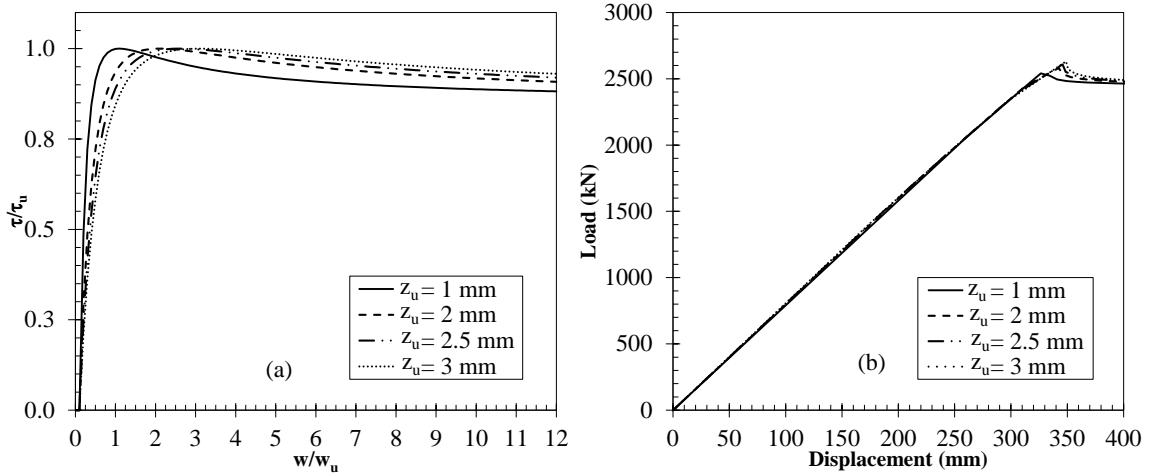


Fig. 3-18. Model 1 Effect of z_u on the load-displacement response: (a) Load transfer curve; (b) Load displacement response

For the softening model 2, Fig. 3-19 shows the results of varying the parameter n . As seen, the variation of the response is analogous to the model 1 when the parameter β ; however, results of this model tend to show the same aspect of load and displacement reduction. This tendency is related with the shape of the load transfer curve; as seen in Fig. 3-12 after the maximum skin friction is reached, model 1 presents a more gentle variation for the mobilized skin friction for an equal value of β .

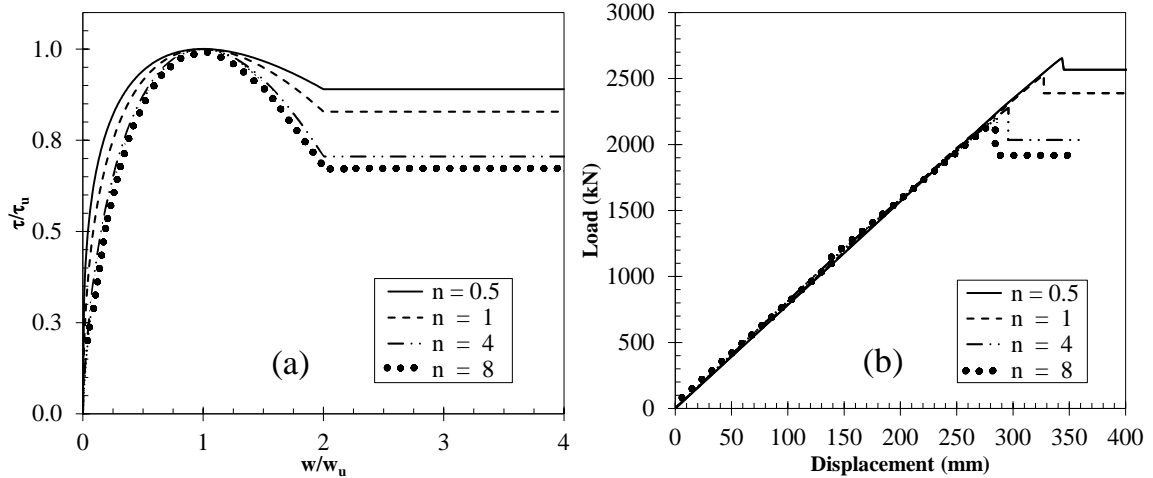


Fig. 3-19. Model 2 Effect of n on the load-displacement response: (a) Load transfer curve; (b) Load displacement response

It can be seen from Fig. 3-17 and Fig. 3-19 that the anchor response is almost linear until the maximum load is reached, this behavior is a consequence of the elongation of the unbonded length which is significantly greater than the movement and elongation of the bonded length. After the ultimate load is reached, a sudden drop in the load is observed to a residual value where the displacement increases and the load remains constant.

3.6 Strain Gages Monitoring for Short and Long-term

Evaluation of the load-transfer mechanism along the bonded length was conducted in anchor 31B through strain gages. Monitoring was conducted using vibrating wire strain gages along the bonded length of the anchors. Gages were installed at 0.9 m, 2.1 m and 3.4 m from top of the bonded length as shown in Fig. 2-7. Changes in deformation were observed during performance tests and after the tests for a period of 185 days considered herein as the long-term analysis. Strain gages were mounted to the strand and wrapped around to protect them during grout installation.

Strains measured along the bonded length of anchor 31B during the performance test are presented in Fig. 3-20. The figure also includes the cracking strain of the concrete grout that was assumed to occur around 100 microstrains Neville (1996). Initially, under small loads tensile strains in the grout and the steel strands were compatible. After increasing the load, the tensile strains in the steel strands exceeded the cracking strain of the grout, as shown in Fig. 3-20. As soon as the cracking strain was surpassed, debonding between the

strand tendon and the grout was observed with the negative strains measured along the bond length (Benmokrane et al., 1995; Weerasinghe and Littlejohn, 1997; Krothapalli, 2013)

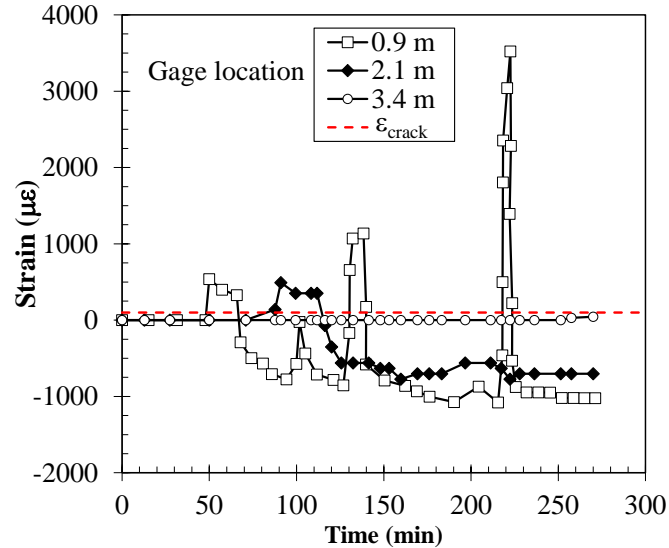


Fig. 3-20. Bonded Length Deformation of anchor 31B during performance test

From the strains measured in the bonded length, axial load were estimated using the axial stiffness of the strands and assuming that the measured strain was equal for all the strands of the anchor. Fig. 3-21 shows the estimated loads along the bonded length. Load was first registered in the top gage; then with the applied load increasing, some tensile load was observed in the second gage installed at 2.1 m from the top of the bonded length. Load variation observed in these gages was similar during the test; initially, it was observed tension and later compression in the gage.

However, the estimated loads in the lowermost gage were almost zero, suggesting that the applied load was distributed, at most, in the top 3.4 m of the bonded length. Similar behavior has been previously reported by other authors (Ostermayer and Scheele 1978; Ludwig 1984). Strain distribution at the end of the test confirms that the bonded length was adequate for the anchors installed in the shale stratum and slippage did not occur at the lowest gage location.

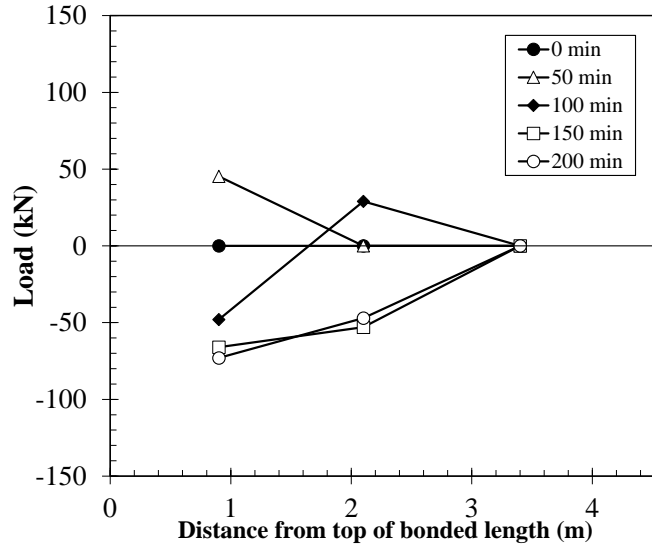


Fig. 3-21. Estimated Load during Performance Test

Long-term performance of ground anchors must be considered in order to guarantee the stability of the structure retained (Benmokrane and Ballivy 1991). Long-term monitoring of strains in the bonded length after locking-off is presented in Fig. 3-22. From the figure it is observed that between Construction Days 155 and 190, there was a gradually redistribution of load along the bonded length with changes observed in all the strain gages.

This redistribution corresponds to the backfilling of the upper wall, gages installed at 0.9 m and 2.1 m from the top of the bonded length showed a decrease in the measured strains, meaning that more relative displacement between the tendons and the grout occurred during this period. In addition, strain measured in the gage located at 3.4 m from top of the bonded length slightly surpassed the assumed cracking strain of the grout. However, as seen from the Fig. 3-22 the strain remain positive indicating that not debonding at the strand/grout interface occurred at this location.

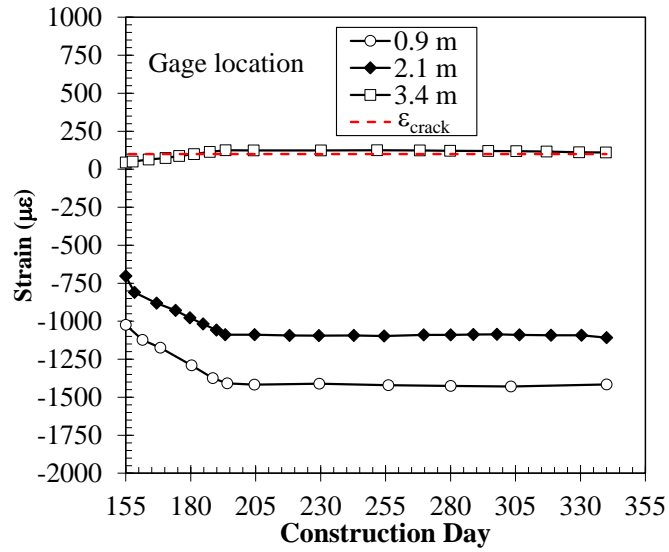


Fig. 3-22. Long-term Monitoring of Anchor Bonded Length

It was observed that after 40 days of the anchors testing, about the time where construction of the walls was almost finished, the anchors reached a state of equilibrium. As shown in Fig. 3-22 the measured strains remained constant after the construction of both walls was finished.

4 Lateral Movements and Pore Water Variation

4.1 Introduction

Landslides impose serious hazard to transportation facilities; stability of natural and cut slopes represents a challenge to construction and operation of these facilities. (Wei et al. 2012). Slope failure results in significant costs associated with reparation and maintenance of roadways and related structures. Retaining structures are used to stabilize landslides and to control ground movements; among these structures, tieback walls are common solutions for permanent slope remediation (Adekunte et al. 2007; Han et al. 2017). Soldier pile and lagging walls are often used due to economic and speedy construction advantages (Lee et al. 2011; Sáez et al. 2015; Urbański and Michalski 2016). Additionally, current corrosion protection techniques and fewer disruptions to traffic during construction make anchored walls a feasible option for effective slide stabilization.

Wall construction imposes significant changes in ground state of stresses and strains; this soil-structure interaction is reflected in complicated relationships between construction sequence and ground response. For anchored soldier pile walls, several studies have been conducted to analyze the behavior during excavations including model and full-scale tests (Briaud et al. 1998; Mueller et al. 1998; Weatherby et al. 1998; Briaud and Lim 1999; Seo et al. 1999). More recently, landslides with retention systems of soldier pile walls (Macciotta et al. 2017; Carlà et al. 2018); these studies revealed the complicated interaction between wall construction and ground response.

The pattern of wall and ground deformations during a typical top-down construction has been of interest to engineers in order to protect surrounding infrastructure. Methods to predict the lateral and settlement profiles have been proposed (Hsieh and Ou 1998; Kung et al. 2007). However, none of these is refer to bottom-up construction; most of these studies imply excavation and they did not consider backfilling behind the retaining structure as part of the construction sequence. Additionally, in order to guarantee safety of adjacent structures to retaining walls; it is necessary to monitor ground and wall responses.

This paper presents the results of a monitoring program during the construction of two tiebacks walls as slope remediation solution. Results are expected to extend the

understanding of the ground response during the construction of tieback walls in a marginally stable slope using a bottom-up technique. Monitoring results during and after construction are presented. Observed ground and wall movements are related with the construction activities to determine the influence of these in the observed performance of the walls and pattern of ground deformation.

4.2 Analysis and Results

Performance of the walls and response of the slope to construction activities is presented in this chapter. Instrumentation techniques and elements were presented in previous chapters.

4.2.1 Ground Inclinerometers

Fig. 4-1 presents the ground movements observed in the downslope direction. Data in the inclinometer 1 was collected until Day 154; after this day, the inclinometer casing was damaged. Based on the construction sequence, at Day 41 the observed ground movements were due to the installation of the soldier piles in the upper wall. Maximum ground displacement until this day was about 35 mm; this maximum was observed in the inclinometer 3 while the other two inclinometers show minor displacements below 5 mm.

This discrepancy in the order of magnitude of ground movements can be attributed to the location of the haul road to the project. Major excavations and ground disturbance were generated during installation of the piles in the area adjacent to the inclinometer 3. It is observed that the lateral deformation of the slope was confined to the upper 5m of the profile; maximum displacement was observed at ground level.

Since Day 41 until Day 51 during installation of the soldier piles for the lower wall, ground movements showed and slight variation as can be seen in the values corresponding to Day 48. Opposite to the behavior observed in the upper wall, soldier pile installation in the lower wall did not affect the ground state.

After soldier pile installation, two failure tests were conducted. During the failure tests in the upper and lower area, minor variation of ground movements was observed in inclinometer 1 and 2 between Days 48 and 63 (Fig. 4-1). However, ground inclinometer 3

measured a maximum increased in the lateral deformation of 19 mm. Construction proceeds with the installation of the steel struts for the middle row of anchors in the upper wall; this activity was finished around Day 84. During this activity, maximum lateral displacement was around 100 mm in the inclinometer 3; inclinometer 2 showed 20 mm of displacement that was only one-fifth of inclinometer 3. Ground displacement variation in the inclinometer 1 was negligible in comparison with the other two inclinometers; however, these movements extended deeper into the ground.

Since Day 84 anchor installation in the middle row proceeded until Day 97; thereafter, anchors were tensioned until Day 106. From that day until Day 115, drill mast was moved to the lower wall to install its lower row of anchors. Simultaneously to the installation of these anchors, ground was excavated in front of the upper wall to install the lower row of anchors (Row C). Temporary wood lagging was used during the excavation. After these activities until Day 120, the same pattern of movement observed in previous days was measured; inclinometer 3 showed a maximum deformation of 133 mm. Although movements increased in the three inclinometers, these tended to concentrate in the upper portion of soil profile.

Although several activities were taking place between Day 84 and Day 120, it is believed, that ground movements were mostly correlation to the activities in the upper wall; lower wall activities were considered as poor correlated. This based on previous inclinometer readings in the slope. During the period of Day 120 until Day 208, the installation of all the anchors and the backfilling activities were finished in both walls. During this period, maximum variation of the ground displacement was about 25 mm. From Fig. 4-1 it is observed that as the construction activities progress, extend of lateral deformation reduces from an initial value of 7 m to approximately 5 m.

After completion of project until the last day of measurements, Day 310, the maximum variation in the ground movements was 55 mm. Inclinometer 2 did not exhibit a significant variation in the measured deformation; in the inclinometer 3 the extends of ground displacement decreases continuously until the last measurement. Based on the rate of displacement observed, both walls effectively contributed to the stability in the slope;

during the post-construction monitoring lateral deformation was observed only in the upper portion of the soil profile.

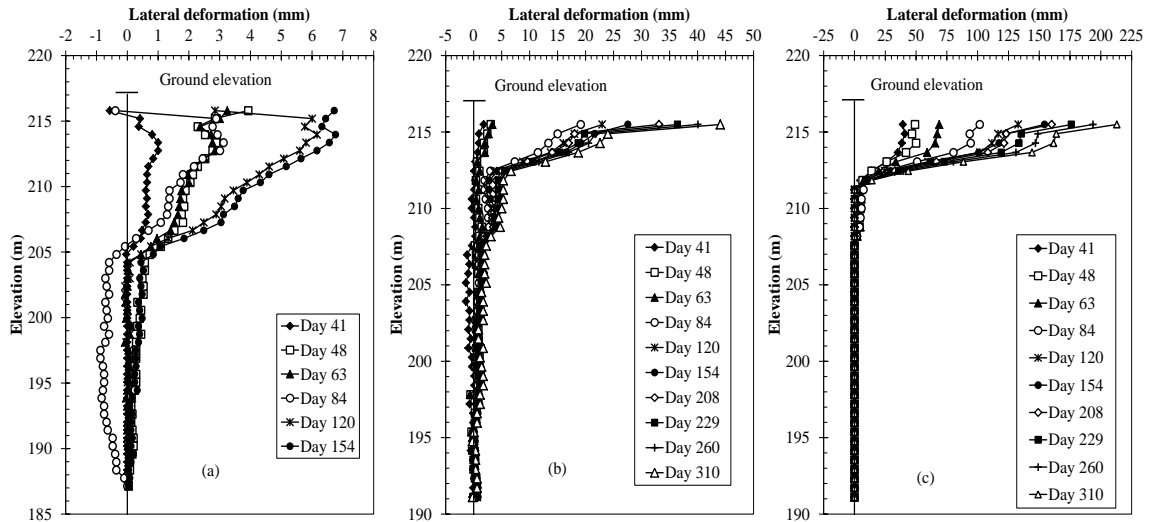


Fig. 4-1. Lateral Deformation Measured in the Slope: (a) Inclinator 1; (b) Inclinator 1 and (c) Inclinator 3

Fig. 4-2 shows the incremental lateral displacement in the inclinometers 2 and 3. Based on the figure deformation was limited over certain depths; ground movement was mostly limited to an interval between elevations 211 m and 215 m approximately. This area was approximately the interface between the brown clayey silt and the gray silty clay deposits. It is observed as well that during all the period of measurement the pattern of deformation was similar; however, after construction of the walls the rate of deformation reduces constantly while keeping the same shape.

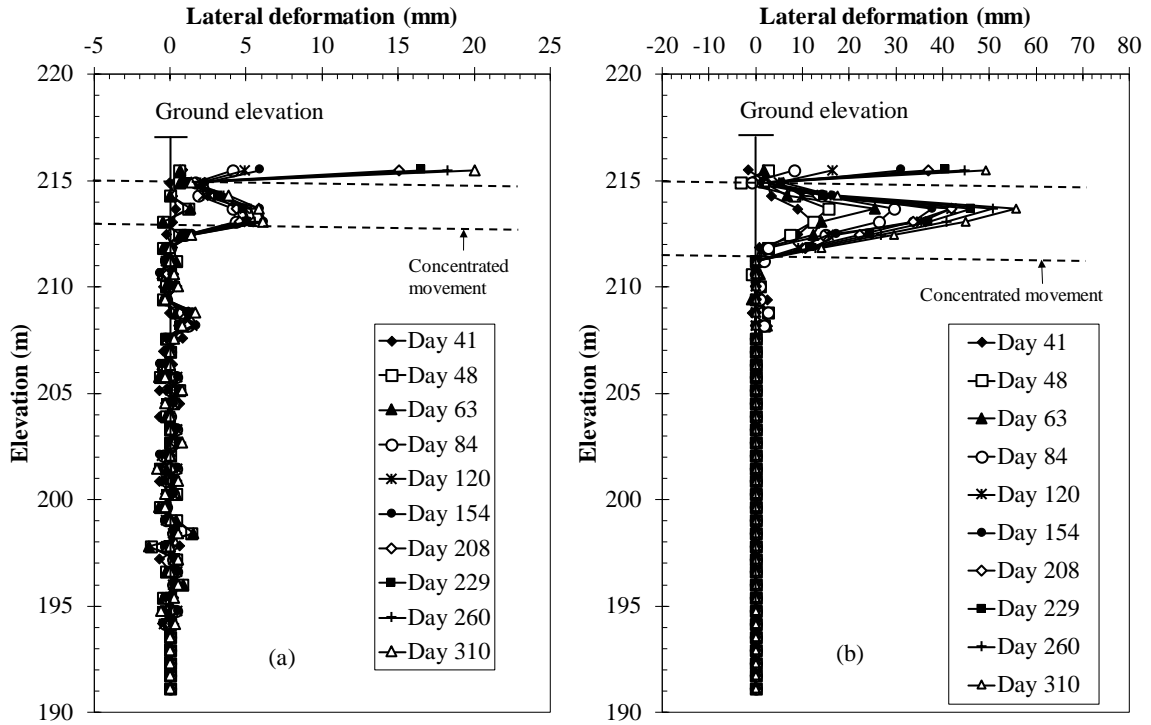


Fig. 4-2. Incremental Lateral Deformation: (a) Inclinator 2; (b) Inclinator 3

4.2.2 Soldier Pile Inclinator

Lateral deformation of the walls and the ground was monitored through inclinometers installed in four soldier piles; location of the soldier piles is presented in Fig. 2-1. Fig. 4-3 presented the observed response in the lower wall; location of the ground anchors is presented in the figure.

At Day 183, upper row of anchor in the lower wall was already installed. During installation of the row A of anchors, backfilling of the wall was at elevation of 200.7 m. Installation of this row of anchors clearly produced a localized effect in the lateral deformation pattern of the wall. As seen in Fig. 4-3a; this installation causes the inclinometer casing to move towards the slope about 5 mm. Fig. 4-3b shows a similar behavior in the soldier pile 12 ; below the upper row of anchors, a bulging profile was observed in both piles. Maximum lateral deformation in the lower wall was near to 3 mm.

At Day 208, lower wall was completely backfilled. During completion of backfilling, the lateral deformation was almost invariant to that measured after installation of the upper anchors; installation of upper anchors successfully reduces ground displacements until the

end of construction. In both piles, the slope response was roughly the same; the bulging profile with the maximum lateral deformation between the anchors was equivalent.

Since the end of construction until the last monitoring day, from Fig. 4-3 slight variation in ground displacements were registered. As seen, both soldier piles exhibited similar behavior below row A; however, soldier pile 12 exhibited a downslope movement of 10 mm on top the pile while in the soldier pile 11 top movement was towards the slope.

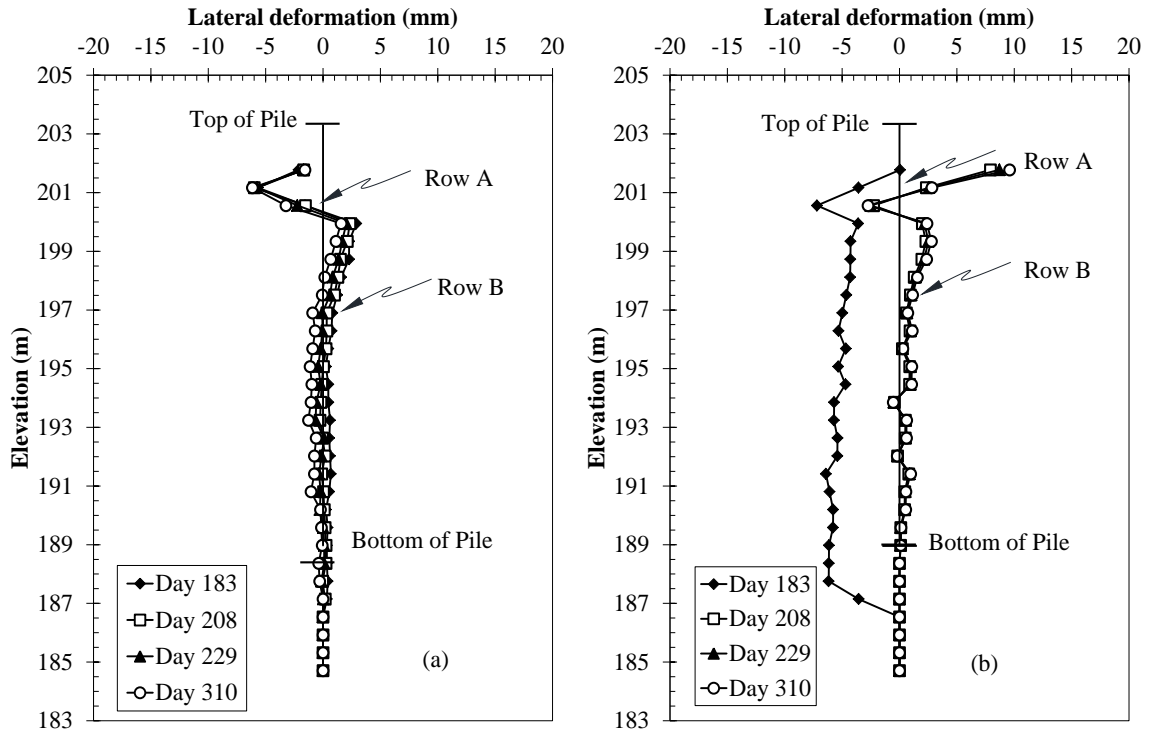


Fig. 4-3. Lateral Deformation Measured in the Lower Wall: (a) Pile 11; (b) Pile 12

Fig. 4-4 presents the measured response in the upper wall. At Day 183, all the rows of anchor were installed in the upper wall; however, backfilling of the wall was incomplete. Installation of the upper row of anchors causes a similar effect that in the lower wall. Inclinometer deformation on top of both soldier piles was towards the slope; this backward movement results from stressing the anchors inn the row A. Below the upper row of anchors, upper wall exhibited a bulging profile with maximum deformations observed between the anchors. Soldier pile 31 registered a maximum displacement of 8 mm while in the pile 30 this value was 4 mm.

At Day 208 construction and backfilling of the upper wall was completed. Post grouting of anchors around this day attenuate the lateral deformation profile in the soldier pile 31 as seen in Fig. 4-4b; soldier pile 30 response was essentially the same as Day 183. Further measurements reported insignificant increase in the wall movement; the observed soil deformation zone was the upper 7 m approximately.

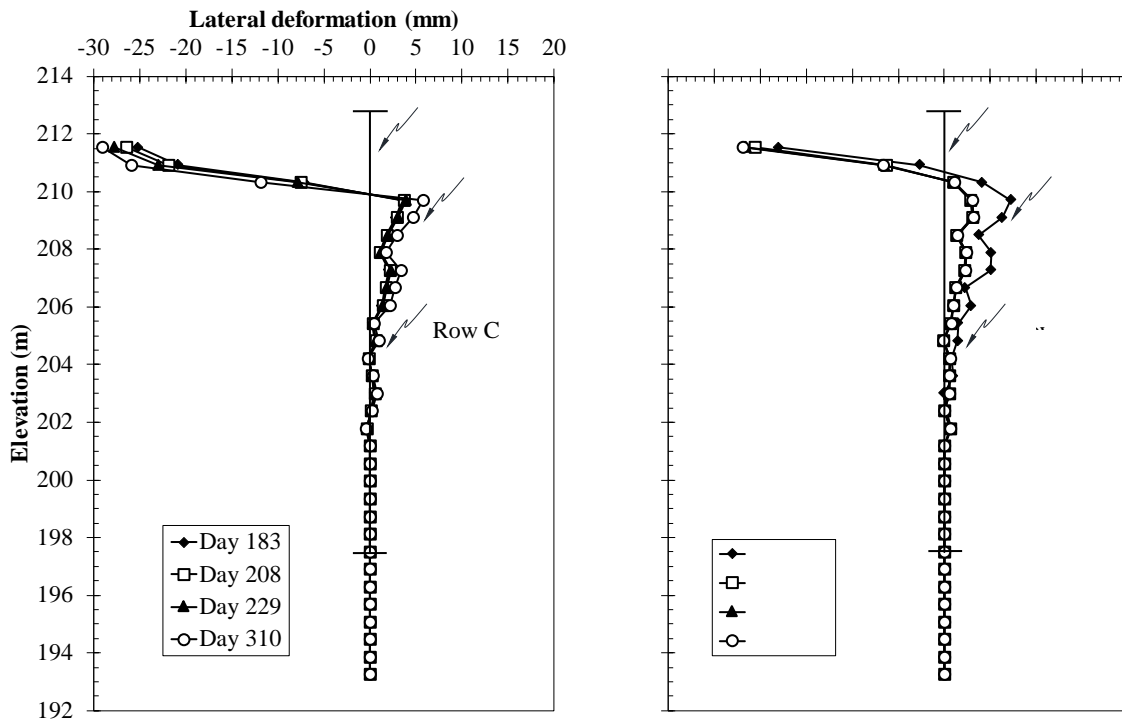


Fig. 4-4. Lateral Deformation Measured in the Upper Wall: (a) Pile 30; (b) Pile 31

Deformation profile at Day 310 confirms that both walls successfully improved the stability in the slope; rate of movement since the end of construction until last monitoring day was almost null. Fig. 4-5 shows the normalized maximum lateral movement in the instrumented piles; also, it is presents the average values reported by Yoo (2001) and Clough and O'Rourke (1990). The height of the excavation was taken as 8.1 m and 7.6 m for the upper and lower wall, respectively. As can be seen in both walls the measured movements are below the average reported by Yoo in H-pile walls and well below to the range given by Clough and O'Rourke.

Although the separation of the soldier piles in the lower wall was greater and the excavated are in from of the upper wall was higher, the level of deformation in both walls was

comparable (Fig. 4-5). The lower values of deformation compared with reported average can also be attributed to the embedded of the toe of the piles in the shale stratum. As reported by other researchers (Long 2001; Yoo 2001; Ma et al. 2010), the presence of bedrock may influence wall deformations; walls in soils overlying rock tend to exhibit smaller lateral movements. Based on Fig. 4-3 and Fig. 4-4, shale stratum effectively support the toe of the piles restraining any lateral movement.

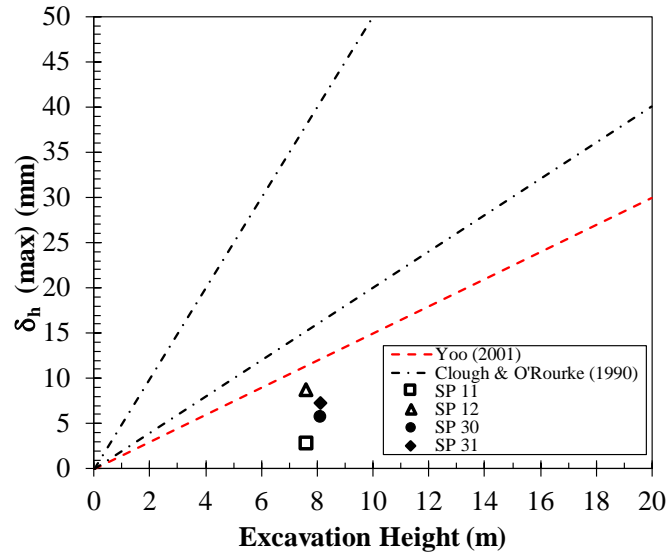


Fig. 4-5. Maximum Lateral Movement Range.

Based on measured movements in the ground and soldier pile inclinometers, the magnitude of the movements measured showed a scarce correlation in the two locations. In the case of inclinometer 1, lateral movement are similar to those in the walls; however, for the other two ground inclinometers the movements registered were remarkably greater than those in the soldier piles. This observation suggests that during construction of backfilled walls, ground disturbance far from the wall location needs to be considered carefully in order to limit damages to adjacent infrastructure. In the case of walls as excavation support systems, the tendency is opposite; typically, the magnitude of lateral movements decrease with increasing distance from the wall.

4.2.3 Pore Water Pressure Response

The vibrating wire piezometer was installed at a depth of 12.8 m from ground elevation (217 m) in the layer where water was encountered. Fig. 4-6 presents the response of the

piezometer since installation at Day 20; as seen, two different responses can be identified and separated at Day 130 approximately. Before Day 130, the drop in the water pressure can be associated to the stress relief during the excavation activities in the slope; that is to say, installation of soldier piles and steel casings in both walls, and row C of anchors in the upper wall.

The other observed response corresponds to a steady increase in the water pressure. After installation of row C in the upper wall, concrete lagging was placed concurrently with the fill behind the wall. The pore water pressure tends to increase while simultaneously the backfill elevation in the upper wall increases. Unfortunately, the piezometer wire was damaged during grading activities in the upper wall area. A maximum increase in the water head of 1.1 m was recorded before the piezometer was dysfunctional; based on the observed response, the change in water head was essentially associated to the construction of the upper wall.

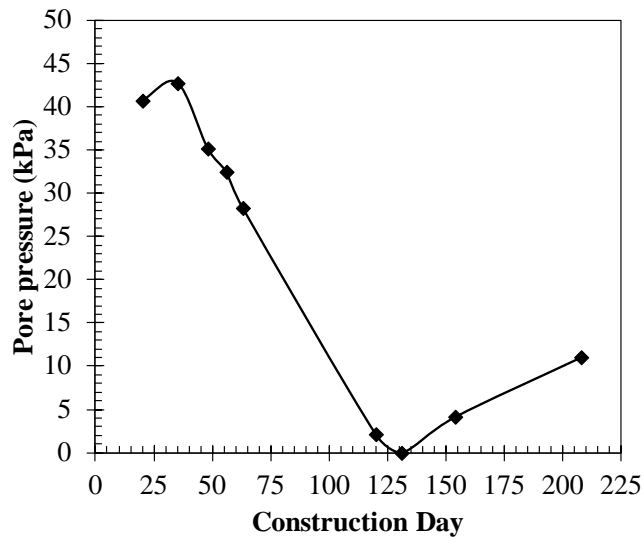


Fig. 4-6. Pore Water Pressure Measurement

5 Analysis of Axial Loads and Bending Moments

5.1 Introduction

Behavior of excavations retaining walls involves a complex interaction of soil and structure. Construction activities impose changes in the in-situ ground stresses; these changes in stress conditions are reflected in thrust acting on the wall and wall deformations. Imposed loads are resisted by wall support systems as anchors or struts, bending of the wall and passive resistance along embedded portion of the wall. Design of retaining walls involves the selection of the lateral pressures acting on the wall compatible with the acceptable level of wall and ground deformation. Typically, at-rest state of stress is prescribed when induced ground movements are critical; otherwise, between active and at-rest conditions are considered where ground deformations are less important.

Apparent earth pressures such as those proposed by Peck (1969), Tschebotarioff (1973), and Sabatini et al. (1999) are commonly used in wall design. Total thrust estimated from these pressures typically range between at-rest and active pressures; therefore, classical earth pressure provide a basis for assessing upper and lower bounds of design lateral thrust (Mueller 2000). When the estimation of deformations is critical to the wall performance, other approaches are used in the design of tieback walls as using finite element methods and beam-column methods.

Commonly, when earth pressures envelopes are used to the design of anchored walls, simplified methods as the tributary area method (Terzaghi and Peck 1967) and hinge method (Lambe et al. 1970) are employed to determine bending moments, anchor loads and embedment depth of the wall.

Measured response of full scale anchored walls have shown that trapezoidal earth pressure envelopes give reasonable predictions of bending moments and anchor loads (Weatherby et al. 1998). However, these findings are the result of a typical top-down excavation sequence; as indicated by Sabatini et al. (1999), during a bottom-up construction sequence, important differences may exist with respect to construction, design, performance of anchored walls.

This chapter presents the analysis and results of the monitoring program conducted in the two walls. Performance of the walls is evaluated in terms of axial loads, bending moments and anchor loads observed during construction and for an extended period after end of construction. Strain gages data was retrieved from the report presented by Liang (2000).

5.2 Data Reduction Process

Fig. 2-6 shows the location of the gages installed in each wall; strain gages were installed by attaching them to end blocks and welding these to the soldier piles. From the strains measured, the bending moment and axial loads in the element were calculated. Fig. 5-1 shows the assumed strain distribution along the piles; the strain distribution was assumed linear and the magnitude of the bending strain proportional to the distance from the neutral axis (Chung and Briaud 1993; Weatherby et al. 1998).

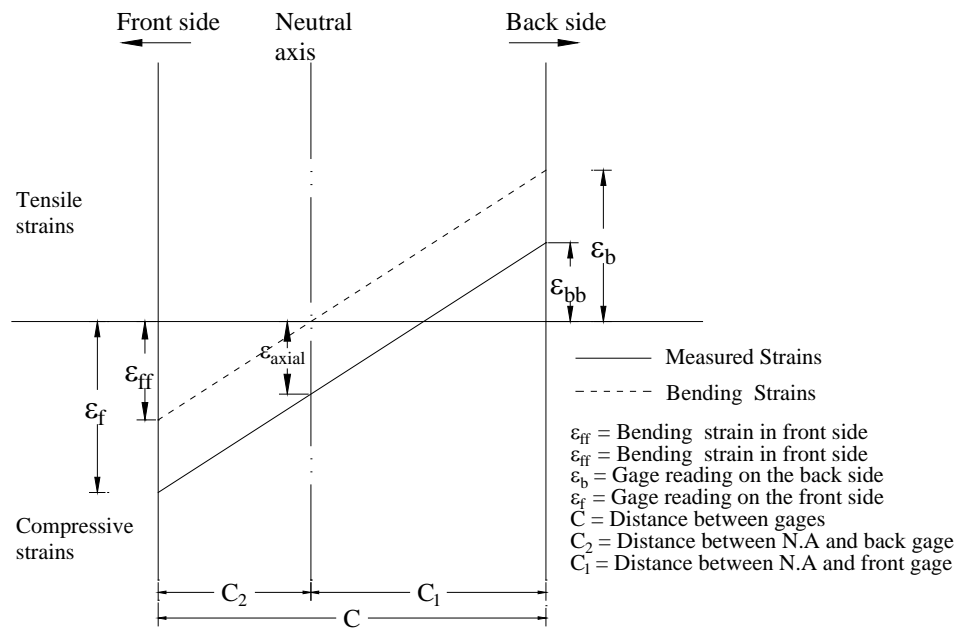


Fig. 5-1. Assumed Distribution of Strains

Based on the symmetry of the section, the neutral axis is align with the centroid of the section; therefore, $C = C_1 = C_2$. The bending and axial strain can be calculated using equations (21) and (22) respectively.

$$\epsilon_{bb} = \frac{\epsilon_b - \epsilon_f}{2} \quad (21)$$

$$\varepsilon_{axial} = \frac{\varepsilon_b + \varepsilon_f}{2} \quad (22)$$

Where ε_{bb} = bending strain and ε_{axial} = axial strain. From elastic theory and using Hooke's law, the bending moment and axial load can be computed with equations (23) and (24)

$$M = \frac{EI}{C_1} \varepsilon_{bb} \quad (23)$$

$$P = A_s E \varepsilon_{axial} \quad (24)$$

Where M = bending moment in the section, P = axial load in the section, A_s = cross-sectional area of the soldier pile and E = Elastic modulus of the steel assumed as 200 GPa.

5.3 Performance of the Wall and Ground Anchors

5.3.1 Bending Moments

Bending moments along the instrumented piles in the lower wall are shown in Fig. 5-2. Day 154 represents the construction state when the upper and lower row of anchors were installed, however, backfilling behind the wall was not complete. Installation of the upper row of anchors in the lower wall caused a negative bending moment in both piles as seen in Fig. 5-2; therefore, during installation process soldier piles bend towards the backfilling material. Upper row of anchors used a steel casing penetrated into the shale stratum to prevent excessive deformation and bending of the piles during anchor installation; based on the magnitude of the upper bending moment, the steel casing was more effective in the soldier pile 12. At the upper strain gage location the bending moment in the soldier pile 11 was almost thirteen times the bending moment induced in the soldier pile number 12.

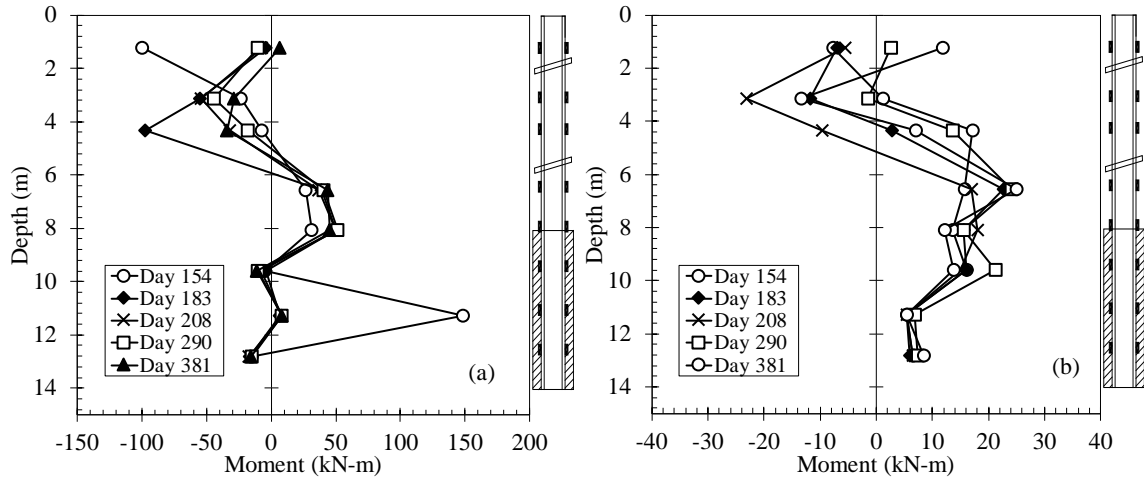


Fig. 5-2. Measured Bending Moments in the Lower Wall: (a) Pile 11. (b) Pile 12

Backfilling activities between days 154 and 183 reduced the moments caused during upper anchor installation in soldier pile 11 as seen in Fig. 5-2(a). In this soldier pile, the bending moment reduces almost to the value of bending moment in soldier pile 12; at pile 12 backfilling activities slightly affect the negative moment above the upper anchor. Decrease in the bending moment observed for the pile 11 was 95 percent from the initial measurement while the moment reduction in the soldier pile 12 was only 12.5 percent. The induced bending moment in the pile 11 during upper anchor installation was counteracted by placing the backfilling.

Backfilling of the wall also increased the positive moment between the Row B and the top of the toe of the piles as seen in Fig. 5-2. Consequently, while backfilling above the Row B, tension was observed in the inner face of the wall. Notice that this portion of the wall was under “cut” conditions where little or no backfill was placed. Measured bending moments distribution showed a disagreement with the distribution reported by Weatherby (2010) in a typical excavation wall with soldier piles; in the latter case, bending moments between the anchors tended to be the same direction that moments between the lower anchor and the toe of the walls

Fig. 5-2 also shows that during post-grouting of the anchors between days 181 and 185 the negative moments between the anchors increase for soldier pile 12; however, for soldier pile 11 during these days negative moments decreased. Positive moments below the lower anchor did not vary significantly.

Between Day 208 and Day 381, bending moments registered above Row B tend to increase; in fact, above the upper row of anchors the bending moment change completely of sign in both soldier piles. Variation in the bending moment distributions reflects the curvature of the wall. Initially, at Day 208, most part of the wall bent towards the slope; however, with time, this tendency was suppressed and most part of the wall had the tendency to bend out of the slope. This behavior was particularly observed in the soldier pile 12 that had almost all the registered bending moments as positive values at Day 381.

Bending moments below the lower anchor remain constant during all the construction process and monitoring period. It seems that the embedded toe of the walls was not affected by the sequence of backfilling and anchor installation in the upper portion of the wall.

It is notable that bending moment distribution observed in the soldier piles of the lower wall was behavior different from the reported by Weatherby et al. (1998) in a full-instrumented soldier pile wall and Mueller et al. (1998) in a model scale test. In fact, measured behavior was similar to the observed by Smethurst and Powrie (2007) in discrete piles used to stabilize a railway embankment and by Cai and Ugai (2003) in case histories studied from flexible piles in landslides. Although the designed capacity of the wall was not exceeded, the use of earth pressure envelopes in the lower wall did not reflect the actual bending moment diagram of the walls.

Fig. 5-3 shows the variation of the bending moments in the soldier piles instrumented in the upper wall. As shown in Fig. 2-5(b) the middle row of anchors was stressed between days 72 and 106; steel pipe casings were used to transfer the load from anchors to the ground without disturbing the soldier piles. However, as seen in Fig. 5-3 at Day 154 negative bending moment developed in soldier piles above the middle row of anchors; the outer face of the piles was in tension and consequently some load was inevitably transferred to the soldier piles. Negative bending moments of 29 kN-m and 4 kN-m were observed in the top gages of soldier pile 30 and 31, respectively.

Lower row of anchors (Row C) was installed between days 115 and 132, steel casings were not used during the installation of these anchors; after installation, backfill was placed to an elevation of 208 m approximately. Under these conditions, Fig. 5-3 shows the bending moment distribution at Day 154. As can be inferred, the effect of backfilling was to increase

the positive bending moment in the soldier piles; that is, tension in the inner face of the wall and curvature out of the slope. This effect was particularly visible below the lower row of anchors.

Posterior backfilling after Day 154 until Day 183 increased the positive bending moments in the piles; positive bending moments increased on average 19 percent below Row C and the toe of the piles. During these days installation and testing of the Row A increased the negative bending moments in the of the wall, as seen in Fig. 5-3, the greatest increase was observed in soldier pile 31 with an increase of approximately 4 times. However, the magnitude of the negative movements was small in comparison with the observed positive values.

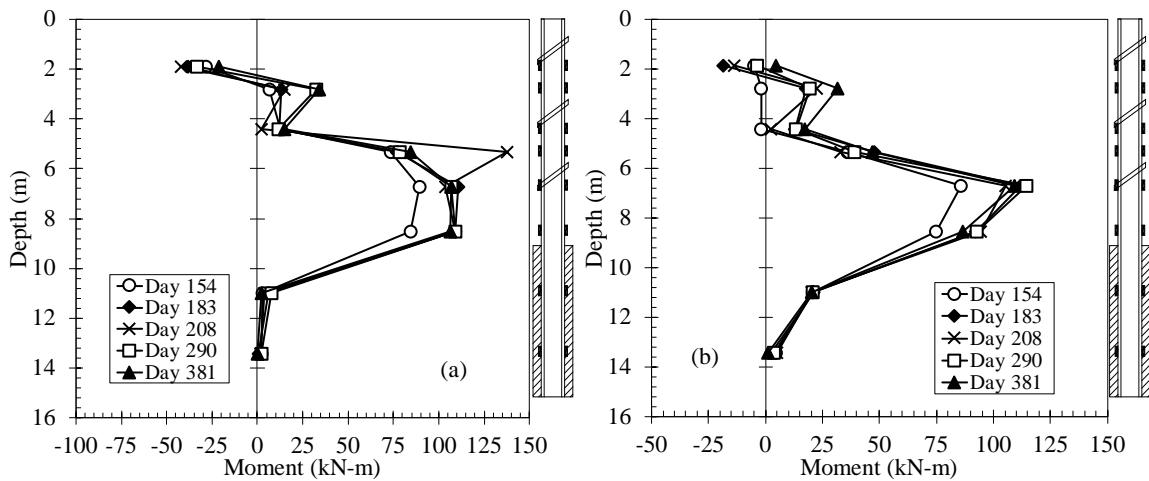


Fig. 5-3 Measured Bending Moments in the Upper Wall: (a) Pile 30. (b) Pile 31

Post grouting of the anchors during days 181 and 185 did not change significantly the distribution of bending moments in the upper wall; between days 183 and 208, a slight decrease in the positive moment and an increase in the negative moment were observed. At Day 208 when the construction was finished and the final graded was established the bending moment distribution remained almost constant with respect to Day 183.

At the last day of analysis, Day 381, the distribution of bending moments was almost identical to that observed at the end of construction. However, the tendency observed was an increase in the bending moments. Although soldier pile 30 presented a negative moment in the top gage location; note that for the soldier pile 31 all the bending moments calculated

were positive at this day, basically the soldier pile behave as a “cantilever” element with all the inner side subject to tension.

On the other hand, some negative bending moment was observed on the top gage location in soldier pile 30. Maximum positive moments were similar in both walls, bending moments of 106 kN-m and 109 kN-m were observed in soldier pile 30 and soldier pile 31, respectively. These moments occurred between the lower row of anchors and the toe of the soldier piles.

Fig. 5-4 shows the variation of bending moments at the toe and at the backfilling portion of both walls. Data was taken from soldier pile 11 and 31. As can be observed, the toe of the walls installed in the shale stratum showed a slight variation during the entire project. Nevertheless, above the embedded length of the both walls, the bending moments, also curvature, show a significant variation related to the construction activities.

Notice that the location of the maximum positive moments in both walls was between the lowest row of anchors and the top of wall toes. Considerable variation of bending moments was observed in early stages of construction; as construction progressed, the variation changes in the bending moments was limited.

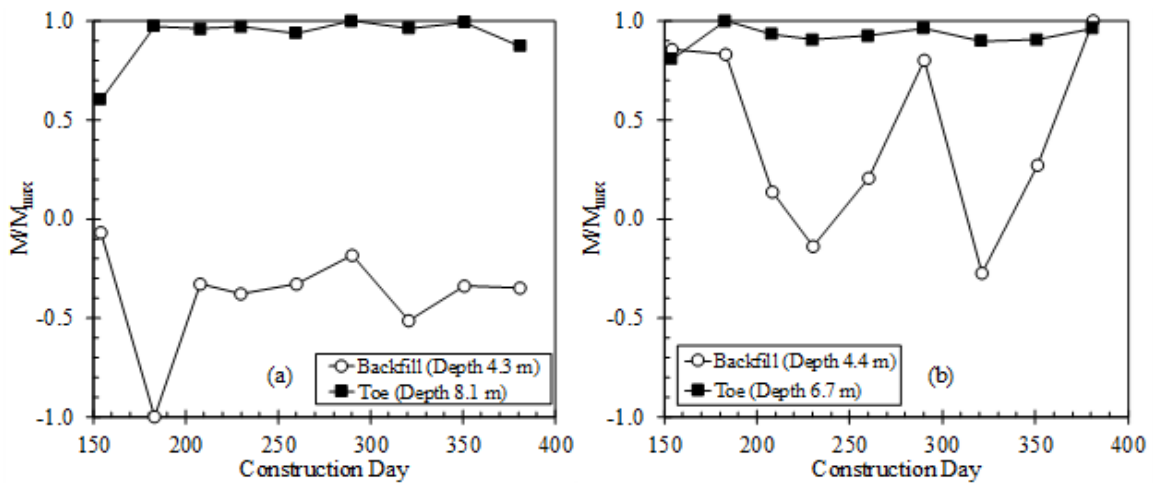


Fig. 5-4. Variation of Bending Moment; (a) Lower wall; (b) Upper wall

The observed performance in both measured walls was different from instrumented full scale test presented by Weatherby et al. (1998); they found that negative bending moments had the tendency to increase and positive bending moments tend to decrease with time.

Measured response of the SUM 82 was distinct. Construction sequence clearly influence the developed of earth pressures which is reflected in bending moments along the wall.

5.3.2 Axial Loads

The required axial capacity of a tieback wall is usually evaluated with consideration only of the vertical loads introduced by tieback prestressing and self-weight. However, additional vertical load can develop due to relative downward movement of the ground with respect to the wall. Fig. 5-5 presents the distribution of axial load along the lower wall in both instrumented piles, at Day 154, both rows of anchors were installed and backfilling was being place. As seen, axial load increased with depth until the gage immediately above the embedded portion of the soldier piles. In the embedded portion of the soldier piles, presumably relative movement between the piles and the grout might cause tension in gages in this portion of the wall.

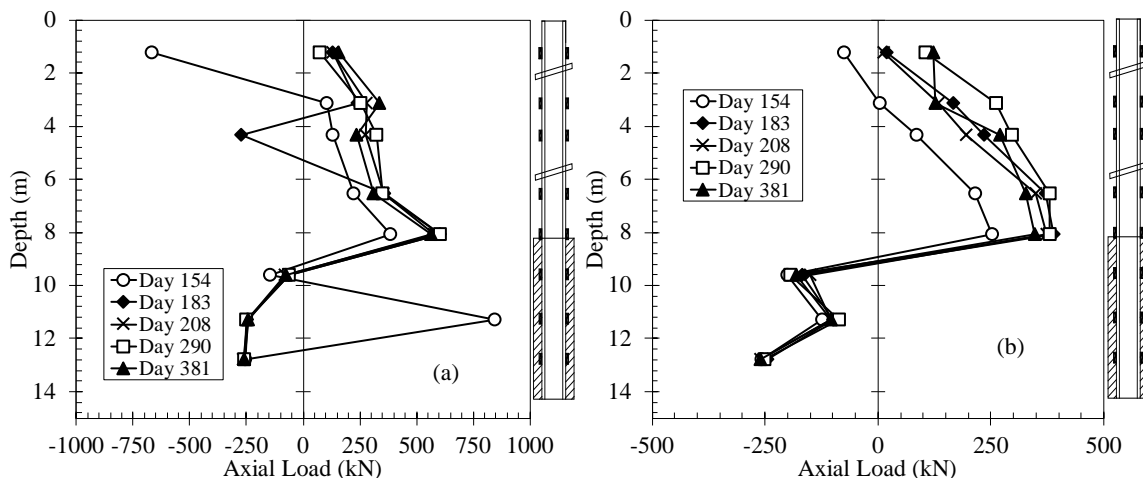


Fig. 5-5. Measured Axial Load in the Lower Wall: (a) Pile 11. (b) Pile 12

Backfilling to the final grade in the lower wall during days 157 and 185 increased the axial forces along the soldier piles through friction along the back side of the lagging. The initial tension observed at the top of the soldier piles became compression along the members as can be see between days 154 and 183. The highest change in force was observed at top of the soldier pile 11, the axial force change for tension of 670 kN to compression of 137 kN approximately. For soldier pile 12 the increase in force was almost uniform along the pile; the greatest increase in vertical load during backfilling for this pile was 154 kN which was immediately below the upper anchor.

From Day 208 to Day 381 the axial force above the upper anchor increased in both anchors, axial loads at the top of the piles incremented 65.6 kN and 110 kN in the soldier pile 11 and 12, respectively. In the embedded portion of the pile, axial loads remained almost the same during all construction states as observed in the Fig. 5-5. As seen in this wall, a significant variation in the axial load distribution was caused during backfilling; load was transfer as friction in backside of the wall.

In general, axial loads computed in the soldier pile 11 were greater than pile 12. The greatest discrepancy of the computed load was observed above the upper anchors; on average, the load in pile 11 was 3.5 times greater than the load in pile 12. Below the upper anchor, maximum variation of the computed load for soldier pile 11 was 1.6 times greater than soldier pile 12.

Fig. 5-6 presents the distribution of axial load in the two piles of the upper wall; axial load distribution was similar to the observed in the lower wall. Stressing the middle row of anchors in the upper wall was finished at Day 106; tensioning the Row C was completed at Day 132. Upon stressing of the lower row of anchors, precast lagging and backfill were installed until 1 m below the upper row of anchors. Day 154 in Fig. 5-6 shows the distribution of axial load under these conditions.

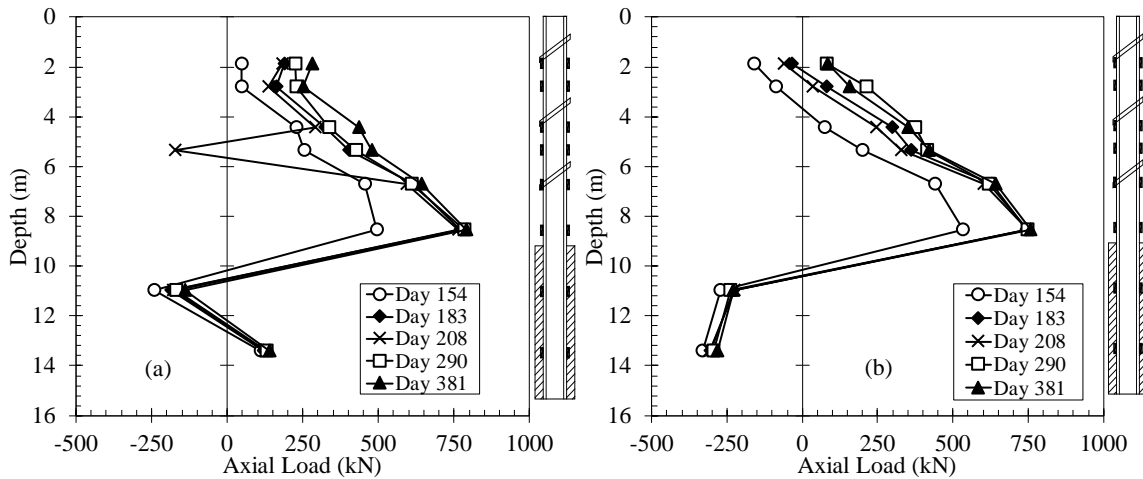


Fig. 5-6. Measured Axial Load in the Upper Wall. (a)Pile 30. (b) Pile 31

The increase in the axial force between days 154 and 183 is the combined effect of stressing the upper row of anchors and backfilling behind the wall. The most significant changes in the axial force were obtain in the gages above the toe of the soldier piles, axial load

increased 281 kN in soldier pile 30 and 219.8 kN in soldier pile 31; these values represent the 116 percent and 91 percent of the vertical component of the anchor load.

At Day 188, grading was finished in both walls; a slight decrease in the axial force in the soldier piles was observed between days 183 and 208. After wall construction, wall movement laterally as a consequence of load reduction in the anchors; during this outward movement, friction was mobilized between the backfill and the wall and increased in the axial force was observed between days 208 and 290. No significant changes were observed in axial forces along the wall after Day 209 until Day 381.

5.3.3 Anchor Loads

Load cells were installed at the head of anchors of the upper and lower wall. In the upper wall, they were installed in the anchors of the soldier pile 30. Analogously, in the anchors of soldier pile 11. Fig. 5-7 shows the load variation versus time on the five instrumented anchors. Lock-off loads of the anchors was 90 percent of the design load. Given that the applied lock-off loads were less than 55 percent of the elastic limit of the steel strands, load losses due to relaxation of the steel can be considered negligible (Benmokrane and Ballivy 1991); therefore, the observed load losses are the results of creep and instantaneous losses during anchor lock-off.

Maximum load loss of 44.7 kN was observed in the middle anchor of the upper wall (30B). Similar average amount of load loss was observed in both walls at the end of the measurement period; the average load reduction in the upper wall was 31.7 kN while in the lower wall this value corresponds to 29.6 kN. These values correspond to load losses of 9.4 and 6.5 percent from the lock-off load in the upper and lower wall, respectively. Although the load loss in the upper wall was unexpected, both values are acceptable based on 10-percent loss in common practice.

According to Benmokrane and Ballivy (1991) the long-term of prestressed rock anchors can be divided in two phases, phase I, where rapid losses of load are observed and phase II where rate of loss becomes small. Based on the measurements in both walls of this project, it is believed that the phase I was completed around construction Day 300 as observed in

Fig. 5-7. This period correspond to almost 6 months since anchor installation; this period corresponds to the suggested of duration of the phase I according to these authors.

Considering the complete monitoring period, the overall load loss per log cycle of time varied from 0.6 percent to 2.5 percent with an average of 1.5 percent. This average corresponding to 7.8 percentage of average of load loss 100 years. This result is similar to the reported by Briaud et al. (1998) of 0.9 percent load loss per log cycle of time and 7 percent in a 100 year period for anchors installed in a soil profile composed of very stiff clay and clay shale.

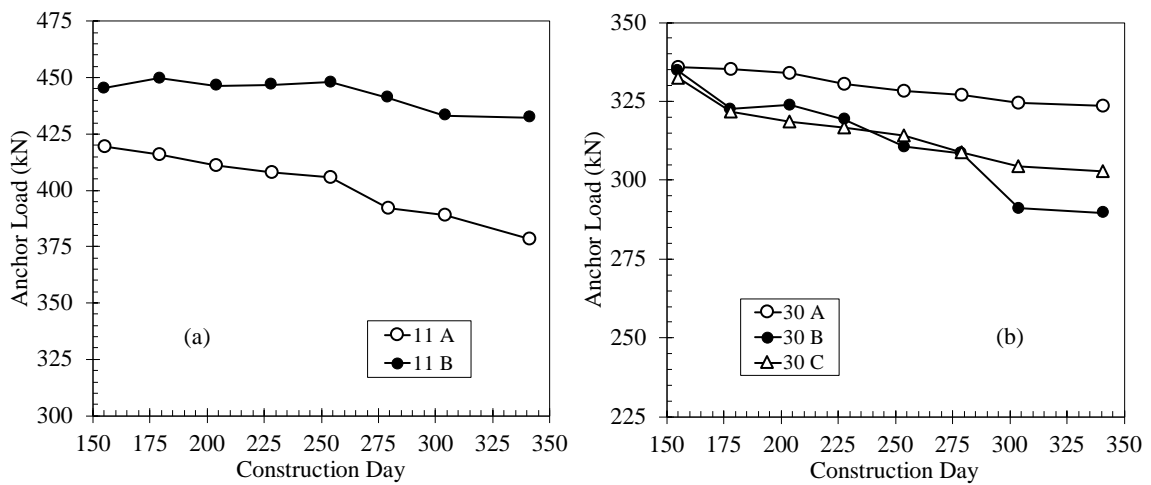


Fig. 5-7. Anchor Load Variation: (a) Lower Wall; (b) Upper Wall

Fig. 5-8 presents the comparison between the loads estimated from the strain gages above the toe of the piles and the vertical component of the load cell for soldier pile 11. Fig. 5-8(a) shows that at Day 154, before backfilling the wall, loads from load cells were similar to those calculated with the strain gages, with the exception of the tensile load above the upper anchor. At Day 208, Fig. 5-8(b), when backfilling was finished, the load determined from the strain gages were greater than vertical component of load cells. This increase in the axial load can be attributed to a high friction developed between the material and the backside of the wall. On average, the load from the strain gages was 2.4 times the load from load cells; at day 38, this proportion remained constant with an average value of 2.6.

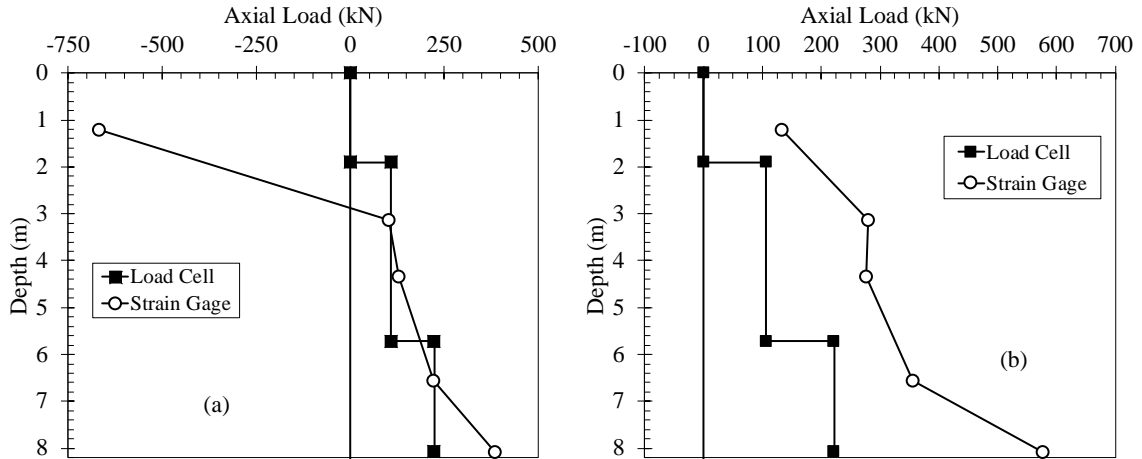


Fig. 5-8. Load Cell versus Strain Gage Load in Soldier Pile 11: (a) Day 154; (b) Day 208

In the soldier pile 30, Fig. 5-9 shows the comparison between axial loads from strain gages and vertical component of load cells. Notice that the anchors of the upper wall were installed at a steeper angle with a high vertical component of anchor load; even though, the results were opposite to the behavior observed in the lower wall; backfilling of the wall did not increase the axial load above the vertical component of the load cells.

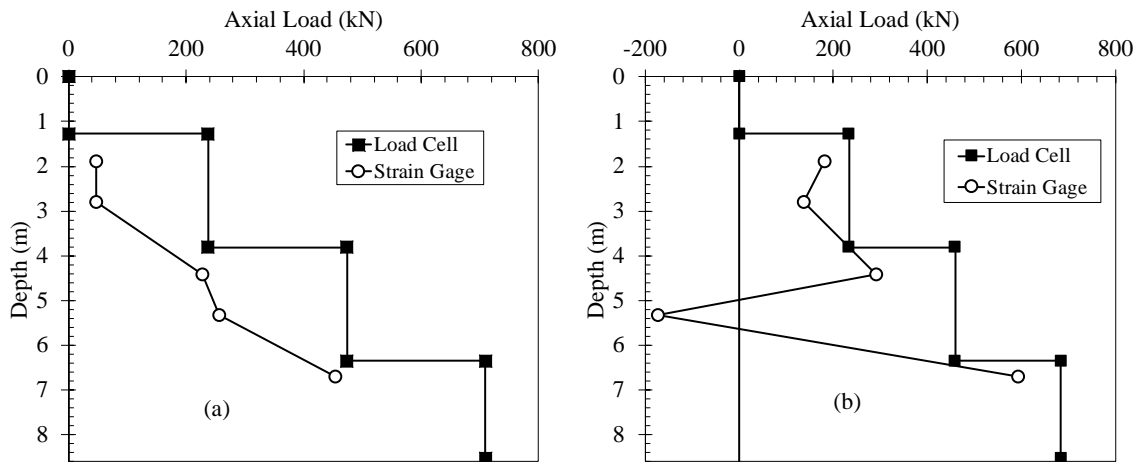


Fig. 5-9. Load Cell versus Strain Gage Load in Soldier Pile 30: (a) Day 154; (b) Day 208

Measurements of axial load in the upper wall are similar to those reported by Grant (1985) and Houghton and Dietz (1990); in soldier pile and lagging walls, the axial load at the tip of the piles was similar or lower than the vertical component of the anchor loads. Consequently, it was possible that some support for the vertical loads developed above the toe of the soldier piles. Axial load transfer in both walls was different,

5.4 Earth Pressures and Wall Design

Anchored wall are commonly dimensioned based on apparent earth pressure, two routinely apparent earth pressures were used to the analysis of both walls, namely those presented by Peck (1969) and the Federal Highway Administration (FHWA) in Sabatini et al. (1999) (1999). Bending moments acting on the wall were determined using three common approaches. The tributary area method and the hinge method, both presented by Sabatini et al. and the approach used by the California Department of Transportation (2011) here referred as Caltrans method.

The difference between Caltrans and Hinge method is that the hinge method assume a pinned support at the subgrade while Caltrans uses a pinned support where shear and moments balance out below the subgrade. Because the backfilling was inclined, a wedge analysis was performed to obtain the maximum load in the walls; then, this load was distributed in the apparent earth pressures.

Both walls were modeled with using a uniform backfilling material with a unit weight of $\gamma = 19.6 \text{ kN/m}^3$ and an angle of internal friction $\phi' = 34^\circ$. The commercial software DeepEX was used in the calculations. The two models used for the lower wall are presented in Fig. 5-10 and the models for the upper wall are presented Fig. 5-11. Both figures include the distribution of lateral earth pressures used in the analysis. Separation between the soldier piles was 3 m and 2.4 m for the lower and the upper wall, respectively.

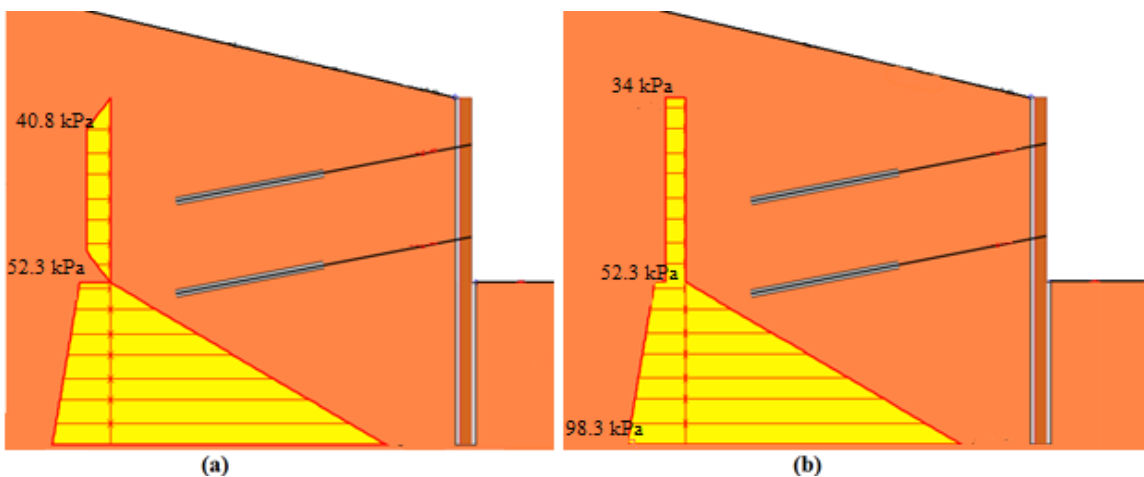


Fig. 5-10. Lower Wall Model: (a) FHWA envelope. (b) Peck envelope

Maximum ordinate of the apparent earth pressures were calculated according to equation (25) and equation (26) for FHWA and Peck apparent earth pressure, respectively

$$\sigma = \frac{P_T}{H - 1/3H_1 - 1/3H_n} \quad (25)$$

Where σ = maximum ordinate of the apparent earth pressure; P_T = total load from wedge analysis; H_1 = distance from the top of the wall to the uppermost anchor; H_n = distance from the bottom of the excavation to the lowermost anchor and H = height of the excavation.

$$\sigma = 0.65\gamma K_a H \quad (26)$$

Where K_a = equivalent lateral earth pressure coefficient and γ = effective unit weight of the soil.

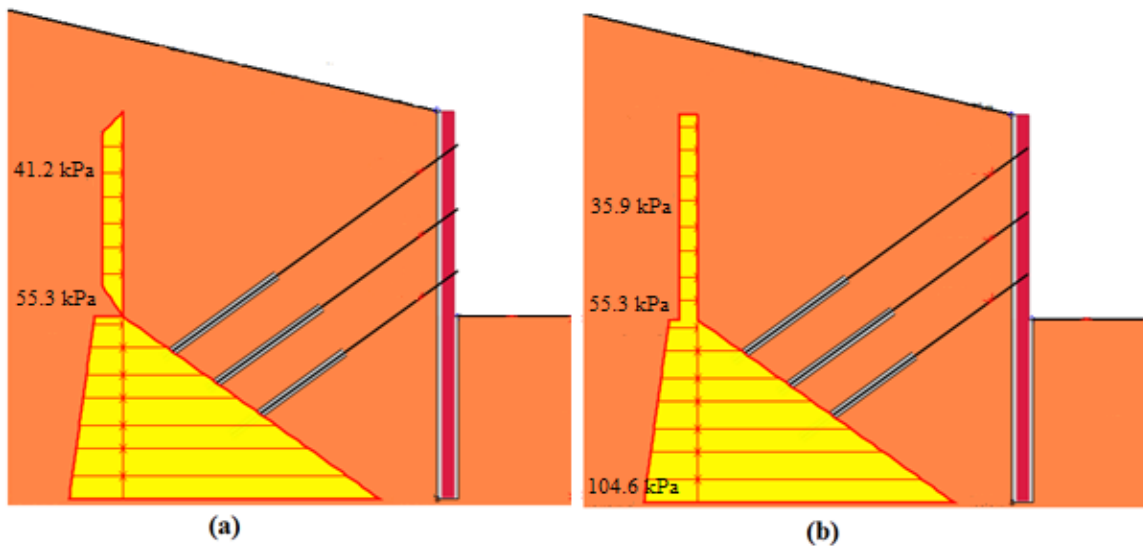


Fig. 5-11. Upper Wall Model: (a) FHWA envelope. (b) Peck envelope

Fig. 5-12 presents the comparison of the bending moments calculated in the lower wall with the aforementioned methods. Moments using the tributary area method were computed following the recommendations from Peck et al. (1974) recommended that the maximum bending moment below the cantilever equal $\sigma l^2 / 10$; where σ = intensity of the earth pressure diagram and l = spacing between the supports. As seen from Fig. 5-12, below the lower support the distribution of bending moments is completely different with

both earth pressure envelopes. Above the lower row of anchors, the moment distribution has a similar tendency. As observed, none of the used methods satisfactorily estimates the bending moments in both of the instrumented soldier piles in the lower wall.

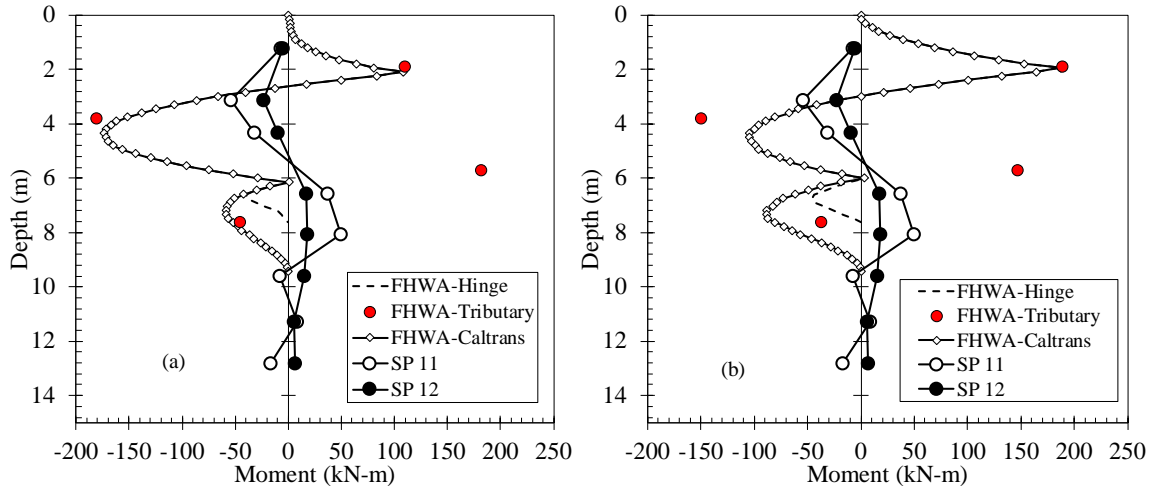


Fig. 5-12. Moment Distributions in Lower Wall Calculated from: (a) FHWA envelope (b) Peck envelope

Results of the analysis for the upper wall are presented in Fig. 5-13. Similar to the results from the lower wall, enormous discrepancies were observed between computed and measured bending moments. Greater differences were observed below the middle anchor, with the measured data approximately three times the calculated. Some reasons may explain the high discrepancy between the measured data and the calculated; computation of bending moments from apparent earth pressures was based on the final state of construction i.e. when the backfill was placed to the final grade. However, this was not the case for the SUM 82 project, backfilling activities clearly impact the response of both walls.

Fig. 5-12 and Fig. 5-13 showed that using earth pressure envelopes to analyze tieback wall in slope stabilization scenarios might result in designs that are not conservative, great moment develop in the early stages of construction can govern the wall requirements. Note that below the lower row of anchors, the computed bending moments are opposite in sign to the measured; this area is precisely where shale stratum was excavated. Considering this material as competent, minor pressures may be expected in this area; in fact, as seen from the calculated moment this zone might acted as cantilever.

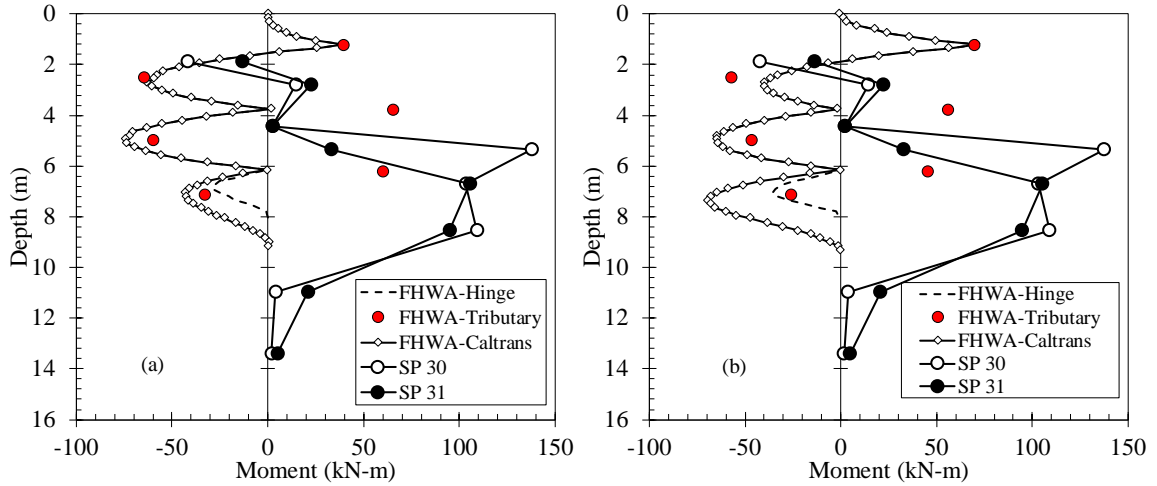


Fig. 5-13. Moment Distributions in Upper Wall Calculated from: (a) FHWA envelope (b) Peck envelope

Fig. 5-14 illustrates the reason for the high positive moments in the upper wall, with the middle and the lower row of anchors installed, backfilling material was placed behind the wall to an elevation of 1 m approximately below the upper row of anchors. Backfilling to this elevation might cause tension in the inner face of the soldier piles; as stated earlier posterior backfilling to the final grade did not modify the significantly the distribution of bending moments along the pile.

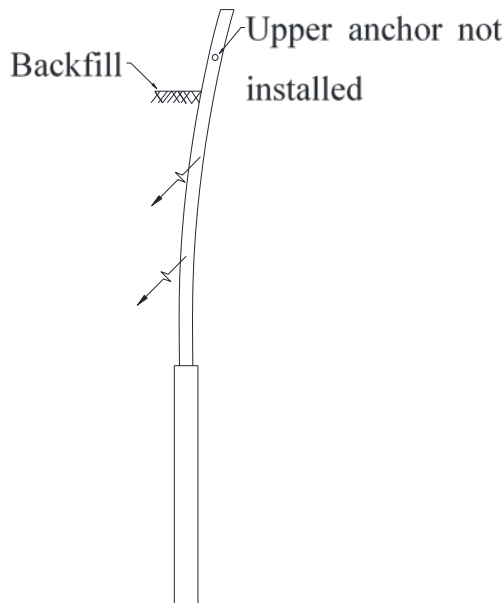


Fig. 5-14. Development of High Positive Moments below the Lowest Anchor

Additionally to the bending moment analysis, apparent pressures used in the analysis were compared with back-calculated values based on the procedure recommended by Terzaghi and Peck (1967). Apparent earth pressures since installation of the anchors until the final monitoring day are presented in Fig. 5-15; also, it includes the apparent earth pressures suggested by Peck (1969) and the FHWA (Sabatini et al. 1999) and computed with DeepEx.

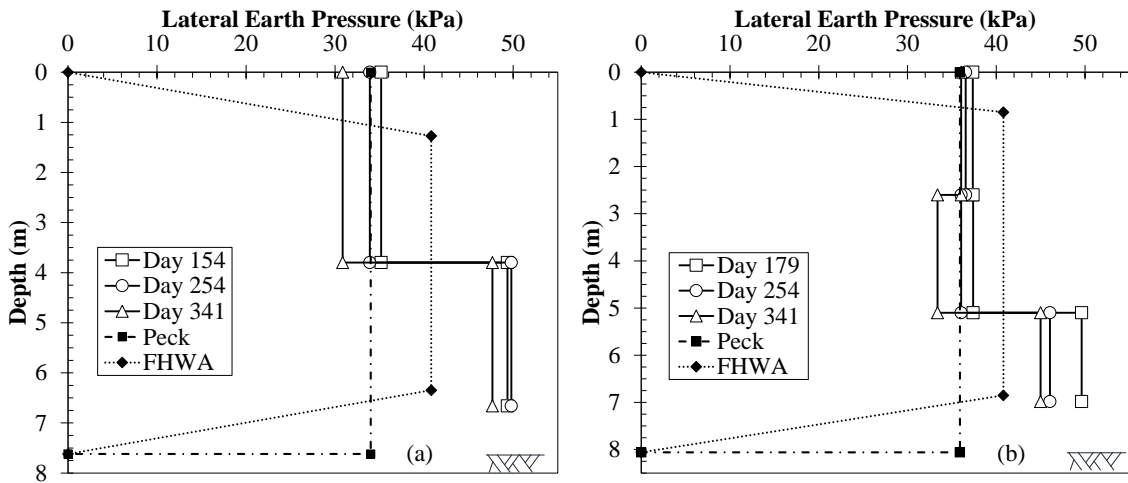


Fig. 5-15. Apparent Earth Pressures: (a) Lower Wall; (b) Upper Wall

In general, both wall exhibit an increase in pressure with depth. After lock-off, it was observed a decrease with time in the estimated lateral pressure in both walls; this reduction is associated with load loss of the anchors. It seems that a balance between earth pressure and anchors was achieved around Day 254; the variation in the pressures after this day until the last day of measurement was slight.

Above the half of the wall approximately, apparent earth pressure suggested by Peck (1969) was closer than the FHWA envelope to the estimated lateral pressures; with the latter overestimating the magnitude of the lateral pressures. However, both methods tend to underestimate the magnitude apparent pressure near the base of the excavation. Similar behavior was observed by Liao and Hsieh (2002) in an alluvial soil deposits.

5.4.1 Bending Moment estimation from inclinometer data.

Based on inclinometer data, bending moment the along the piles can be estimated. Usually, a fitting curve is adjusted to the inclinometer data and using beam theory (equation 27) considering that all transverse deflections, rotations, and strains along the member are small.

$$M \approx EI \frac{d^2 y}{dx^2} \quad (27)$$

Where M = bending moment along the soldier pile; E = modulus of elasticity of the pile material; I = inertia of the soldier pile and $d^2 y / dx^2$ is the soldier pile curvature. Material properties used were $E=200$ GPa and $I= 3.03 \times 10^{-4} \text{m}^4$.Several techniques can be used to estimate the curvature, piecewise quadratic fitting, B-splines, piecewise fitting of circular arcs, high order polynomial curve, etc. A piecewise cubic polynomial curve, equation (28) , with a moving window of five inclinometers data points was used to estimate the bending moments for the lower and upper wall (Ooi and Ramsey 2003).

$$\delta = Az^3 + Bz^2 + Cz + D \quad (28)$$

Where A, B, C and D are constants. These constants were determined using least square fitting for the selected five successive points. Lateral displacements measured along piles used to estimate the bending moments are presented in Fig. 5-16. Data from the soldier piles 12 and 30 was used in the calculation of the bending moments in the lower and upper wall, respectively. During installation of the upper row of anchors (Row A) and backfilling of the walls, the casings of the inclinometers were moved and data in the upper portion of the soldier piles was questionable; dotted lines in Fig. 5-16 show these data which was omitted during the estimation of the bending moments. Note that inclinometer data was collected until a depth of 4.6 m below the bottom of the soldier pile.

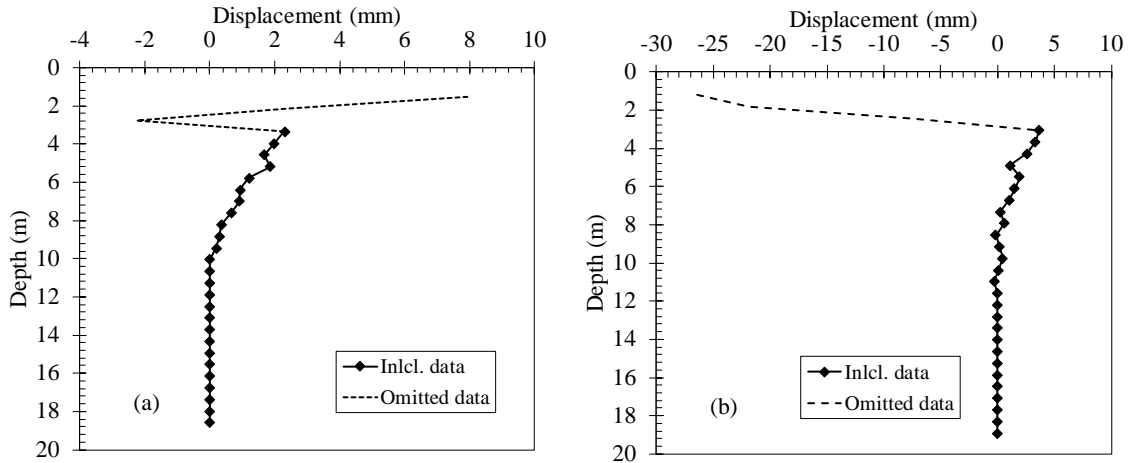


Fig. 5-16. Inclinometer Data: (a) Lower Wall; (b) Upper Wall

Based on the calculated bending moments, Fig. 5-17, it is observed that inclinometer data provides a satisfactory estimative of the bending moment distribution. In the case of the lower wall, estimated moments showed a noticeable correlation with the measured values above the embedded depth of the soldier pile. Maximum positive and negative bending moments estimated with inclinometer data corresponded to 77 and 98 percent the measured values; however, location of the maximum negative moment showed an offset distance of 1.5 m approximately.

For the upper wall, although the bending moment distribution was similar to the measured, the overall magnitude of the moments was underestimated in the case of positive bending moments. Maximum positive estimated moment was 33 percent the measured value, while the maximum negative estimated value was 155 percent the measured. This poor correlation between the measured and estimated bending moments can be attributed to displacement of the inclinometer casing during backfilling in the upper wall. Moment distribution from the strain gages and inclinometer data correspond to the construction Day 230 and Day 229, respectively.

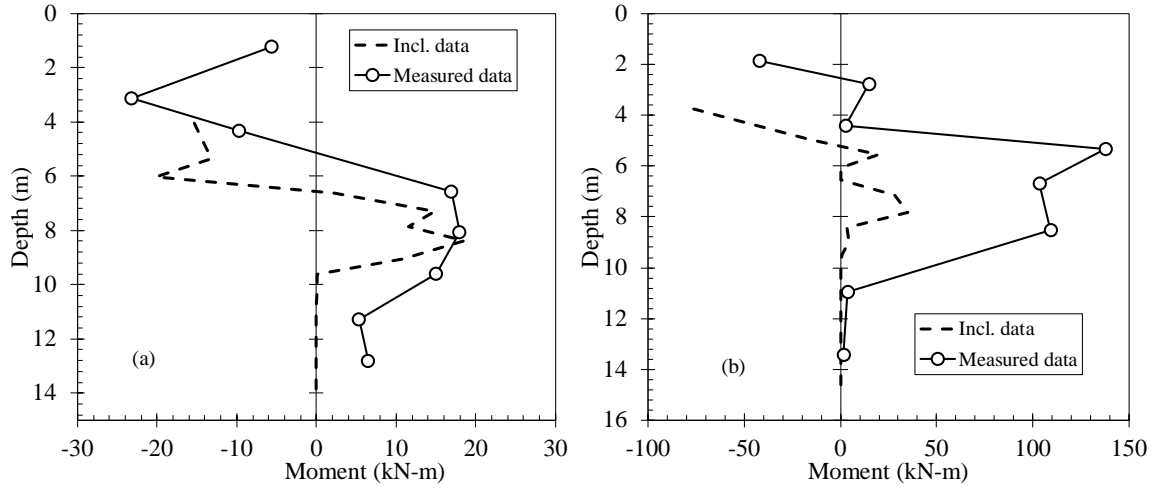


Fig. 5-17. Estimated Moments from Inclinator Data (a) Lower Wall; (b) Upper Wall

6 Empirical Method to Estimate Lateral Wall Deformation Profiles and Bending Moment in Excavation Retaining Walls

6.1 Introduction

Development of underground space is a necessary practice worldwide. This tendency makes imperative the use of deep excavations in urban environments, where induced ground movements may be critical and damage to adjacent structures and utilities may occur. Thus, prediction of ground movements during design is necessary in order to evaluate the suitability of a support system Mueller (2000). Traditionally, estimation of ground movements is based on local experience obtained from past excavation projects while the excavation support system is sized using simplified limit equilibrium methods such as the internal hinge method (Lambe et al. 1970) (Lambe and Wolfskill, 1970) and the tributary area method (Terzaghi and Peck, 1967).

However, deficiencies of these methods emerge from their simplifying assumptions and the empirical representation of the soil-structure interaction problem. Additionally, more sophisticated methods such as finite element and finite difference analyses have shown the importance of considering three-dimensional (3D) effects of the excavation geometry. However, quantification of input parameters for the numerical analyses is a formidable task and variation of ground conditions makes the modelling process laborious and time-consuming. Additionally, a general lack of understanding concerning sources of wall movements makes the predicted response uncertain.

Commonly, the main concern in excavation support system design is the possible excavation-induced damages in adjacent infrastructure and utilities. Consequently, the performance of a support system is evaluated based on the maximum deformations observed during and after construction. Numerous empirical and semi-empirical relationships to determine lateral wall deformation and settlement profiles have been proposed (Mana and Clough 1981; Clough and O'Rourke 1990; Hsieh and Ou 1998; Kung et al. 2007; Zhang et al. 2015). In these approaches, the relationship between the excavation-induced movements and support system is well recognized. Therefore, these methods include the systems stiffness factor defined by Clough et al. (1989).

Based on 3D finite-element analyses and a collected database, Bryson and Zapata-Medina (2012) developed a relative stiffness ratio, which takes into account the main variables that relate system stiffness and maximum lateral movement. The authors reported that their relative stiffness ratio outperformed the systems stiffness factor defined by Clough et al. (1989). This chapter uses research presented by (Bryson and Zapata-Medina) to estimate lateral deformation profiles for various soil types.

Few cases are reported where the structural response of the wall is evaluated, that is, bending moment and shear forces along the wall. From a structural design standpoint, variation of the bending moments along the wall allows designers to optimize the amount of steel; however, at the same time it is necessary to guarantee the serviceability of the wall by limiting the ground movements. Monitoring of wall deformations is generally carry out using inclinometers and optical surveys during construction. Inclinometers provide not only deformation data, but also a mean to obtain curvature along the retaining wall. Curvature can be directly linked with bending moments and shear forces along the wall using fundamental relationships from mechanics of materials. Ooi and Ramsey (2003) conducted studies about common methods to estimate bending moments from inclinometers data. They suggested that a piecewise polynomial curve fitting was practical to derived the bending moments. This chapter presents empirical relations, based on data interpolation with a unique continuous polynomial function, to determine the variation of internal bending moment in excavation retaining walls.

The focus of this chapter is to present an empirical approach to obtain characteristic distributions of bending moments and lateral wall displacements for excavations in clays. The method is based on inclinometer data collected from thirty case histories worldwide and allows the designer, having the maximum lateral wall displacement and the height of the wall, to predict the shape of lateral wall deformations for deep excavations based on soil type (i.e., based on the undrained shear strength parameter). The internal bending moment along the wall is derived from the fundamental relations of mechanics of materials and the classical theory of beams that relate the internal bending moment to the components of translation of the member.

6.2 Development of the Empirical Method

The proposed methodology is based on well-reported case histories worldwide. Table 6-1 lists the case histories that form the basics of the proposed empirical method (Zapata-Medina 2007). The cases are distinguished by soil type based on the undrained shear strength (Stiff Clay, $s_u > 50kPa$; Medium Clay, $25kPa \leq s_u \leq 50kPa$; and Soft Clay, $s_u < 25kPa$) found at the dredge level of the excavation.

Table 6-1 Excavation Cases after Zapata-Medina (2007)

| Soil type | Case ID | Project name, Location | Wall type | Reference |
|-----------|---------|--|-----------|--------------------------|
| Stiff | St1 | Lion Yard Development, Cambridge | Diap | Ng (1992) |
| | St2 | New Palace Yard Park Project, London | Diap | Burland and Hancock |
| | St3 | Far-East Enterprise Center Project, | Diap | Hsieh and Ou (1998) |
| | St4 | Oxley Rise Development, Singapore | Diap | Poh et al. (1997) |
| | St5 | Central Insurance Building, Taipei | Diap | Ou and Shiau (1998) |
| | St6 | Post Office Square Garage, Boston | Diap | Whittle et al. (1993) |
| | St7 | National Taiwan University Hospital, | Diap | Liao and Hsieh (2002) |
| | St8 | Taipei County Administration Center, | Diap | Liao and Hsieh (2002) |
| | St9 | 75 State Street, Boston | Diap | Becker and Haley |
| | St10 | Smith Tower, Houston | Secan | Ulrich (1989) |
| Mediu | M1 | Taipei National Enterprise Center | Diap | Ou et al. (1998) |
| | M2 | Robert H. Lurie Medical Building, | Sheet | Finno and Roboski |
| | M3 | Robert H. Lurie Medical Building, | Sheet | Finno and Roboski |
| | M4 | Taiwan Formosa, Taipei | Diap | Hsieh and Ou (1998) |
| | M5 | Tokyo Subway Excavation Project, | S-C. | Miyoshi (1977) |
| | M6 | HDR - 4 Project for the Chicago Subway | Sheet | Finno et al. (1989) |
| | M7 | Oslo Subway Excavation Project, Oslo | Sheet | NGI (1962) |
| | M8 | Embarcadero BART Zone 1, San | Diap | Clough and Buchignani |
| | M9 | Metro Station South Xizan Road, | Diap | Wang et al. (2005) |
| | M10 | Open Cut in Oslo | Sheet | Peck (1969) |
| Soft | So1 | Chicago and State Street Excavation, | Secan | Finno et al. (2002) |
| | So2 | Mass Rapid Transit Line, Singapore | Diap | Goh et al. (2003) |
| | So3 | Deep Excavation adjacent to the | Diap | Hu et al. (2003) |
| | So4 | Excavation in Downtown Chicago | Sheet | Gill and Lucas (1990) |
| | So5 | Peninsula Hotel Project, Bangkok | Sheet | Teparaksa (1993) |
| | So6 | AT&T Corporate Center, Chicago | Diap | Baker et al. (1989) |
| | So7 | Museum of Science and Industry | Diap | Konstantakos (2000) |
| | So8 | One Market Plaza Building, San | Soldi | Clough and Buchignani |
| | So9 | Sheet Pile Wall Field Test, Rotterdam | Sheet | Kort (2002) |
| | So10 | MUNI Metro Turnback Project, San | Soldi | Koutsoftas et al. (2000) |

Note: Sheet = sheet pile wall; Diaph. = diaphragm wall; S-C = steel with concrete lagging wall; and Secant = secant pile wall.

6.3 Lateral Profile Deformation

Fig. 6-1 Normalized Lateral Deformations for Case Histories: (a) Stiff Clay; (b) Medium Clay; and (c) Soft Clay. Fig. 6-1 shows lateral wall deformations versus depth for the case histories of stiff, medium and soft clay. In the figure, lateral deformations are normalized with respect to the maximum horizontal movement recorded at the end of excavation, and the depth axis is normalized with respect to the height of the wall.

Note that a three-linear plot was included for each soil type in order to show the lateral deformation profile tendency of the case history data. These empirical three-linear plots allow the designer, having the maximum lateral wall displacement and the height of the wall, to predict the shape of lateral wall deformations for deep excavations based on soil type (i.e., based on the undrained shear strength parameter).

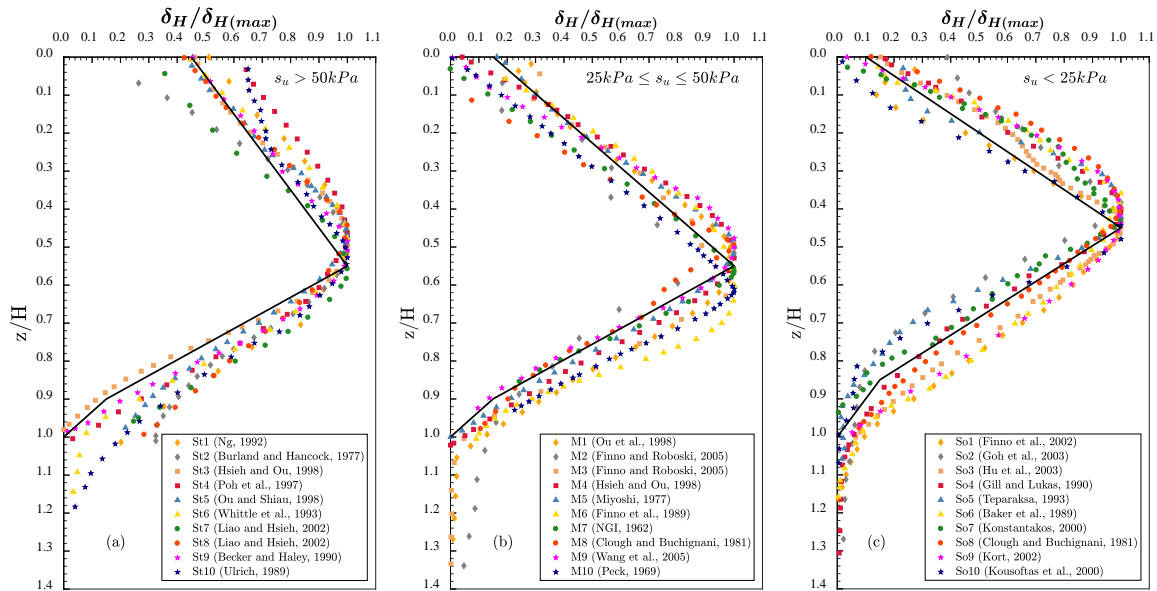


Fig. 6-1. Normalized Lateral Deformations for Case Histories: (a) Stiff Clay; (b) Medium Clay; and (c) Soft Clay.

6.4 Bending Moments

The bending moment in the wall is derived from the fundamental relations of mechanics of materials and the classical theory of beams. It is expressed as:

$$M = -\kappa EI \quad (29)$$

Where M = bending moment, κ = curvature, E = elasticity modulus of the material, and I = moment of inertia of the cross-section. From calculus, the curvature of a beam expressed in terms of its displacements is given by the relation:

$$k = \frac{1}{\rho} = \frac{\frac{d^2 \delta_H}{dz^2}}{\left[1 + \left(\frac{d\delta_H}{dz} \right)^2 \right]^{3/2}} \quad (30)$$

Where δ_H = lateral displacement and z = abscissa along the element. Assuming that all transverse deflections, rotations, and strains along the member are small so that the principle of superposition is applicable, the term $(d\delta_H / dz)^2$ can be approximated to zero yielding:

$$k = \frac{1}{\rho} \approx \frac{d^2 \delta_H}{dz^2} \quad (31)$$

Substituting equation (31) into equation (29), the following expression is obtained:

$$M = -EI \frac{d^2 \delta_H}{dz^2} \quad (32)$$

which is the classical equation that relates the internal bending moment and the components of translation of the member. Introducing the following non-dimensional terms: $\bar{\delta}_H = \delta_H / \delta_{H(\max)}$ and $\bar{z} = z / H$, equation (32) becomes:

$$\bar{M} = \frac{M \times H^2}{EI \times \delta_{H(\max)}} = -\frac{d^2 \bar{\delta}_H}{d\bar{z}^2} \quad (33)$$

Equation (33) is the non-dimensional bending moment expression to be used in this analysis to design the retaining walls of excavation support systems. In order to define the bending moment along the retaining wall, it is necessary to develop a function for lateral deformation along the member. For this purpose, the empirical lateral wall deformation

profiles presented in Fig. 6-1 are used as a reference. A six-order polynomial function having the following form was fitted to each soil type:

$$\bar{\delta}_H(\bar{z}) = A_1(\bar{z})^6 + A_2(\bar{z})^5 + A_3(\bar{z})^4 + A_4(\bar{z})^3 + A_5(\bar{z})^2 + A_6(\bar{z}) + A_7 \quad (34)$$

To find the constants A_1 to A_7 , seven different conditions are necessary. Based on the shape of the three-linear plots presented in Fig. 6-1 and assuming that the bending moment at the top and bottom of the wall are equal to zero, the conditions summarized in Table 6-2 were applied.

Table 6-2 Initial and boundary conditions.

| For stiff clay | For medium clay | For soft clay |
|--|--|--|
| $\bar{\delta}_H(0) = 0.45$ at $\bar{z} = 0$ | $\bar{\delta}_H(0) = 0.1$ at $\bar{z} = 0$ | $\bar{\delta}_H(0) = 0.1$ at $\bar{z} = 0$ |
| $\bar{\delta}_H(0.55) = 1$ at $\bar{z} = 0.55$ | $\bar{\delta}_H(0.55) = 1$ at $\bar{z} = 0.55$ | $\bar{\delta}_H(0.45) = 1$ at $\bar{z} = 0.45$ |
| $\bar{\delta}_H(1) = 0$ at $\bar{z} = 1$ | $\bar{\delta}_H(1) = 0$ at $\bar{z} = 1$ | $\bar{\delta}_H(1) = 0$ at $\bar{z} = 1$ |
| $\frac{d\bar{\delta}_H(0)}{d\bar{z}} = 1$ at $\bar{z} = 0$ | $\frac{d\bar{\delta}_H(0)}{d\bar{z}} = 1.6364$ at $\bar{z} = 0$ | $\frac{d\bar{\delta}_H(0)}{d\bar{z}} = 2$ at $\bar{z} = 0$ |
| $\frac{d\bar{\delta}_H(0.55)}{d\bar{z}} = 0$ at $\bar{z} = 0.55$ | $\frac{d\bar{\delta}_H(0.55)}{d\bar{z}} = 0$ at $\bar{z} = 0.55$ | $\frac{d\bar{\delta}_H(0.45)}{d\bar{z}} = 0$ at $\bar{z} = 0.45$ |
| $\frac{d^2\bar{\delta}_H(0)}{d\bar{z}^2} = 0$ at $\bar{z} = 0$ | $\frac{d^2\bar{\delta}_H(0)}{d\bar{z}^2} = 0$ at $\bar{z} = 0$ | $\frac{d^2\bar{\delta}_H(0)}{d\bar{z}^2} = 0$ at $\bar{z} = 0$ |
| $\frac{d^2\bar{\delta}_H(1)}{d\bar{z}^2} = 0$ at $\bar{z} = 1$ | $\frac{d^2\bar{\delta}_H(1)}{d\bar{z}^2} = 0$ at $\bar{z} = 1$ | $\frac{d^2\bar{\delta}_H(1)}{d\bar{z}^2} = 0$ at $\bar{z} = 1$ |

Substituting equation (34) and its respective initial and boundary conditions (Table 6-2), a linear system of seven equations is obtained. After solving the system of equations, the expressions for computing the normalized lateral wall movements in stiff, medium and soft clays, respectively, are obtained:

$$\bar{\delta}_H(\bar{z}) = -0.3612(\bar{z})^6 + 6.9546(\bar{z})^5 - 13.3329(\bar{z})^4 + 5.2894(\bar{z})^3 + 1.0(\bar{z}) + 0.45 \quad (35)$$

$$\bar{\delta}_H(\bar{z}) = -6.8282(\bar{z})^6 + 25.215(\bar{z})^5 - 29.7366(\bar{z})^4 + 9.5624(\bar{z})^3 + 1.6364(\bar{z}) + 0.15 \quad (36)$$

$$\bar{\delta}_H(\bar{z}) = -34.688(\bar{z})^6 + 98.8338(\bar{z})^5 - 89.837(\bar{z})^4 + 23.572(\bar{z})^3 + 2(\bar{z}) + 0.1 \quad (37)$$

Fig. 2-1. Site Conditions before Construction of the Walls Fig. 6-2 shows the six-order polynomial function curves fitted for each soil case and compared them with the case history data. The three-linear plots previously defined in Fig. 6-1 are also included. Note that the fitted six-order polynomial functions describe well the tendency showed by the empirical data above the point of maximum lateral displacement. Below the point of maximum lateral displacement, the assumption that the wall rotates around the toe constrained the polynomial fitting and make the adjusted function move slightly below the data; nevertheless, due the empirical approximation the polynomials were satisfactory.

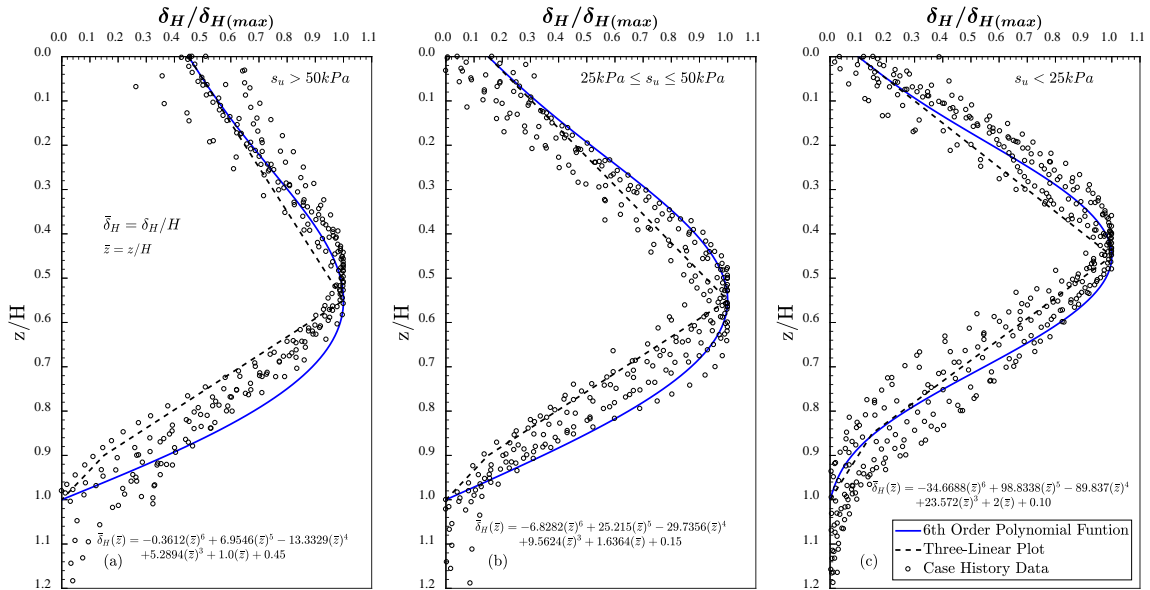


Fig. 6-2. Six-Order Polynomial Functions: (a) Stiff Clay; (b) Medium Clay; and (c) Soft Clay.

The non-dimensional bending moment expressions for stiff, medium, and soft clays are found by differentiating twice the equations (35), (36), (37) and substituting in equation 33. The obtained expressions are:

For Stiff Clay:

$$\bar{M} = 10.8345(\bar{z})^4 - 139.0930(\bar{z})^3 + 159.9944(\bar{z})^2 - 31.7363(\bar{z}) \quad (38)$$

For Medium Clay:

$$\bar{M} = 204.8475(\bar{z})^4 - 504.30(\bar{z})^3 + 356.8269(\bar{z})^2 - 57.3746(\bar{z}) \quad (39)$$

For Soft Clay:

$$\bar{M} = 1040.06(\bar{z})^4 - 1976.68(\bar{z})^3 + 1078.04(\bar{z})^2 - 141.43(\bar{z}) \quad (40)$$

The shape for the above non-dimensional moment expressions is presented in Fig. 6-3. Note that the locations of the maximum positive moment increase with decreasing the soil strength; also, the soft clay exhibit a negative bending moment near the bottom of the wall which is not observed in the other two types of soil. As expected bending moments at the bottom and the top of the wall are zero.

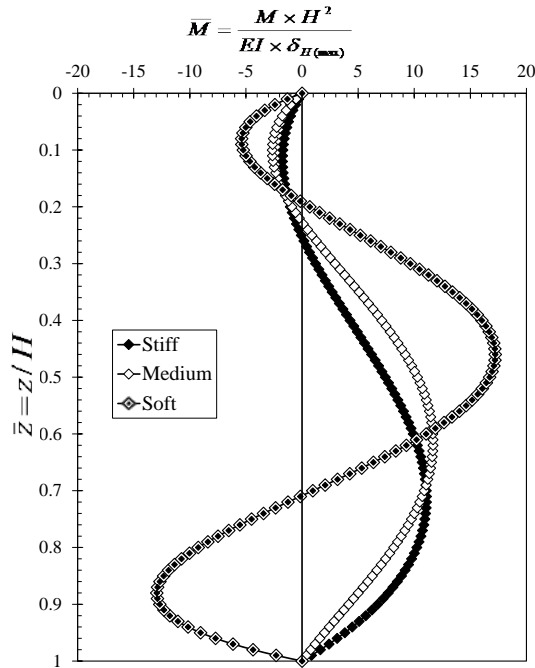


Fig. 6-3. Non-dimensional Bending Moment versus Normalized Depth

6.5 Method Validation

Three different projects were selected to validate the proposed methodology, each one corresponding to one type of soil on average as classified. Tan and Wang (2013) studied the response on a cylindrical excavation in Taiwan soft Clay. In addition, Tan and Wang presented in a companion paper the performance of an adjacent pit, which was not cylindrical. This case was purposely selected to evaluate if the proposed method is susceptible to any geometric effects. It is noted that most common semi empirical approaches (Clough and O'Rourke 1990; Hsieh and Ou 1998; Kung et al. 2007) used to determine lateral movements might not yield accurate estimations as they were derived from mostly rectangular excavations. Fig. 6-4 shows two sets of data from four inclinometers from a project involving a soft clay (Tan and Wang, 2013). The solid symbols in the figure correspond to the cylindrical excavation.

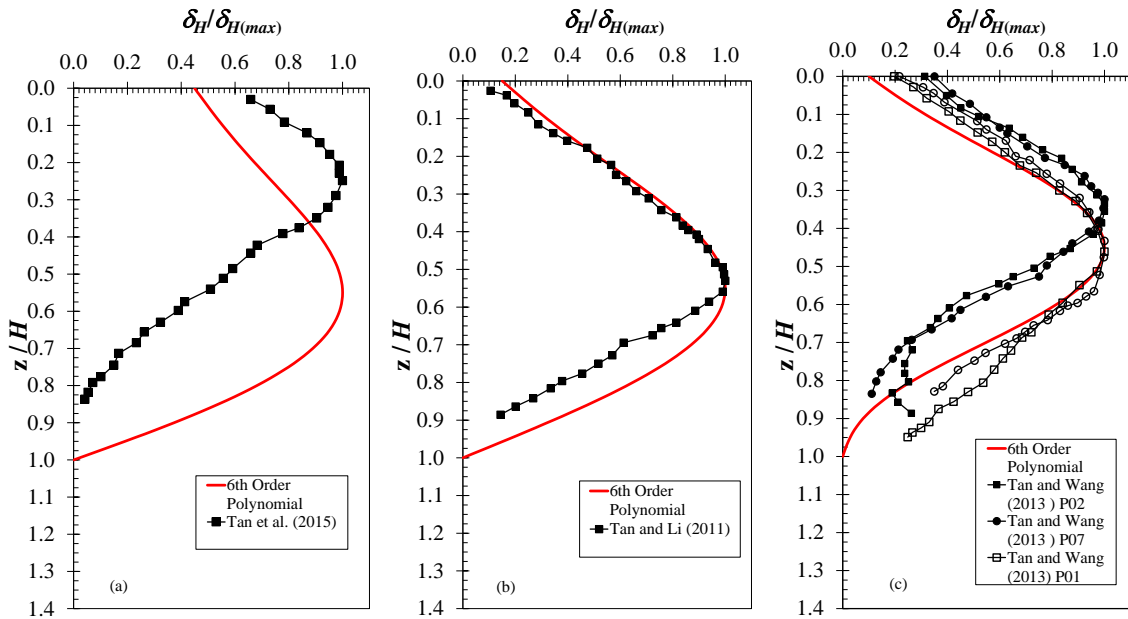


Fig. 6-4. Predicted and Measured Lateral Deformation for: (a) Stiff Clay; (b) Medium Clay; (c) Soft Clay

A good agreement is observed between the measured data and the proposed polynomial function. In particular, the polynomial function shows a better correlation with the data measured in the rectangular excavation. It was specifically noted for the soft clay that the location of the maximum displacement observed in the cylindrical excavation is slightly above of the maximum observed from the rectangular excavation. However, above this point the data between the two set of data had a good agreement.

Fig. 6-4 also presents the computed lateral deformation profiles for excavations in stiff and medium clays. There is a good correlation between the observed displacements and the prediction from the polynomial equation for the case of medium clay (Tan and Li 2011) as shown in Fig. 6-4b. Note that Fig. 6-4a shows a vertical offset between the lateral deformation profiles; however, it is observed the same trend between the predicted and calculated. As reported by Tan et al. (2015) the soil near the toe of the wall was jet grouted, to prevent lateral movement of adjacent utilities and a metro station near the excavation. This discrepancy certainly arrives from the fact that the database used to develop the polynomial approximation did not included excavations with grouting processes at the excavation subgrade; additionally, not recent cases of excavations in stiff clays were found.

In order to address the bending moment distribution along the member, a model from a hypothetical excavation was develop using the commercial software DeepEX. As shown in Fig. 6-5, the excavation has a height of 12 m with three levels of anchors and a width of 20 m. The analysis was conducted using a uniform soil type for the stiff soil profile. However, for the medium and soft clay it was assumed that the wall penetrated into a hard stratum.

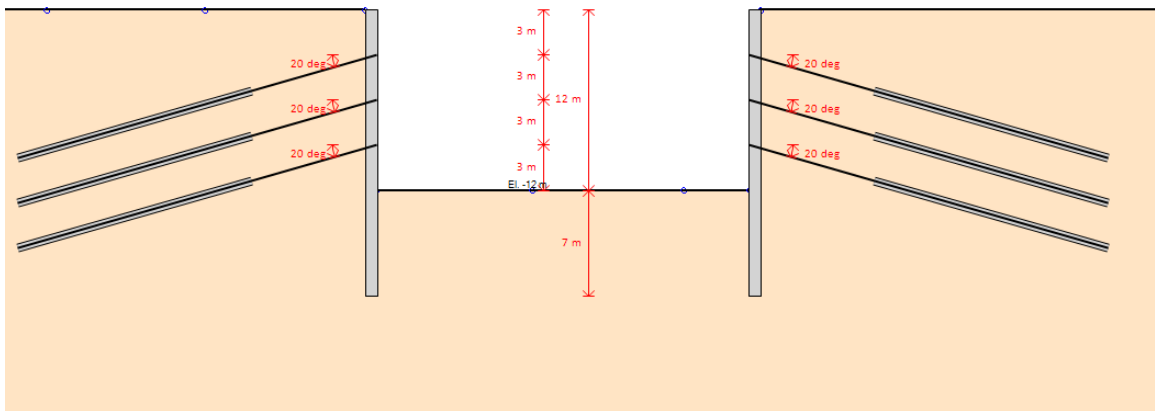


Fig. 6-5. DeepEX Model for Standard Excavation

Lateral displacement of the wall will cause a redistribution in lateral pressures and the bending moments; therefore, as the lateral deformation profiles for each soil are different it is expected a distinct redistribution of the wall bending moments. Analogously to the procedure suggested by Rowe (1957) a reduction factor can be applied to the proposed bending distribution in order to obtain a distribution which more precisely describe the

computed bending moments in the fictitious excavation. For each type of soil, an empirical factor was applied until the proposed distribution was similar to the computed.

Fig. 6-6 presents the obtained moment reduction factors; as seen, despite the fact that only three soil types were modeled, there is a correlation between the reduction factor and the strength of the material. As an initial approximation to the relationship between this two parameters, a straight line was adjusted through the data; however, it is recognized that further analysis are necessary to improve the obtained relationship between s_u and the proposed moments distribution. The moment reduction factor can be obtained from equation (41).

$$f = 0.046 \times s_u + 0.2605 \quad (41)$$

Where s_u has units in kPa . Fig. 6-7 presents the results of the proposed normalized relationship and the result from the models computed for the three types of soil. As seen in the figure, after applying the reduction factor to the bending moment diagram, the bending moments agree satisfactorily with the calculated. Discrepancy arises mostly below the half portion of the wall, this fact can be attributed to the boundary conditions imposed in the model and those observed in the database.

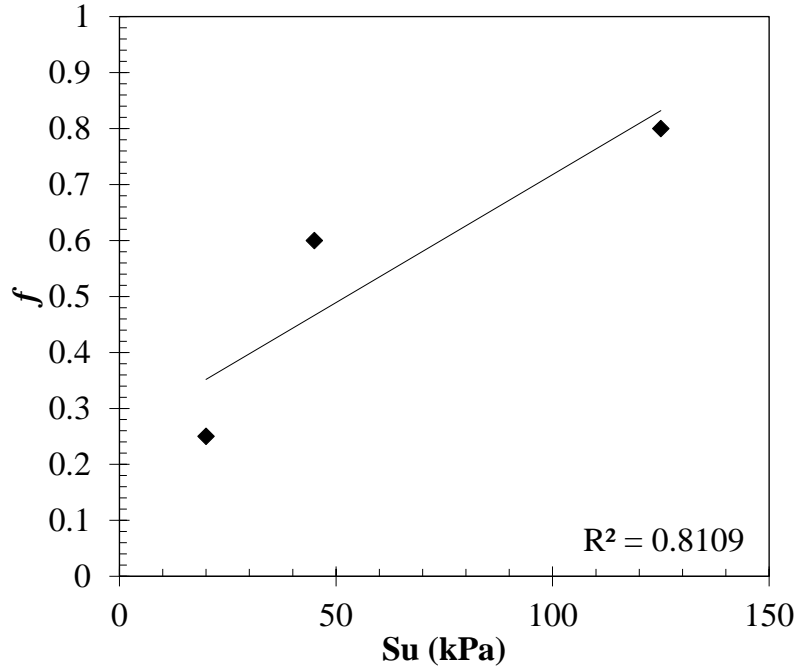


Fig. 6-6. Moment Reduction Factor Versus s_u

Notice that the several of cases from the database presented movement at the bottom of the wall and below it. As can be seen in Fig. 6-2, the lateral profiles proposed do not include any movement at the bottom of the wall; however, these profiles were derived from data which have implicitly wall movement at the bottom. This reason, may explain that the proposed distributions present high moments in the lower part of the wall. On the other hand, the hypothetical excavation was model in a firm stratum; consequently, lateral wall movement at the wall tip were limited which is the ideal case in order to reduced excavation-induced movements.

The bending moment distribution along the wall, when the final level of excavation is reached, may be calculated using Fig. 6-3 with the proposed factor from equation (41). Note that it is assumed that at the final excavation level, the lateral movements are the maximum movements observed during all the excavation process, therefore the maximum curvature is obtained which is represented by the bending moments along the wall.

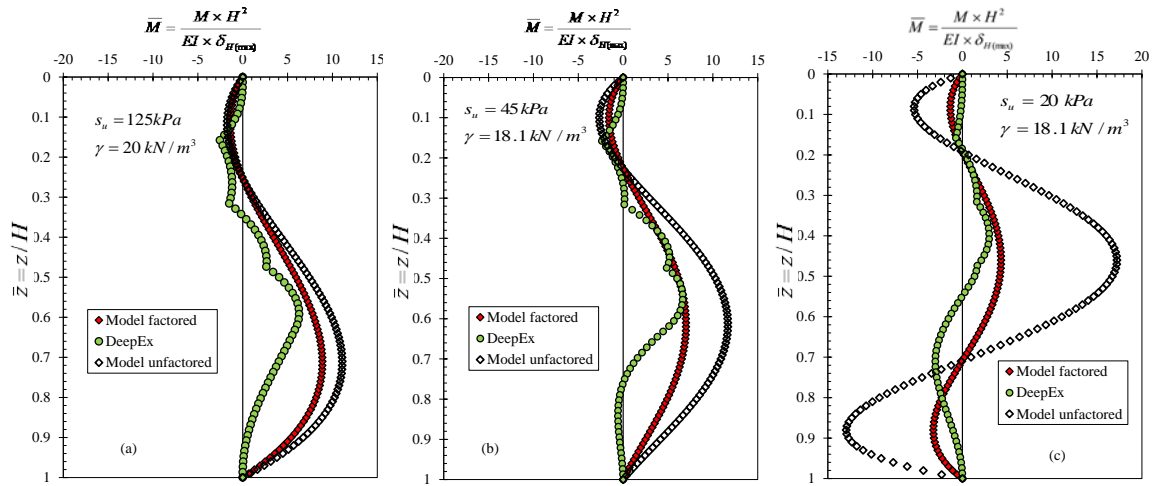


Fig. 6-7. Model Bending Moment versus Proposed Bending Moment Distribution: (a) Stiff Clay; (b) Medium Clay; (c) Soft Clay

7 Conclusions

Using the t-z approach and the two softening models presented, the calculated response of the anchors was satisfactory; however, more research is necessary to calibrate the softening models curves under ultimate conditions for ground anchors installed in shale. Although the displacement measured at the anchor head during a performance or proof test in anchors is mostly due to the elongation of the unbonded length; the presented softening models can be used to estimate the post peak response of ground anchors.

Although some slippage was observed between the strain gages and the strands, load-transfer mechanism along the bonded length was identified using strain gages; it was noted that slippage increased as the anchor head load increased. After the construction period and during the long-term monitoring, only minor variations in the strain gage data were observed suggesting that the anchor bonded length reached equilibrium and that these anchors installed in the shale stratum did not show significant creep susceptibility.

Based on the data collected in the gage installed 3.4 m. It is believed that anchor load was distributed from the top of the bonded length to this location; therefore, confirming a satisfactory anchor bonded length. Based on the presented approach the prediction of load-displacement curve for the anchors is more influenced by the selected ultimate side frictional resistance along the anchor-rock interface than the shear stiffness of the interface.

To define clearly the load transfer characteristic and degree of softening of anchors installed rock, it is necessary the analysis of additional pullout tests under ultimate load conditions. Load test where the peak and residual load are obtained are fundamental to calibrate the presented softening models.

The results show that the use of the two soldier-pile walls significantly improved the stability in the slope in consideration. Measured lateral deformations showed smaller values that commonly reported values in literature for this type of walls. It was identified that installing the soldier piles in the bedrock had a beneficial effect in controlling the lateral deformations.

Although both wall were parallel, it seems that the upper wall construction activities showed a greater correlation with the slope movements. Additionally, during excavation

of the upper wall, it was observed a decrease in the pore water pressures that tended to increasing during backfilling. Long-term data showed that the two walls effectively control the stability problems in the area and preserve the bridge foundation.

Construction sequence considerably affect the performance of the installed tie-back walls. Although the flexural capacity of both wall was not reached, the bending moment below the lowest row of anchors were opposite as the predicting using apparent earth pressures.

Observed performance of both tieback walls showed that for both walls, positive bending moments tend to increase with time while negative to decrease. In this study, the positive bending moments caused tension in the backside of the wall. The estimated bending moments using common design methodologies showed a clear discrepancy with the moments calculated from the strain gages; the main reason for this difference is attributed to the construction sequence of both walls.

During backfilling activities, a notable variation in the axial load along the walls was observed. Apparently, friction developed between the backside of the walls and the backfilling material was the reason the increase in the axial load. In general the location of the maximum moment was below the lowest row of anchors and the embedded toe of the walls; presumably, this value was achieved during intermediate states of construction during backfilling the walls. At the embedded portion of the walls, the walls bending moments remain almost constant.

A fair estimation of the bending moment distribution along the soldier piles was computed from inclinometer data. Even though part of the data was discarded due to disturbances during backfilling, estimation from survey data seems reasonable. Observed tendency in the anchor loads was to decrease with time; although, at the end of the monitoring period the change in loads was negligible.

From the database presented, the proposed empirical relationships show a good agreement with observed data reported in the literature. The discrepancy in lateral wall deformation observed with the stiff clay data can be attributed to the mixed-in-place (MIP) wall used to limit the lateral deformations in the presented validation. Nevertheless, the other two proposed distributions, show a satisfactory agreement with the measured data.

Validation with the software DeepEx showed a good agreement between the proposed distribution and the numerical calculations. However, more efforts are necessary to adjust the proposed relationship to a more exact distribution of bending moment. The proposed relation was derived from a continuous function adjusted to the inclinometer data, therefore, any concentrated bending moment along the wall, as a result of construction procedures, is not included and it has to be analyzed differently.

Bending moment along the wall is highly influenced by the construction sequence. The aforementioned relationships in the empirical methods were based on a typical construction sequence where no special excavation conditions are considered.

Further analysis with more advanced constitutive models and computational methods are necessary to address the proposed distribution of lateral deformation and bending moments; so far, the results from the empirical methodology are encouraging. Additionally, field validation of the proposed bending moment distributions is required.

Appendix A

Tieback Notes

During the development of this thesis some note about the design of tieback wall were developed. This appendix presents these notes; Appendix B presents the handouts developed for the notes.

Tieback Wall

- A tieback wall is wall that uses prestressed grouted anchors installed in soil/rock to transmit a tensile load to the ground.
- Tieback walls are commonly used to stabilize excavations temporarily or permanently.
- Anchored wall support relies lateral resistance provided by the ground anchors to resist horizontal pressures as well as the support provided through the shear and bending stiffness of the vertical wall elements and passive resistance from the soil below the finished excavation grade.

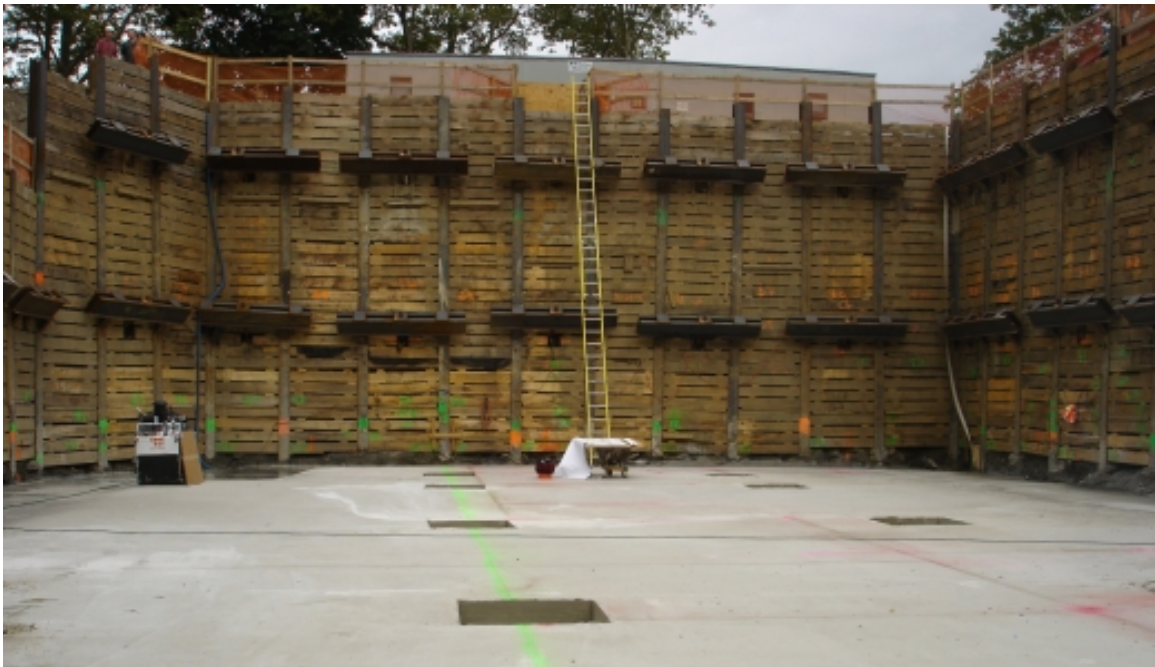


Fig. A-1 Tieback wall.

The tieback element of the wall can be broken down into three components: (See Handout 1)

- The anchorage: Anchor Head, Bearing Plate, and Trumpet

- Unbonded length: Portion of prestressed steel which is free to elongate elastically and transfers the resisting force from the bond length to the tieback wall
- Bonded Length: Portion of ground anchor that is bonded to the grout and is capable of transmitting the applied force to the surrounding ground. This portion of the anchor should be placed behind the critical failure surface.

Types of Tieback Walls

Several construction materials and methods are used for the wall elements of an anchored wall. These wall elements can be classified as discrete and continuous.

- Discrete wall elements: Consist of steel piles or drilled shafts that are spanned by a structural facing. Permanent facing can be precast concrete panels, cast-in-place concrete and timber lagging. These wall systems can be constructed in most ground types, however, in cohesionless soils and soft clays that may have limited “stand-up” time for lagging installation. These wall systems are also highly pervious. Horizontal spacing of the soldier beams typically varies from 5ft to 10ft.
- Continuous wall elements: Include steel sheet-piles, diaphragm walls, tangent/secant piles and jet-grouted columns. These walls do not require separate structural facing. Unlike soldier beam and lagging walls, continuous walls act as both vertical and horizontal wall elements. Because of the relative continuity of these wall systems, water pressure behind continuous walls must be considered in design.

Ground Anchor Types

Main types of ground anchors are presented in Handout 1. The three common types used in the United States. These ground anchors are:

- Straight-Shaft gravity-grouted
 - Typically installed in rock or stiff to hard cohesive soil
 - Installed using either rotary drilling or hollow-stem auger
 - Tremie (gravity displacement) methods used to grout anchors
 - Borehole can be cased if stability of borehole is an issue.

- Anchor resistance to pullout is based on shear resistance at the grout/ground interface
- Straight-Shaft pressure-grouted
 - Typically installed in coarse granular soils, weak fissured rock, or fine-grained cohesionless soils
 - Installed using either hollow-stem auger or rotary techniques with drill casing
 - Grout is injected into the bonded section at a pressure greater than 50psi
 - Grout is injected as either the auger or casing is withdrawn until the entire bond length is grouted
 - Advantage of pressure grouted over gravity grouted in terms of resistance to pullout
 - Increases the normal stress resulting from compaction of surrounding material around the grout bulb.
 - Increases the effective diameter of grout bulb
- Post-grouted
 - Initial grout is placed using gravity grout methods
 - Additional grout is placed 1-2 days after initial grout placement
 - Accomplished by use of sealed grout tube that is installed with tendons
 - Tube is equipped with check valves in the bonded length that allow for additional grout to be injected into the initial grout
 - High pressure grout fractures initial set grout and wedges it into the surrounding soil which enlarges the grout body

Tieback Wall Construction Sequence

- Installation of the wall element; soldier piles, tangent/secant piles, sheet pile, etc.
- Excavation in front of wall to just below elevation of the first row of ground anchors. For discrete walls, excavation is done in lifts of 4 to 5 ft. followed by installation of lagging. The soil face should be excavated to create a reasonably smooth contact surface for the lagging.
- Installation of first row of anchors.

- Continue excavation down to next set of anchors and install lagging. This cycle of excavations, lagging installation continues until the excavation depth is reached (See Handout 2)

Tendon Material

- Bar and Strand Tendons are used for soil and rock anchors
- Bar tendons are available in diameters of 1-3 inches and uncouple bar lengths up to 60ft. When longer sections are needed, the bars can be coupled.
- Strand tendons consist of multiple wire strands. Strands normally come in 0.5-0.6 inch diameter. Unlike bar systems, strand can be produced in any length. (See Handout 3)

Ground Anchor Design

- An anchored wall system conceptually is a stable mass of soil that will resist external failure modes at an adequate level of serviceability.
- The procedure to design a tieback wall is the following:
 - Calculate the ground anchor loads using apparent pressure diagrams.
 - Location of the critical potential failure surface.
 - Design of the unbonded and bonded lengths of the anchor.
 - Allowable load requirements for prestressing steel element.
 - Horizontal and Vertical spacing and inclination of the anchors.

Apparent Pressure Diagrams

- Earth pressures acting on an anchor installation depend not only on soil strengths but also on wall and soil stiffnesses, anchor spacing, anchor yield, the pre-stress locked into the anchors as installed and loss of pre-stress with time.
- Terzaghi and Peck (1967) and Peck (1969) developed apparent earth pressure diagrams to compute loadings of struts in braced excavations. Apparent earth pressure envelopes has resulted in reasonable estimates of ground anchor loads and conservative estimates of wall bending moments between anchors for flexible walls.

- After Terzaghi and Peck (1967) several authors that proposed earth pressures envelopes; Schnabel (1982), Winter (1990), Ulrich (1989) and the Federal Highway Administration in the publication FHWA-IF-99-015.
- Peck 1969 earth pressure envelopes (See Handout 4)
- Federal Highway Administration in the publication FHWA-IF-99-015 (See Handout 5)

If the soil behind the wall is a cohesionless soil, then the following equations will be used to find the maximum ordinate

- Total Load for Cohesionless soils

$$P = 0.65 \cdot K_a \cdot \gamma_s \cdot H^2$$

$P = \text{Total Load}$

$K_a = \text{Coefficient of active lateral Earth Pressure}$

$\gamma_s = \text{Total unit weight of soil}$

$H = \text{Wall height}$

- Single Level of Anchors

$$\sigma_a = \frac{P}{\frac{2}{3} \cdot H}$$

- Multi-Level Anchor System

$$\sigma_a = \frac{P}{H - \frac{1}{3}(H_1 + H_{n+1})}$$

Where:

$H_1 = \text{Distance from ground surface at top of wall to uppermost level of anchors}$

$H_{n+1} = \text{Distance from ground at bottom of wall to lowermost level of anchors}$

$n = \text{number of anchor levels}$

If the soil behind the wall is cohesive, then first the stability number needs to be determined to classify the soil as either “stiff to hard” or “soft to medium”. The equation for stability number (N_s) is defined as:

$$N_s = \frac{\gamma_s H}{S_u}$$

Where;

S_u = Average undrained Shear Strength

γ_s = Total unit weight of soil

H = Excavation depth

- If $N_s \leq 4$, then the soil is considered stiff to hard and the following equation is

used to determine the maximum ordinate (σ_a) of the earth pressure envelope:

$$0.2 \gamma_s H \leq \sigma_a \leq 0.4 \gamma_s H$$

- If $N_s \geq 5.14$, then the soil is considered soft to medium and the equation used for determining the maximum ordinate is :

$$\sigma_a = K_a \gamma_s H$$

Where the value of the coefficient K_a is obtained as follows

If $N_s \geq 5.14$

$$K_a = 1 - \frac{4 \cdot S_u}{\gamma \cdot H} + \frac{2\sqrt{2} \cdot d}{H} \left(1 - \frac{5.14 \cdot S_{ub}}{\gamma \cdot H} \right)$$

for $4 < N_s < 5.14$

$$K_a = 0.22$$

S_u = Undrained shear strength of the soil through which the excavation extends

S_{ub} = Undrained strength of the soil providing bearing resistance

γ_s = Total unit weight of soil

d = Depth to potential failure surface

H = Excavation depth

Load in stratified Soil profiles

- In stratified soil profiles, the following approach can be used to evaluate earth pressures acting on the wall.
 - Evaluate the total active earth pressure acting over the height of the wall; used conventional analysis methods or trial wedge stability analysis assuming full mobilization of soil shear strength.
 - Apply a factor of safety to the total load computed, usually a factor of 1.3 is applied.
 - Distribute the total force into an apparent earth pressure diagram

Note: When potential failure surfaces are deep-seated or surcharge loading is irregular, slope stability analysis may be used to calculate earth pressure loading. (See Handout 6)

Water Pressures

- For temporary systems water pressures associated with static conditions and with seepage behind and beneath the wall; water pressures can be computed using the simplified procedure presented by the FHWA- IF-99-015. (See Handout 7)
- For permanent systems water is usually collected using drainage elements between the facing of the wall and the retained soil therefore the wall is not design to resist this pressures.

Earth Pressures Due to Surface Loads

- For uniform surcharge loads the lateral stress can be computed as

$$\Delta\sigma = K_a \cdot q_s$$

Where:

$\Delta\sigma$ = Increase in lateral earth pressure

K = Appropriate earth pressure coefficient

q_s = vertical surcharge load

- Point loads, line loads, and strip loads are typically calculated using equations based on elasticity theory for lateral stress distribution with depth

Ground anchor loads

- Ground anchor loads can be estimated from apparent earth pressure envelopes. Methods commonly used include the tributary area method and the hinge method. (See Handout 8)
- Both methods assume a hinge support (i.e., no bending moment) at the excavation subgrade.
- For walls constructed in competent materials, the reaction force is assumed to be supported by the passive resistance of the soil below the excavation subgrade. In this case, the lowest anchor carries only the tributary area of the apparent pressure diagram, and the reaction force is equivalent to the load from the apparent pressure diagram from the base of the excavation to the midheight between the base of the excavation and the lowest anchor.
- For walls that penetrate weak materials, sufficient passive capacity below the base of the excavation may not be available to resist the reaction force regardless of the wall embedment depth. In this case, the lowest anchor may be designed to carry the tributary area of the apparent pressure diagram plus the load corresponding to the reaction force.
- The values calculated using the earth pressure envelopes are the horizontal component of the anchor load per unit width length of wall. The anchor load for designing the bond zone can be calculated as:

$$T = \frac{T_{hi} \cdot s}{\cos(\theta)}$$

Where:

T = Total anchor load

T_{hi} = Horizontal component of the anchor load per width

s = Horizontal spacing between anchors

Critical Potential Failure Surface

- It is important to know the location of the failure surface in the soil behind the wall for placement of the bonded length; the bonded length must be located sufficiently behind this surface such that the load is not transferred from the bond zone into the failure zone.
- In general, the minimum distance that the unbonded length is extended past the critical failure surface is the larger between $H/5$ where H is the height of the wall or 5 ft.
- For Cohesionless soils, the failure surface is assumed to extend from the corner of the excavation at an angle of $45 + \frac{\phi'}{2}$ from the horizontal.

Design of the Unbonded Length

- The minimum length is 15ft (4.5m) for strand tendons and 10ft(3m) for bar tendons (Sabatini et al. 1999)
- These minimum are set to prevent reductions in load from seating losses from load transfer to the structure after anchor load testing
- Longer unbonded sections could be required due to the following reasons:
 - To have the bond length a minimum distance behind the failure surface
 - To locate the anchor bond in suitable ground conditions
 - Ensure system stability
 - Accommodate long-term movements

Ground Anchor Spacing

- The minimum horizontal spacing between the ground anchors is 4 ft. to ensure that group effects between the anchors are minimized and to ensure that anchors don't intersect as a result of drilling deviations

Ground anchor capacity

- The capacity of an anchor in the field depends on:
 - Method of Drilling: drill hole cleaning quality & period left open

- Diameter of drill hole
- Method and pressure used for grouting
- Length of anchor bond zone
- Designer is responsible for defining the minimum capacity for a given soil condition
- The estimation of the anchor capacity should be based on the simplest installed anchor, the straight-shaft gravity-grouted anchor
- Bonded Length is designed based on the following equation:

$$L_b = \frac{T * FS}{\pi d S_b}$$

L_b = Bonded Length

T = Anchor design load

FS = Factor of safety for Ultimate Bond Strength

d = Diameter of drill hole

S_b = Average Ultimate Bond Strength at the soil/grout interface

- For prestressing steel, the safety factor should not be less than 1.67 (PTI, 2014)
- The average ultimate Bond strengths for cohesive and non-cohesive soils can be found in the tables on Handout 10
- The anchor capacity will be verified by field testing once installed

Depth of Embedment of Wall

- The process of finding the depth of embedment is based on force or moment equilibrium. This would include the active and passive forces on the wall below the excavation. See the example #1 for process of using moment equilibrium.

Effective width

- For soldier pile systems an effective width (b) is determined to compute active and passive forces below the excavation level.

- The effective width is generally considered to be the dimension of the soldier pile parallel to the wall; for driven piles is the dimensions of the soldier pile and drilled piles backfilled with concrete is the diameter of the drilled-hole.
- When soil arching is considered the effective width of a soldier pile can increase up to 3 times for granular soil and 2 times for cohesive soils. See tables

$$\text{Adjusted width} = \text{Effective Width} * \text{Arching Capability Factor}$$

Table A.1 Arching factor. (After CALTRANS (2011))

| <i>Pile spacing (s)</i> | <i>Arching capability factor</i> |
|-------------------------|----------------------------------|
| $\leq 3 \cdot b$ | 3 |
| $> 3 \cdot b$ | $0.08 \cdot \phi (\leq 3)$ |

Table A.2 Arching capability factor for cohesive soil (After CALTRANS (2011))

| <i>Consistency</i> | <i>Very soft</i> | <i>Soft</i> | <i>Medium</i> | <i>Stiff</i> | <i>Very stiff</i> | <i>Hard</i> |
|----------------------------------|------------------|-------------|---------------|--------------|-------------------|-------------|
| q_u (psf) | 500 | 100 | 2000 | 4000 | 8000 | |
| <i>Unit weight</i> (psf) | 100-120 | 100-130 | | 120-140 | 130+ | |
| <i>Arching capability factor</i> | 1 to 2 | 1 to 2 | 2 | 2 | 2 | |

Other Notes for Ground Anchors

- For both vertical sheet-pile walls and soldier beam walls, the anchor design load will generally range between 60kips and 260kips (260kN and 1160kN).
- The total length of anchor is generally between 30 and 60ft (9-18m).
- Ground anchors are usually installed at angles of 15-30 degrees
- The center of anchor bond zones must have a minimum of 15ft of overburden to prevent grout leakage during installation of anchors and to prevent heave at ground surface from large grouting pressures.

Wall System Design

Wall Section

- For sheet pile systems, the wall section can be found based on the maximum moment as determined by tributary area or the hinge method.
- Based on the hinge method results, plot the shear and bending moment diagram. In this plotting, ignore the embedded section of the wall. Determine the Maximum moment from the bending moment diagram.

Steel

Section Modulus:

$$S_{wall} = \frac{M_{max}}{F_b}$$

S_{wall} = Section modulus of Steel section

$$F_b = 0.55 F_y$$

F_y = yield strength of the steel

- Based on the Section Modulus, use manufacturing guides to determine the required member to be used. AZ sheet Piles are commonly used. A sample manufacturing guide is provided in Handout 11

Concrete

- For concrete piles, the maximum moment of the wall has to be compared to the nominal moment of the designed reinforced pile.

$$0.9 * M_n \geq M_{max}$$

$$M_n = A_s * f_y \left(d - \frac{a}{2} \right)$$

M_n = Nominal Moment

A_s = Area of Reinforcing Steel

f_y = Yield Strength of Reinforcing Steel

d = distance from top of beam to reinforcing concrete

$$a = \frac{A_s f_y}{0.85 f'_c b}$$

f'_c = compressive strength of concrete

b = width of the column

Wales and Permanent Facing

- Wales are often used in anchored walls, they are used to transfer the lateral soil load forces to the wall.
- Normally a double channel member is used as walling.
- The design moment for wales and support facing depend on the support condition and soil condition

Table A.3 Arching capability factor for cohesive soil

| Support and soil condition | Design moment M_{\max} |
|---|-------------------------------|
| Simple span – soft cohesive soils; rigid facing placed against soil. | $\frac{\sigma \cdot l^2}{8}$ |
| Simple span – granular cohesive soils or stiff cohesive soil; | $\frac{\sigma \cdot l^2}{12}$ |
| Continuous facing – soft cohesive soil; rigid facing | $\frac{\sigma \cdot l^2}{10}$ |
| Continuous facing - granular cohesive soils or stiff cohesive soil | $\frac{\sigma \cdot l^2}{12}$ |

(After AASHTO 1996)

Where:

σ = maximum ordinate of the total earth pressure envelope

l = span between supports

Note: Continuous spans are considered than extends more than three supports.

The required section modulus of the wale is calculated as:

$$S_{wale} = \frac{M_{max}}{F_b}$$

Where:

M_{max} = *desing moment*

$F_b = 0.55 \cdot F_y$

F_b = *allowable bending stress*

F_y = *yield stress of the steel*

- Once the section modulus is determined, use the AISC Manual to determine member required. Sample can be found in Handout # #_.4.
- For concrete facing
- Permanent facings that are cast-in-place (CIP) are typically 200 to 300 mm thick.

Timber Lagging

- Timber lagging is also used as temporary facing is placed usually between the flanges of the piles; also can be placed Lagging placed behind the front flange may be and transfers the lateral soil load to the soldier pile system similar to the wales.
- Due to flexibility of the timber lagging and the soil arching capability, the maximum earth pressure is multiplied by a reduction factor of 0.6; therefore the maximum moment on the lagging is calculated as:

$$M_{max} = 0.6 \frac{\sigma \cdot l^2}{8}$$

Where:

M_{max} = *desing moment*

σ = *maximum ordinate of the total earth pressure envelope*

l = *span between supports*

Note: For the arching effect to occur the backside of the soldier pile must bear against the soil.

- The section modulus is determined

$$S_{req} = \frac{M_{max}}{F_b}$$

Where:

S_{req} = required section modulus

F_b = allowable bending stress in the timber lagging

Minimum Recommended timber thicknesses are presented in Handout 12.

Safety factor against basal heave

For tieback walls are constructed in clays, heave can occur in the bottom of the excavation when weight of the retained soil exceeds or approaches the soil bearing capacity at the base of the excavation.

$$FS = \frac{S_u \cdot N_c}{(\gamma_s + q_s/H - S_u/B) \cdot H}$$

Where:

B' = minimum of $B/\sqrt{2}$ or T

B = Width of the excavation

T = Depth to hard stratum below the excavation

q_s = Surcharge loading

γ_s = Unit weight of the soil

N_c = Bearing capacity factor

S_u = Undrained shear strength

H = Excavation depth

(See Handout 13)

External Stability

External Stability of anchored systems is commonly address using conventional methods for slope stability. A minimum factor of safety of 1.3 is required for potential slip surfaces passing behind or through the anchors

For walls with multiple levels of anchors, failure surfaces that pass behind each anchor should be checked. Where external stability requirements cannot be met, the anchors may be lengthened or methods to improve anchor bond or load transfer mechanisms may be used.

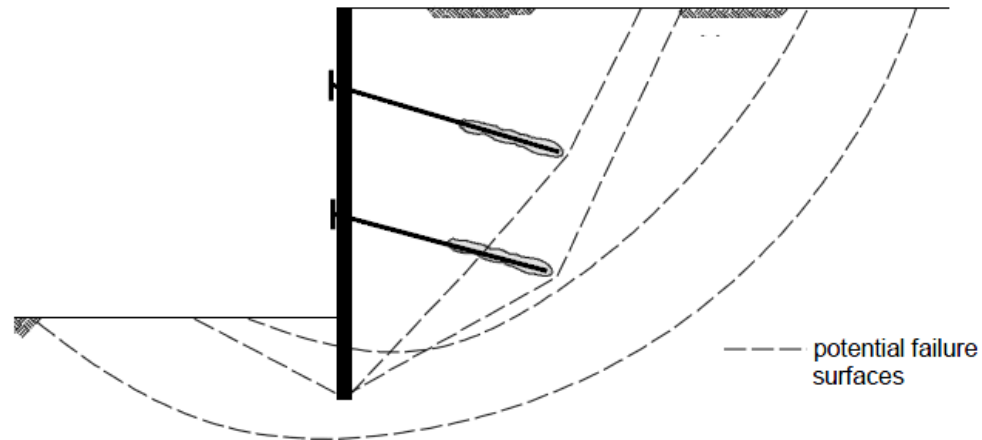


Fig. A-2 Tieback wall.

Ground Anchor Load Testing

- Each ground anchor is tested before it is allowed to be put into service.
- Testing of each anchor occurs at the ground surface and consists of tensioning the prestressing the anchor and measuring the load and movement.
- Load testing normally consists of the following equipment:
 - Hydraulic jack and pump: used to apply the load to anchor
 - Stressing anchorage: used in front of jack head to grip prestressing element during loading.
 - Pressure gauges and load cells: used to monitor pressure of jack pump and determine load applied.
 - Dial gauge: used to measure movement
- Acceptance of ground anchor depends on the results from one of three separate tests: performance tests, proof test, and extended creep test

Performance Test

- This test involves incremental loading and unloading cycles of a ground anchor. The maximum applied load during the test vary between 120 and 150 percent the

design load of the anchor; however, 133 percent of the design load is the common practice.

- Performance test is used to verify the following:
 - Anchor Capacity
 - Establish load-deformation behavior
 - Identify any causes of anchor movement
 - Verify the unbonded length is equal to or greater than anchor design
- First step in performance test is to apply and alignment load of approximately 5% of the design load which ensures stressing and testing equipment are properly aligned.
- Multiple cycles are performed increasing the maximum load applied between each load cycle.
- From the recordings from the performance test, the elastic movement can be determined and used to determine if the anchor meets the acceptability criteria.
- For soil anchors, the elastic movement at the test load must exceed a specified minimum value.
- If acceptable, a lock-off load is applied before taking off testing equipment. If not accepted, please see acceptance criteria section below.

Proof Test

- Involves a single load cycle and holding a load for a period of ten minutes.
- The loading schedule of this test is the same as the load test for the performance test.
- If test results meet the acceptance criteria for total movement, then the load is reduced to the lock-off load.
- If results of test are not accepted, then see section below titled acceptance criteria.

Extended Creep Testing

- This test is required when anchors are installed in cohesive soils having a $PI > 20$ or a $LL > 50$.
- Test evaluates the creep deformation of the anchor installed.

- The load schedule used in extended creep test can be seen on Handout 14.
- The results of this test are plotted creep movement vs time with time being on a log scale. Creep movement is defined as the difference between the total movement and the movement at 1 minute for each increment.
- The creep rate is found as the slope of the curve per log cycle of time. This rate is calculated for each curve and then that value is compared to the maximum specified rate.
- If accepted, the anchor load is set to the lock-off load, if not meet, see acceptance criteria in the following section.

Testing Acceptance Criteria

The acceptance of an anchor is based on the creep and elastic movement of the anchor during the testing.

Creep

- Acceptance criteria for creep, in performance or proof testing, demand a maximum movement of 1mm between 1 and 10 minutes. If the movement is less than 1mm then the anchor meets creep acceptance. If not accepted during the 1 to 10 minute criteria, the anchor is held at that load for an additional 50-minute period. If the total movement is less than 2 mm from 6 to 60 minutes then it is accepted.
- Acceptance criteria for extended creep test, the total movement of any load hold should not exceed 2mm per log cycle over the final log cycle of time of each load increment.

Apparent Free Length

- Elastic movement criteria acceptance is based on a calculation of apparent free length. Apparent free length is the length of the tendon not bonded to the surrounding ground or grout as measured from the elastic movement at the test load.
- The apparent free length has to be greater than a minimum specified apparent free length.
- Minimum Apparent Free Length Criterion:

$$L_{a,\min} = 0.8 * \text{Unbonded length} + \text{jack length}$$

- Apparent Free Length in meters, L_a , is calculated using the following equation

$$L_a = \frac{A_i E_s \delta_e}{P} * \frac{1}{10^9}$$

A_i = Cross Sectional Area of Prestressing steel (mm^2)

E_s = Young's Modulus (kPa)

δ_e = Elastic Movements at the Test Load (mm)

P = Test Load (kN) - Load Alignment load (kN)

- The possible options of how these tests could ultimately turn out can be found in the decision tree in Handout 14.

Appendix B

Handouts for the Tieback Notes

Handout 1 Components of a Ground Anchor

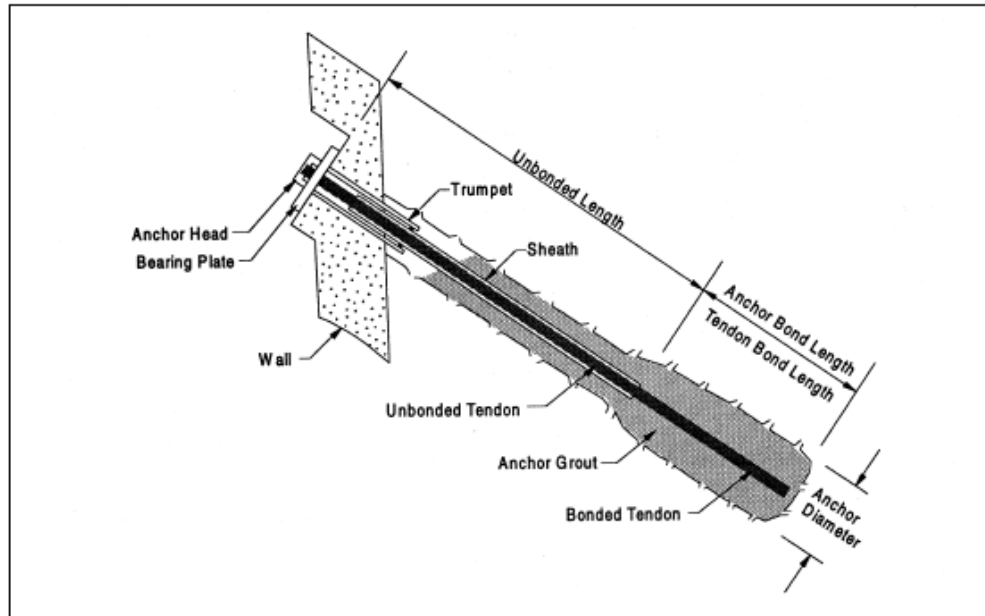


Fig. B-2 Components of a ground anchor (Sabatini et al. 1999)

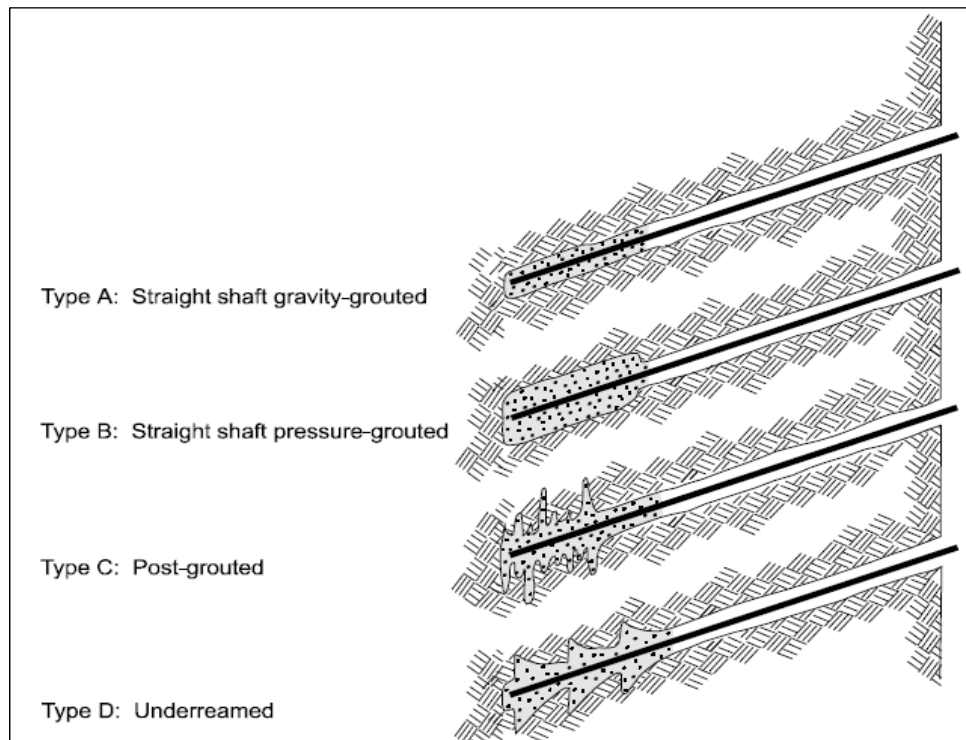
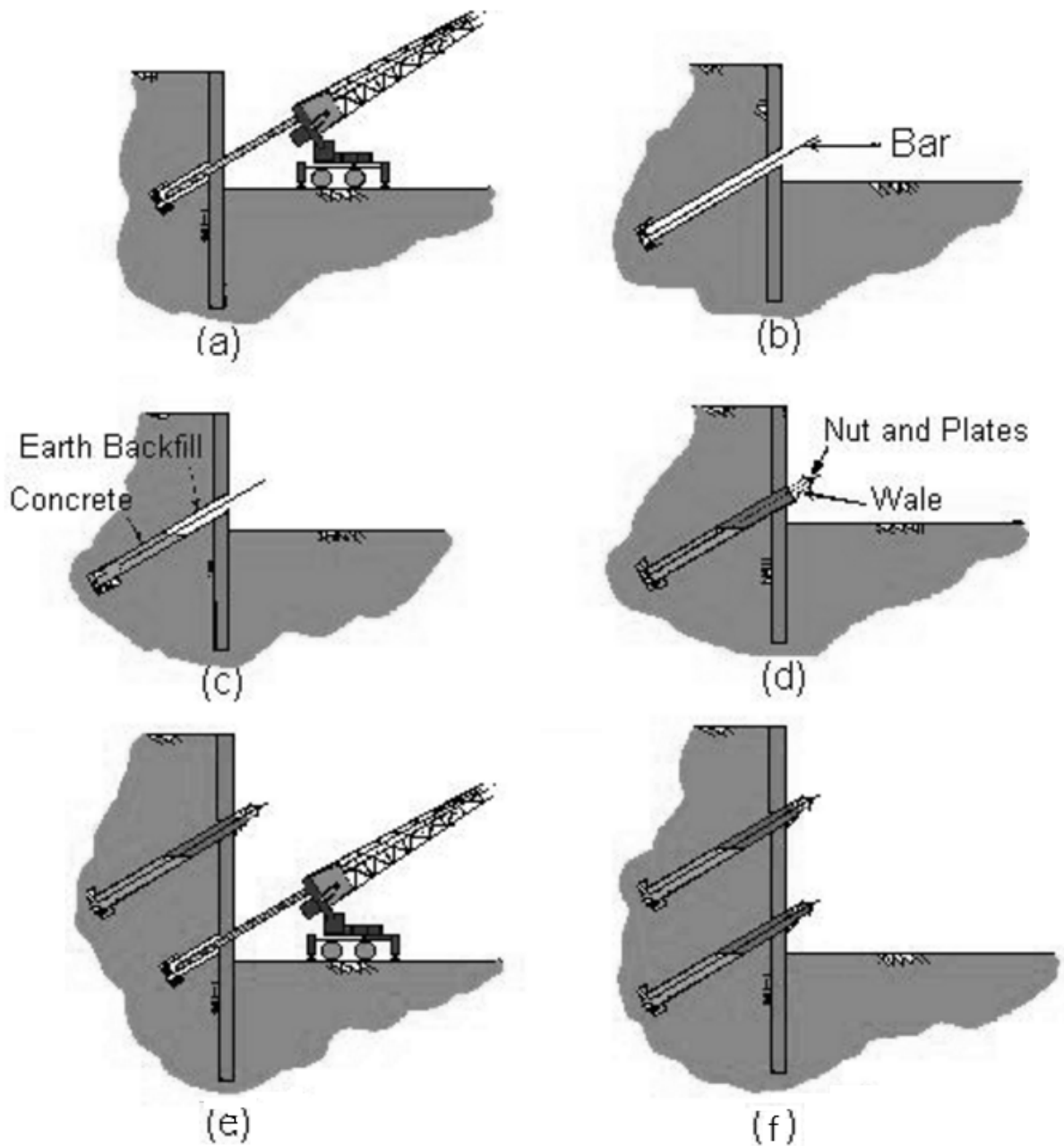


Fig. B-2 Types of grouted anchors (Sabatini et al. 1999)

Handout 2 Typical Construction Sequence



- (a) Excavation to the first level of anchors and hole drilled.
- (b) Tendon placed in hole.
- (c) Concrete poured around anchor.
- (d) Wall connection made.
- (e) Excavation to the next level.
- (f) Installation of the next level of anchors.

Fig. B-3 Typical Construction Sequence

Handout 3 Tendon Materials



Grout Bonded MCP Anchors

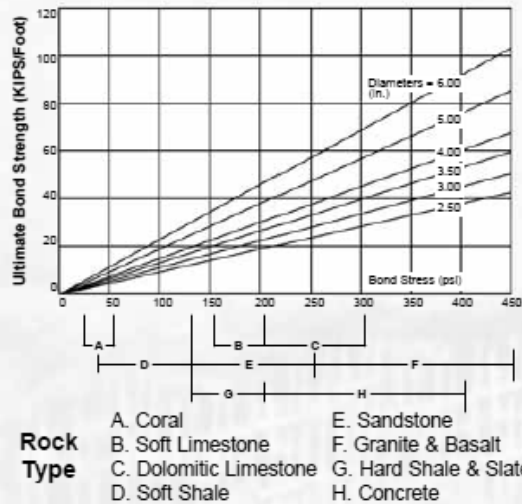
Multiple Corrosion Protection Anchors

Williams standard grout bonded rock & soil anchors consist of a plain or epoxy coated bar, grouted in an oversized drill hole. Centralizers should be used to assure good grout cover (approximately 25 mm) around the bar. Where anchors will penetrate aggressive soils that are low in pH value (<5.5) and high in sulfate, additional corrosion protection may be desirable. The degree of protection should be matched against the aggressivity of the environment and the expected life of the anchorage system. Williams Multiple Corrosion Protection (MCP) systems offer increasing barriers against corrosion attack for confidence in permanent anchorage in all ground environments. Williams protective outer end caps may also be used to seal the nut and washer from the environment when the outer end of the anchorage will not be encased in concrete.

Typically, Williams MCP anchors are supplied in 150 KSI All-Thread Grade (as shown below) and used in various applications such as externally supported earth structures and tension tie-down systems.



Ultimate Bond Strength
Per Linear Foot of Cement Grout by Diameter of Drill Hole



150 KSI All-Thread Bar

| Bar Diameter | Minimum Net Area Thru Threads | Minimum Ultimate Strength | Minimum Yield Strength |
|----------------|--|---------------------------|------------------------|
| 1" (26 mm) | 0.85 in ² (549 mm ²) | 128 kips (567.1 kN) | 102 kips (453.6 kN) |
| 1-1/4" (32 mm) | 1.25 in ² (807 mm ²) | 189 kips (834 kN) | 150 kips (667.2 kN) |
| 1-3/8" (36 mm) | 1.58 in ² (1019 mm ²) | 237 kips (1054.2 kN) | 190 kips (843.4 kN) |
| 1-3/4" (45 mm) | 2.60 in ² (1684 mm ²) | 400 kips (1779.2 kN) | 320 kips (1423.4 kN) |
| 2-1/4" (57 mm) | 4.08 in ² (2632 mm ²) | 613 kips (2727 kN) | 490 kips (2181 kN) |
| 2-1/2" (65 mm) | 5.19 in ² (3350 mm ²) | 778 kips (3457.0 kN) | 622 kips (2765.8 kN) |
| 3" (75 mm) | 6.46 in ² (4169 mm ²) | 969 kips (4311 kN) | 775 kips (3448 kN) |

For complete 150 KSI All-Thread-Bar chart see page 62.

For Grade 75 All-Thread Rebar strengths, see page 64

Structural Properties

| Bar Type | Yield Stress | Ultimate Stress | Typical Elongation | Reduction of Area |
|----------|---------------------|--------------------|--------------------------|-------------------|
| 150 KSI | 127.7 KSI (881 MPa) | 150 KSI (1034 MPa) | 4% over 20 bar diameters | 20% |
| Grade 75 | 75 KSI (517 MPa) | 100 KSI (699 MPa) | 6% - 7% in 8" bar | - |

Notes: If overall length is over 50' (or 45' for 3" diameter), anchor coupling should be located in bond zone with field-applied barrier, such as heat shrink tube installed across splice joint. At minimum drill hole size, centralizers will only fit around anchor in the bond zone. Drill hole diameters and bond lengths are based on geologic conditions. Consult your geotechnical engineer for recommendations.



Fig. B-4 Tendon materials

Strand Anchor Systems



Strand Anchor System - ASTM A416

| Number of Strands | Cross-Sectional Area (Aps) | Ultimate Load (fpu*Aps) | Maximum Jacking Load (0.8*fpu*Aps) | Maximum Design Load (0.6*fpu*Aps) | HDPE Tubing | Anchor Heads | Weight per Foot |
|-------------------|---|-------------------------|------------------------------------|-----------------------------------|-----------------------|----------------------------------|----------------------|
| 1 | 0.217 in ² (140 mm ²) | 58.6 kips (261 kN) | 46.9 kips (209 kN) | 35.2 kips (157 kN) | 3" nom. (3-1/2" O.D.) | C4.6 | 0.74 lbs (0.34 kg) |
| 2 | 0.434 in ² (280 mm ²) | 117 kips (522 kN) | 93.8 kips (418 kN) | 70.4 kips (314 kN) | 3" nom. (3-1/2" O.D.) | C4.6 | 1.48 lbs (0.67 kg) |
| 3 | 0.651 in ² (420 mm ²) | 176 kips (783 kN) | 141 kips (627 kN) | 106 kips (471 kN) | 3" nom. (3-1/2" O.D.) | C4.6 | 2.22 lbs (1.01 kg) |
| 4 | 0.868 in ² (560 mm ²) | 234 kips (1044 kN) | 188 kips (836 kN) | 141 kips (626 kN) | 3" nom. (3-1/2" O.D.) | C7.6 - Class 1 C4.6 - Class 2 | 2.96 lbs (1.34 kg) |
| 5 | 1.09 in ² (700 mm ²) | 293 kips (1305 kN) | 235 kips (1045 kN) | 178 kips (785 kN) | 3" nom. (3-1/2" O.D.) | C7.6 | 3.70 lbs (1.68 kg) |
| 6 | 1.30 in ² (840 mm ²) | 352 kips (1566 kN) | 281 kips (1254 kN) | 211 kips (942 kN) | 3" nom. (3-1/2" O.D.) | C7.6 | 4.44 lbs (2.01 kg) |
| 7 | 1.52 in ² (980 mm ²) | 410 kips (1827 kN) | 328 kips (1463 kN) | 246 kips (1099 kN) | 3" nom. (3-1/2" O.D.) | C7.6 | 5.18 lbs (2.35 kg) |
| 8 | 1.74 in ² (1120 mm ²) | 469 kips (2088 kN) | 375 kips (1672 kN) | 282 kips (1256 kN) | 3" nom. (3-1/2" O.D.) | C9.6 | 5.92 lbs (2.69 kg) |
| 9 | 1.95 in ² (1260 mm ²) | 527 kips (2349 kN) | 422 kips (1881 kN) | 317 kips (1413 kN) | 4" nom. (4.6" O.D.) | C9.6 | 6.66 lbs (3.02 kg) |
| 10 | 2.17 in ² (1400 mm ²) | 586 kips (2610 kN) | 469 kips (2090 kN) | 352 kips (1570 kN) | 4" nom. (4.6" O.D.) | C12.6 | 7.40 lbs (3.36 kg) |
| 11 | 2.39 in ² (1540 mm ²) | 645 kips (2871 kN) | 516 kips (2299 kN) | 387 kips (1727 kN) | 4" nom. (4.6" O.D.) | C12.6 | 8.14 lbs (3.69 kg) |
| 12 | 2.60 in ² (1680 mm ²) | 703 kips (3132 kN) | 563 kips (2508 kN) | 422 kips (1884 kN) | 4" nom. (4.6" O.D.) | C12.6 | 8.88 lbs (4.03 kg) |
| 13 | 2.82 in ² (1820 mm ²) | 762 kips (3393 kN) | 610 kips (2717 kN) | 458 kips (2041 kN) | 4" nom. (4.6" O.D.) | C19.6 | 9.62 lbs (4.36 kg) |
| 14 | 3.04 in ² (1960 mm ²) | 820 kips (3654 kN) | 657 kips (2926 kN) | 493 kips (2198 kN) | 4" nom. (4.6" O.D.) | C19.6 | 10.36 lbs (4.70 kg) |
| 15 | 3.26 in ² (2100 mm ²) | 879 kips (3915 kN) | 704 kips (3135 kN) | 528 kips (2355 kN) | 4" nom. (4.6" O.D.) | C19.6 | 11.10 lbs (5.03 kg) |
| 16 | 3.47 in ² (2240 mm ²) | 938 kips (4176 kN) | 750 kips (3344 kN) | 563 kips (2512 kN) | 5" nom. (5.6" O.D.) | C19.6 | 11.84 lbs (5.37 kg) |
| 17 | 3.69 in ² (2380 mm ²) | 996 kips (4437 kN) | 797 kips (3553 kN) | 598 kips (2669 kN) | 5" nom. (5.6" O.D.) | C19.6 | 12.58 lbs (5.71 kg) |
| 18 | 3.91 in ² (2520 mm ²) | 1055 kips (4698 kN) | 844 kips (3762 kN) | 634 kips (2826 kN) | 5" nom. (5.6" O.D.) | C19.6 | 13.32 lbs (6.04 kg) |
| 19 | 4.12 in ² (2660 mm ²) | 1113 kips (4959 kN) | 891 kips (3971 kN) | 669 kips (2983 kN) | 5" nom. (5.6" O.D.) | C19.6 | 14.06 lbs (6.38 kg) |
| 20 | 4.34 in ² (2800 mm ²) | 1172 kips (5220 kN) | 938 kips (4180 kN) | 704 kips (3140 kN) | 5" nom. (5.6" O.D.) | C22.6 | 14.80 lbs (6.71 kg) |
| 21 | 4.56 in ² (2940 mm ²) | 1231 kips (5481 kN) | 985 kips (4369 kN) | 739 kips (3297 kN) | 6" nom. (6.6" O.D.) | C22.6 | 15.54 lbs (7.05 kg) |
| 22 | 4.77 in ² (3080 mm ²) | 1289 kips (5742 kN) | 1032 kips (4598 kN) | 774 kips (3454 kN) | 6" nom. (6.6" O.D.) | C22.6 | 16.28 lbs (7.38 kg) |
| 23 | 4.99 in ² (3220 mm ²) | 1348 kips (6003 kN) | 1079 kips (4807 kN) | 810 kips (3611 kN) | 6" nom. (6.6" O.D.) | C27.6 | 17.02 lbs (7.72 kg) |
| 24 | 5.21 in ² (3360 mm ²) | 1406 kips (6264 kN) | 1126 kips (5016 kN) | 845 kips (3768 kN) | 6" nom. (6.6" O.D.) | C27.6 | 17.76 lbs (8.06 kg) |
| 25 | 5.43 in ² (3500 mm ²) | 1465 kips (6525 kN) | 1173 kips (5225 kN) | 880 kips (3925 kN) | 6" nom. (6.6" O.D.) | C27.6 | 18.50 lbs (8.39 kg) |
| 26 | 5.64 in ² (3640 mm ²) | 1524 kips (6786 kN) | 1219 kips (5434 kN) | 915 kips (4082 kN) | 6" nom. (6.6" O.D.) | C27.6 | 19.24 lbs (8.73 kg) |
| 27 | 5.86 in ² (3780 mm ²) | 1582 kips (7047 kN) | 1266 kips (5643 kN) | 950 kips (4239 kN) | 6" nom. (6.6" O.D.) | C27.6 | 19.98 lbs (9.06 kg) |
| 28 | 6.08 in ² (3920 mm ²) | 1640 kips (7308 kN) | 1313 kips (5852 kN) | 986 kips (4396 kN) | 6" nom. (6.6" O.D.) | C31.6 | 20.72 lbs (9.40 kg) |
| 29 | 6.29 in ² (4060 mm ²) | 1699 kips (7569 kN) | 1360 kips (6061 kN) | 1021 kips (4553 kN) | 6" nom. (6.6" O.D.) | C31.6 | 21.46 lbs (9.73 kg) |
| 30 | 6.51 in ² (4200 mm ²) | 1758 kips (7820 kN) | 1407 kips (6270 kN) | 1056 kips (4710 kN) | 6" nom. (6.6" O.D.) | C31.6 | 22.20 lbs (10.07 kg) |
| 31 | 6.73 in ² (4340 mm ²) | 1816 kips (8091 kN) | 1454 kips (6479 kN) | 1091 kips (4867 kN) | 6" nom. (6.6" O.D.) | C31.6 | 22.94 lbs (10.41 kg) |
| 32 | 6.94 in ² (4480 mm ²) | 1875 kips (8352 kN) | 1500 kips (6688 kN) | 1126 kips (5024 kN) | 8" nom. (9-1/2" O.D.) | C37.6 | 23.68 lbs (10.74 kg) |
| 37 | 8.03 in ² (5180 mm ²) | 2168 kips (9657 kN) | 1735 kips (7733 kN) | 1302 kips (5809 kN) | 8" nom. (9-1/2" O.D.) | C37.6 | 27.38 lbs (12.42 kg) |
| 55 | 11.94 in ² (7700 mm ²) | 3223 kips (14337 kN) | 2578 kips (11468 kN) | 1934 kips (8603 kN) | 10" nom. (11.9" O.D.) | C55.6 | 40.70 lbs (18.46 kg) |
| 61 | 13.24 in ² (8540 mm ²) | 3575 kips (15901 kN) | 2860 kips (12722 kN) | 2145 kips (9541 kN) | 10" nom. (11.9" O.D.) | C61.6 | 45.14 lbs (20.48 kg) |

- 1) Mill certification provided upon request to indicate the actual tensile strength of the 7-wire strand with each shipment of Williams strand anchors.
- 2) Larger diameter anchors available upon request.
- 3) Minimum grout cover shall be 1/2" (13mm) over the OD of the encapsulation in a Class I Protected anchor and 1/2" (13mm) over the tendon bond length in a Class II protected anchor.



Fig. B-5 Strand Anchors

Handout 4 Recommended Apparent Earth Pressure (Peck 1969)

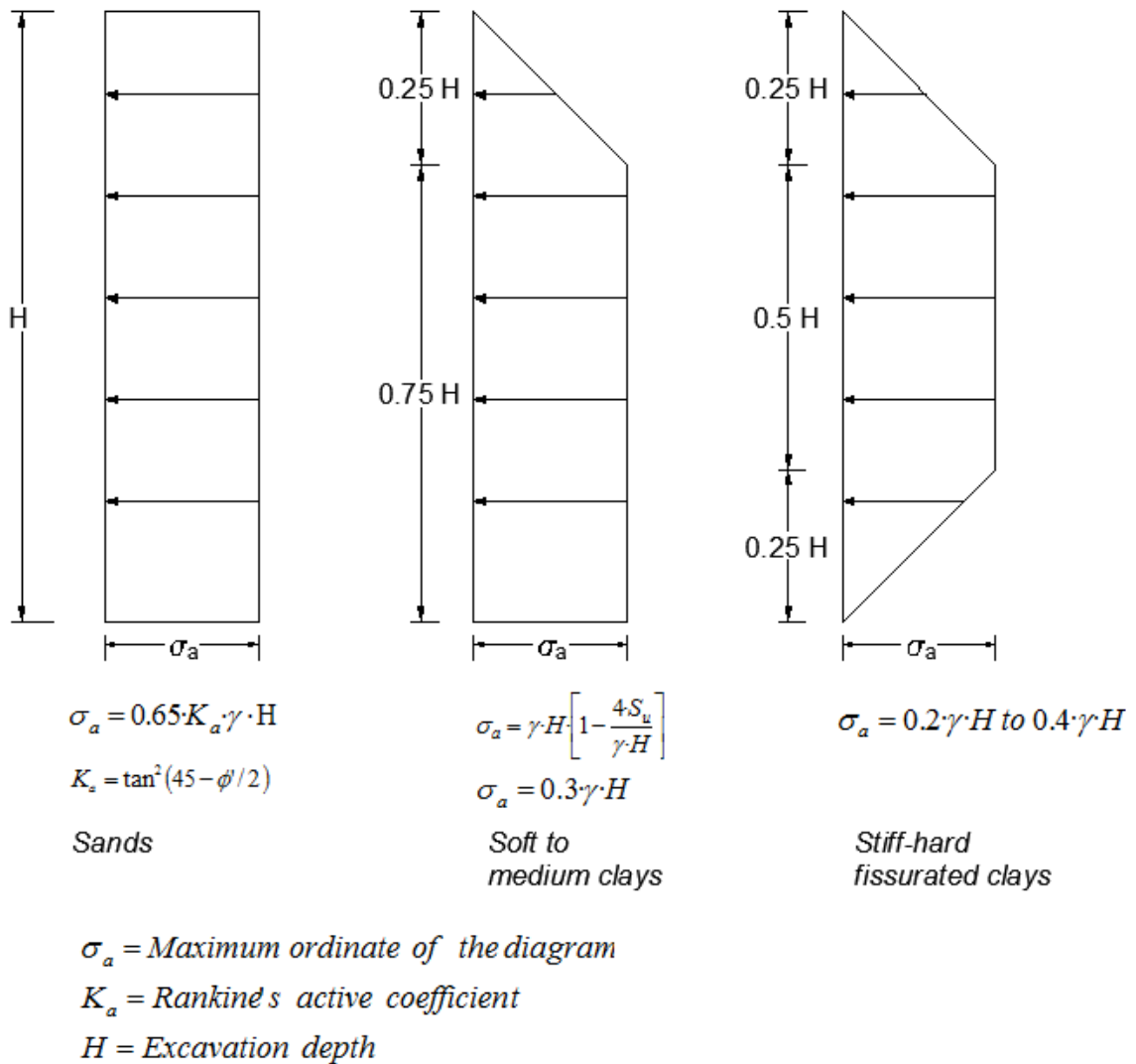


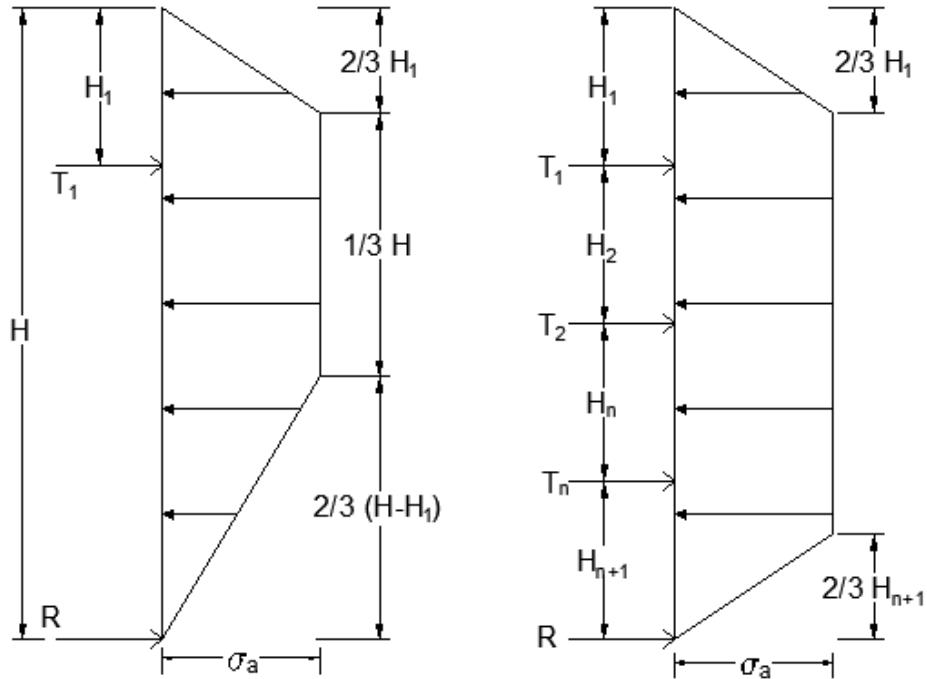
Fig. B-6 Apparent Pressure Envelopes (After Peck, 1969).

Note: These diagrams consider undrained conditions and only total stresses for the clays; in sands, drained conditions are assumed.

Handout 5 Recommended Apparent Earth Pressure (Sabatini et al. 1999)

Sands

- For both temporary (short-term) and permanent (long-term) loadings.



$$\sigma_a = \frac{P}{2/3 H} \approx K_a \cdot \gamma H$$

(a) Walls with one level of ground anchor

$$P = 0.65 \cdot K_a \cdot \gamma H^2$$

H_1 = Distance from ground surface to uppermost ground anchor

H_{n+1} = Distance from base of excavation to lowermost ground anchor

T_i = Horizontal load in ground anchor i

R = Reaction force to be resisted by subgrade (i.e below of excavation level)

σ_a = Maximum ordinate of diagram

P = Total load of the diagram

γ = Total unit weight of soil

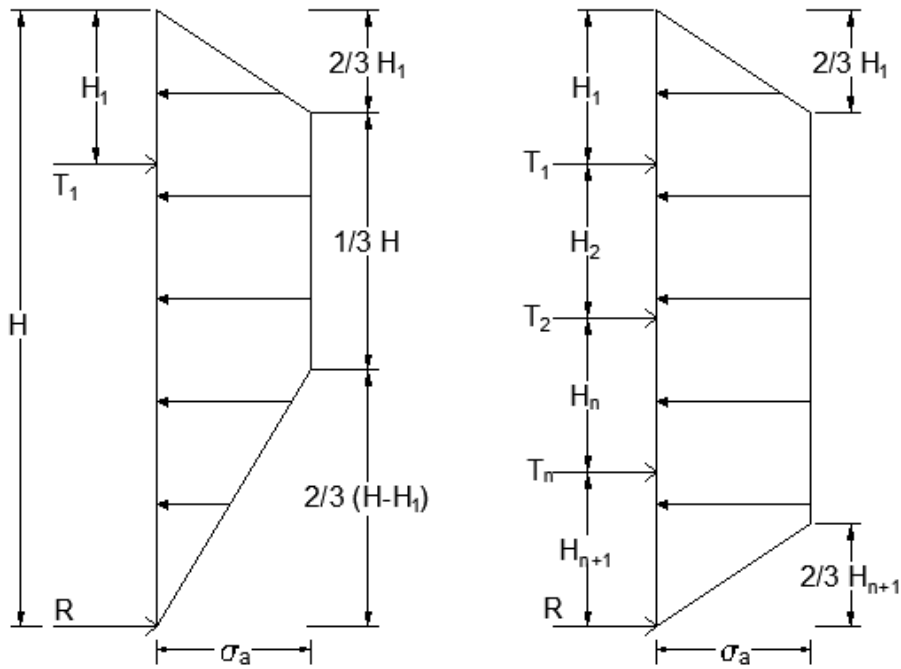
$$\sigma_a = \frac{P}{H - 1/3(H_1 - H_{n+1})}$$

(b) Walls with multiple levels of ground anchor

Fig. B-7 Recommended apparent earth pressure diagram for stiff sands

Stiff to Hard Fissured clays

- Temporary (short-term) loadings.



$$\sigma_a \approx 0.2 \cdot \gamma H - 0.4 \cdot \gamma H_1$$

$$\sigma_a \approx 0.2 \cdot \gamma H - 0.4 \cdot \gamma H_1$$

(a) Walls with one level of ground anchor

(b) Walls with multiple levels of ground anchor

H_1 = Distance from ground surface to uppermost ground anchor

H_{n+1} = Distance from base of excavation to lowermost ground anchor

T_{ni} = Horizontal load in ground anchor i

R = Reaction force to be resisted by subgrade (i.e below of excavation level)

σ_a = Maximum ordinate of diagram

γ = Total unit weight of soil

H = Excavation depth

Fig. B-8 Recommended apparent earth pressure diagram for stiff clays

- Permanent (long-term) loadings.

Excavation induces negative excess pore water pressures; therefore, the soil to exhibit a greater shear strength than is available in the long term. Soil behind the wall and in front of the wall (i.e., at the base of the excavation) experience

unloading to which the soil responds by drawing in water, resulting in softening (i.e., weakening) of the soil with time.

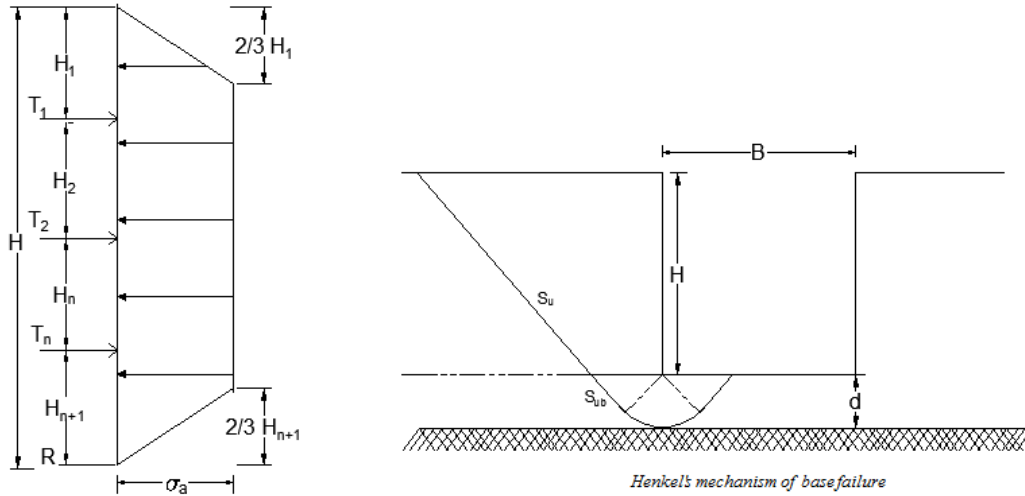
The development of tension cracks at the surface and the possible presence of sandy or silty layers or cracks and fissures serve to increase the rate at which soil softening may occur.

Based on the above discussion, earth pressures associated with long-term drained conditions for excavations in stiff to hard fissured clays may be greater than those computed based on envelopes for temporary conditions.

The total resultant force calculated using a diagram for temporary conditions can be compared to the total resultant force associated with the recommended apparent earth pressure envelope for stiff to hard clays using a total resultant force of $0.65K_a\gamma H^2$, where K_a is based on the drained friction angle of the clay soil. For most anchored wall applications, the drained friction angle should correspond to the fully softened friction angle. The larger of the resultant forces from the two diagrams should be used for design.

Soft to Medium clays

- For both temporary (short-term) and permanent (long-term) loadings.



$$\sigma_a = K_a \cdot \gamma \cdot H$$

for $N_s \geq 5.14$

$$K_a = 1 - \frac{4 \cdot S_u}{\gamma \cdot H} + \frac{2 \cdot \sqrt{2} \cdot d}{H} \left(1 - \frac{5.14 \cdot S_{ub}}{\gamma \cdot H} \right)$$

for $4 < N_s < 5.14$

$$K_a = 0.22$$

S_u = Undrained shear strength of the soil through which the excavation extends

S_{ub} = Undrained strength of the soil providing bearing resistance

γ_s = Total unit weight of soil

d = depth of the failure surface below the cut; limited to $B/\sqrt{2}$

H = Excavation depth

Fig. B-9 Recommended apparent earth pressure diagram for soft clays

Where N_s is the stability number given as:

$$N_s = \frac{\gamma_s H}{S_u}$$

Note: Henkel's method is valid to cases where the clay soils on the retained side and below the excavation subgrade can each be reasonably characterized using a constant value for undrained shear strength. Where a more detailed shear strength profile is required, limit equilibrium methods may be used to evaluate the earth pressure loadings on the wall.

Handout 6 Sliding Wedge Analysis Method

For complicated stratification, irregular ground surface, or irregular surcharge loading, the lateral force required to provide stability to the excavation may be evaluated using a trial wedge stability analysis.

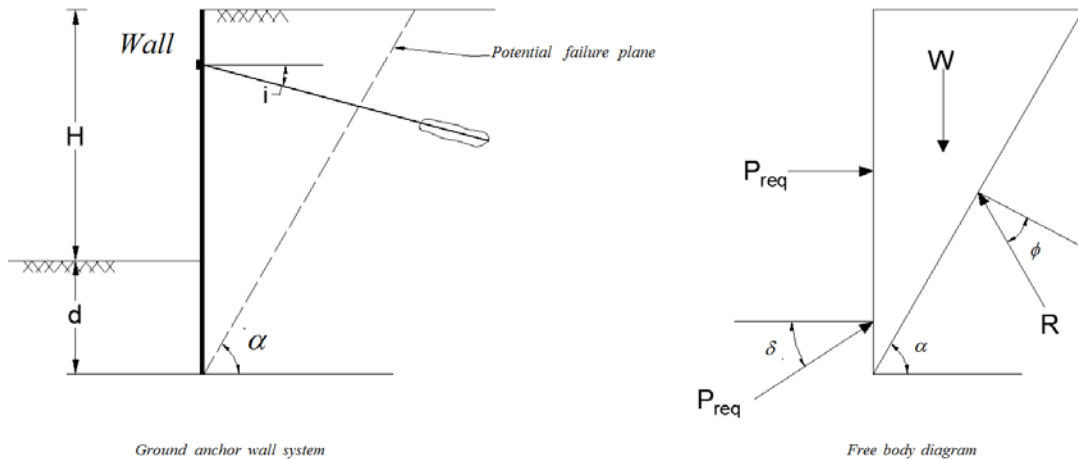


Fig. B-10 Sliding Wedge Analysis Method

The required force P_{req} represents the horizontal component of the anchor forces and the lateral resistance provided by the embedded portion of the wall. This force is then calculated as:

$$P_{req} = \frac{1}{2} \gamma \cdot H^2 \left[\frac{(1 + \xi)^2}{\tan(\alpha)} - K_p \cdot \zeta^2 \left(\sin(\delta) + \frac{\cos(\delta)}{\tan(\alpha - \phi)} \right) \right] \cdot \tan(\alpha - \phi) \quad \xi = d / H$$

Where:

W = Weight of soil mass

R = Frictional component of soil strength

P_p = Passive earth pressure resultant force

T = Total anchor force

ϕ = Friction angle of the soil

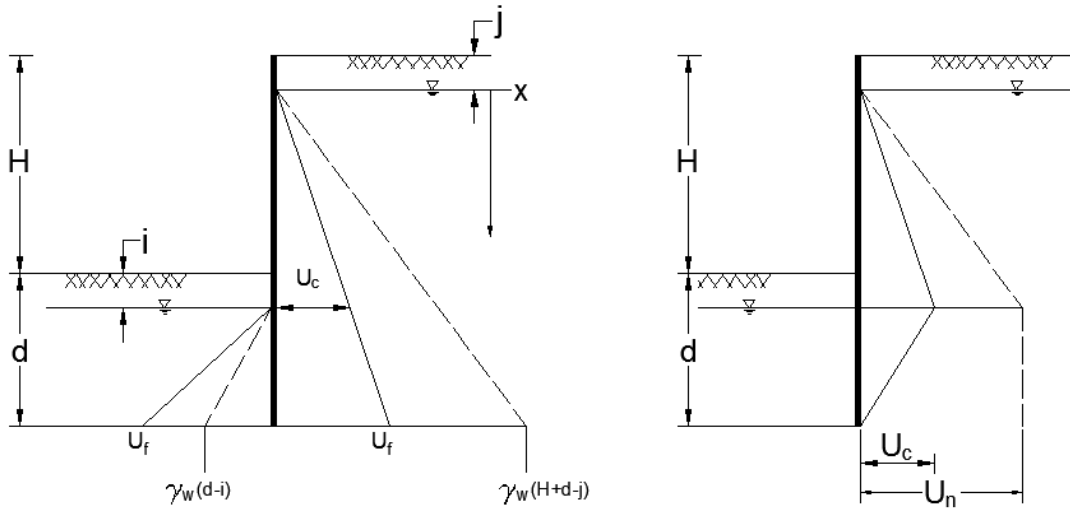
α = Inclination of potential failure surface

δ = Interface friction angle of the soil

P_{req} = Required resisting force

The required force is found by adjusting the angle of the potential failure surface (α) and the wall depth of embedment, d , until the greatest P_{req} is found. This load is then redistributed into an apparent pressure envelope; then, the hinge or the tributary method is used to calculate the ground anchor loads and bending moments in the wall.

Handout 7 Water Pressures Evaluation



U_f = pore water pressures at bottom of the wall

(a) Gross water pressures

(b) Net water pressures

Seepage conditions —————

$$U_f = \frac{2(d+H-j)(d-i)}{2d+H-i-j} \gamma_w$$

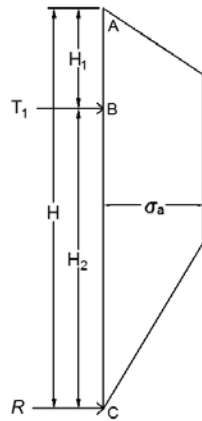
$$U_c = (H+i-j) \frac{2(d-i)}{2d+H-i-j} \gamma_w$$

Static conditions —————

$$U_n = (H+i-j) \gamma_w$$

Fig. B-11 Sliding Wedge Analysis Method

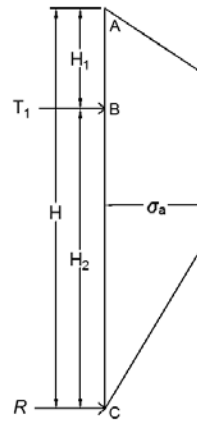
Handout 8 Calculation of Anchor Loads



Tributary area method

$$T_1 = \text{Load over length } H_1 + H_2 / 2$$

$$R = \text{Load over length } H_2 / 2$$

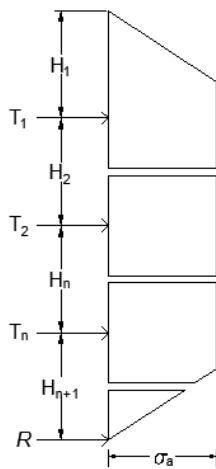


Hinge method

$$T_1 = \text{Calculate from } \sum M_c = 0$$

$$R = \text{Total earth pressure} \cdot T_1$$

Fig. B-12 Anchor Loads for One Row of Anchors



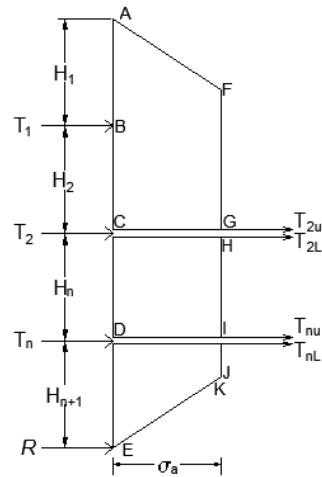
Tributary area method

$$T_1 = \text{Load over length } H_1 + H_2 / 2$$

$$T_2 = \text{Load over length } H_2 + H_n / 2$$

$$T_n = \text{Load over length } H_n + H_{n+1} / 2$$

$$R = \text{Load over length } H_{n+1} / 2$$



Hinge method

$$T_1 = \text{Calculate from } \sum M_c = 0$$

$$T_1 = \text{Calculate from } \sum M_c = 0$$

$$T_{2u} = \text{Total earth pressure (ABCGF)} - T_1$$

$$T_{2L} = \text{Calculate from } \sum M_D = 0$$

$$T_{nu} = \text{Total earth pressure (CDIH)} - T_{2L}$$

$$T_{nL} = \text{Calculate from } \sum M_c = 0$$

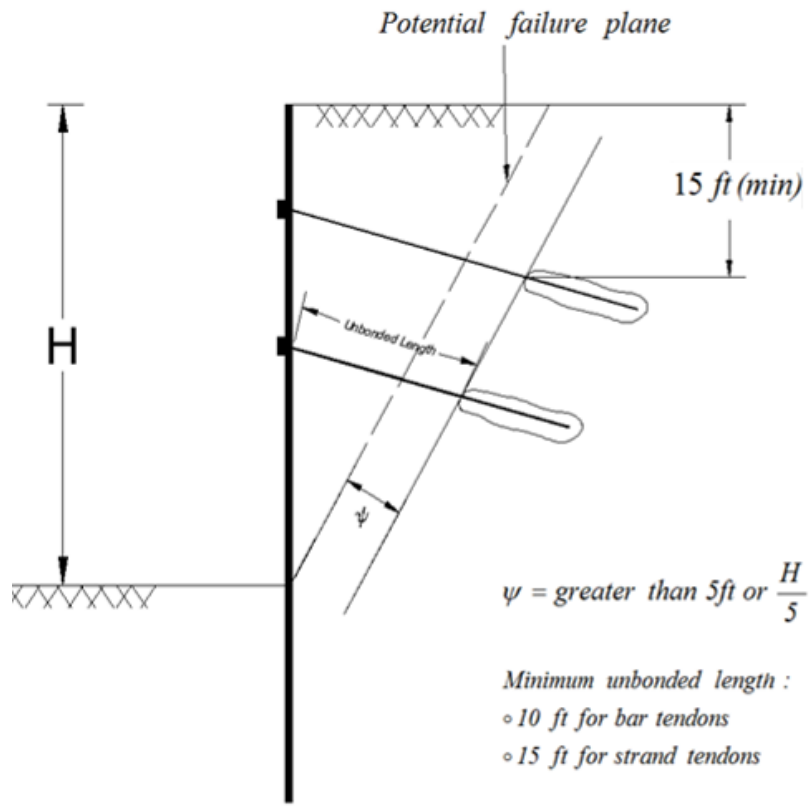
$$R = \text{Total earth pressure} - T_1 - T_2 - T_n$$

$$T_2 = T_{2u} + T_{2L}$$

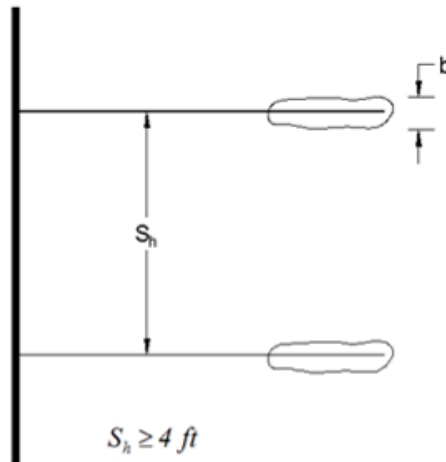
$$T_n = T_{nu} + T_{nL}$$

Fig. B-13 Multiple rows of Anchors

Handout 9 Vertical and Horizontal Spacing Requirements for Ground Anchors



(a) Cross Section



(b) Plan view

Fig. B-1 Spacing Requirements for Anchors

Handout 10 Ultimate Bond Strengths

Table B.1 Typical average ultimate bond strengths-cohesive soils

| Anchor Type | Average ultimate bond strength-soil/grout, MPa(psi) |
|--|---|
| Gravity-grouted anchors(straight shaft) | 0.03 to 0.07 (5 to 10) |
| Pressure-grouted anchors (Straight Shaft) | |
| ○ Soft silty clay | 0.03 to 0.07 (5 to 10) |
| ○ Silty clay | 0.03 to 0.07 (5 to 10) |
| ○ Stiff clay, medium to high plasticity | 0.03 to 0.05 (5 to 15) |
| ○ Very stiff clay, medium to high plasticity | 0.07 to 0.17 (10 to 25) |
| ○ Stiff clay, medium plasticity | 0.10 to 0.25 (15 to 36) |
| ○ Very stiff clay, medium plasticity | 0.14 to 0.35 (20 to 50) |
| ○ Very Stiff sandy silt, medium plasticity | 0.28 to 0.38 (40 to 55) |

Note: Actual values for pressure-grouted anchors depend on the ability to develop pressures in each soil type

Table B.2 Typical average ultimate bond strengths-cohesive soils

| Anchor Type | Average ultimate bond strength-soil/grout, MPa(psi) |
|--|---|
| Gravity-grouted anchors(straight shaft) | 0.07 to 0.14 (10 to 20) |
| Pressure-grouted anchors (Straight Shaft) | 0.08 to 0.38 (12 to 55) |
| ○ Fine-med. sand, med. dense – dense | 0.11 to 0.66 (16 to 95) |
| ○ Med.–coarse sand (w/gravel), med-dense | 0.25 to 0.97 (35 to 140) |
| ○ Med.–coarse sand (w/gravel), dense-very dense. | 0.17 to 0.41 (25 to 60) |
| ○ Silty sands. | 0.30 to 0.52 (43 to 75) |
| ○ Dense glacial till | 0.21 to 1.38 (31 to 200) |
| ○ Sandy gravel, med. dense-dense | 0.28 to 1.38 (40 to 200) |
| ○ Sandy gravel, dense- very dense | |

Note: Actual values for pressure-grouted anchors depend on the ability to develop pressures in each soil type

Handout 11 Manufacturing Guides for Wall Section, and Wale Channels

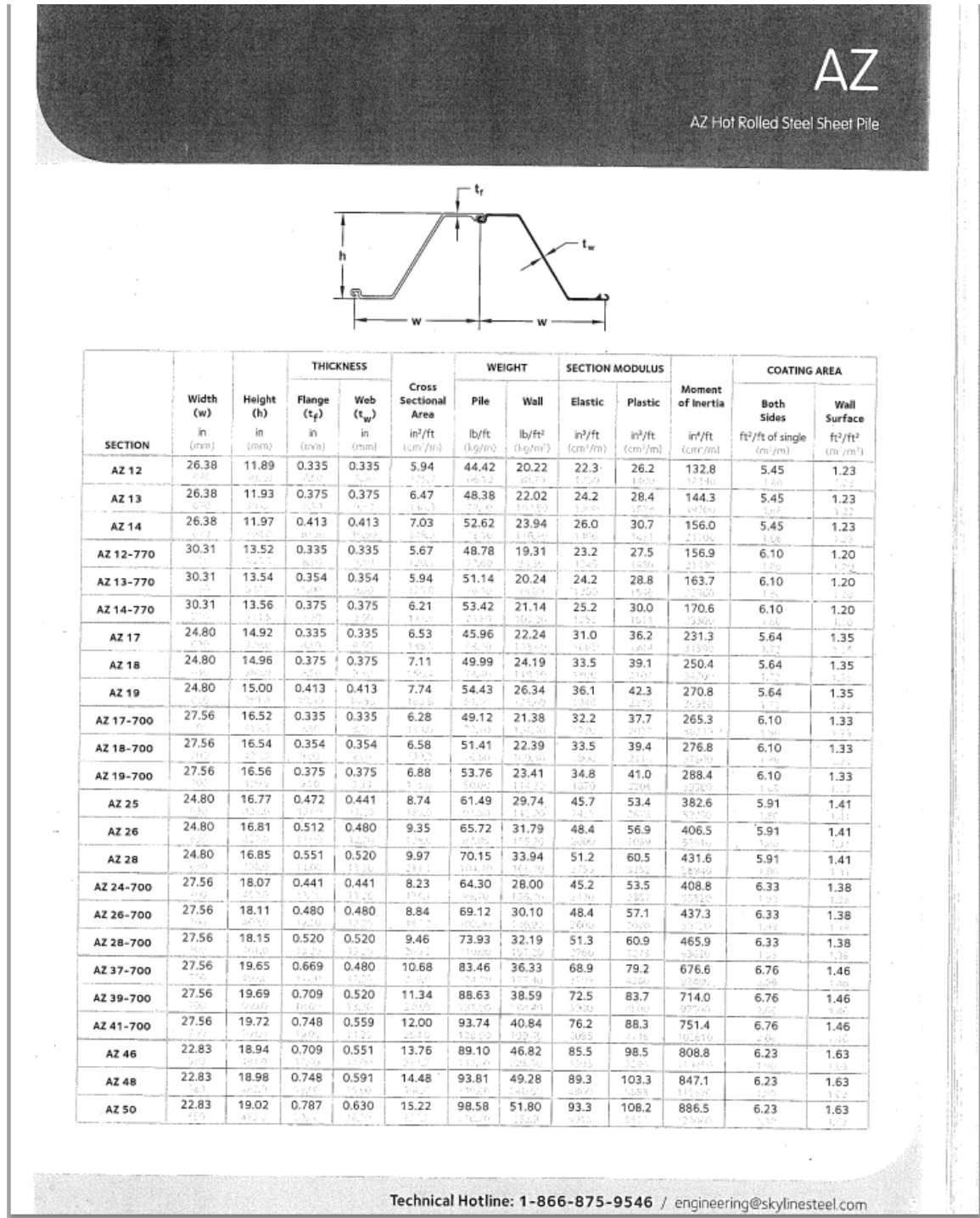


Fig. B-15 Typical Wall Sections, Anchor Strands, and Wale Channels

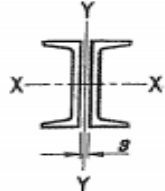



Table 1-17
2MC-Shapes
Properties



2MC18-2MC7

| Shape | Area, A | | Axis Y-Y | | | | | | | | | | | Axis X-X |
|-------------------------|------------------|------------------|--------------------|------------------|------------------|-----------------------------|----------|------------------|------------------|-----------------------------|----------|------------------|----------------------|----------|
| | | | Separation, s, in. | | | | | | | | | | | |
| | 0 | | | | | ³ / ₈ | | | | ³ / ₄ | | | | |
| | <i>I</i> | <i>S</i> | <i>r</i> | <i>Z</i> | <i>I</i> | <i>S</i> | <i>r</i> | <i>Z</i> | <i>I</i> | <i>S</i> | <i>r</i> | <i>Z</i> | <i>r_x</i> | |
| in. ² | in. ⁴ | in. ³ | in. | in. ³ | in. ⁴ | in. ³ | in. | in. ³ | in. ⁴ | in. ³ | in. | in. ³ | in. | |
| 2MC18×58 | 34.2 | 60.6 | 14.4 | 1.33 | 29.5 | 72.8 | 16.6 | 1.46 | 35.9 | 87.5 | 19.1 | 1.60 | 42.3 | 6.29 |
| ×51.9 | 30.6 | 55.0 | 13.4 | 1.34 | 26.3 | 65.9 | 15.4 | 1.47 | 32.0 | 79.0 | 17.6 | 1.61 | 37.7 | 6.41 |
| ×45.8 | 27.0 | 50.1 | 12.5 | 1.36 | 23.4 | 59.8 | 14.3 | 1.49 | 28.4 | 71.4 | 16.3 | 1.63 | 33.5 | 6.55 |
| ×42.7 | 25.2 | 47.8 | 12.1 | 1.38 | 22.1 | 57.0 | 13.8 | 1.51 | 26.8 | 67.9 | 15.7 | 1.64 | 31.6 | 6.64 |
| 2MC13×50 | 29.4 | 60.7 | 13.8 | 1.44 | 28.6 | 72.5 | 15.8 | 1.57 | 34.1 | 86.3 | 18.0 | 1.71 | 39.7 | 4.62 |
| ×40 | 23.4 | 49.1 | 11.7 | 1.45 | 22.7 | 58.4 | 13.4 | 1.58 | 27.2 | 69.4 | 15.2 | 1.72 | 31.6 | 4.82 |
| ×35 | 20.6 | 44.3 | 10.9 | 1.47 | 20.2 | 52.6 | 12.3 | 1.60 | 24.1 | 62.3 | 14.0 | 1.74 | 27.9 | 4.95 |
| ×31.8 | 18.7 | 41.5 | 10.4 | 1.49 | 18.7 | 49.2 | 11.7 | 1.62 | 22.2 | 58.2 | 13.3 | 1.76 | 25.7 | 5.05 |
| 2MC12×50 | 29.4 | 67.2 | 16.2 | 1.51 | 30.9 | 79.8 | 18.5 | 1.65 | 36.4 | 94.5 | 20.9 | 1.79 | 41.9 | 4.28 |
| ×45 | 26.4 | 59.9 | 14.9 | 1.51 | 27.5 | 71.1 | 16.9 | 1.64 | 32.4 | 84.1 | 19.2 | 1.79 | 37.4 | 4.36 |
| ×40 | 23.6 | 53.7 | 13.8 | 1.51 | 24.5 | 63.7 | 15.6 | 1.65 | 29.0 | 75.3 | 17.7 | 1.79 | 33.4 | 4.46 |
| ×35 | 20.6 | 48.0 | 12.7 | 1.53 | 21.6 | 56.8 | 14.4 | 1.66 | 25.5 | 67.1 | 16.2 | 1.81 | 29.4 | 4.59 |
| ×31 | 18.2 | 44.0 | 12.0 | 1.55 | 19.7 | 52.1 | 13.5 | 1.69 | 23.1 | 61.4 | 15.2 | 1.83 | 26.5 | 4.71 |
| 2MC12×14.3 | 8.36 | 3.19 | 1.50 | 0.618 | 3.15 | 4.66 | 2.02 | 0.747 | 4.72 | 6.73 | 2.70 | 0.897 | 6.29 | 4.27 |
| 2MC12×10.6 ⁶ | 6.20 | 1.21 | 0.804 | 0.441 | 1.67 | 2.05 | 1.21 | 0.575 | 2.83 | 3.33 | 1.78 | 0.733 | 3.99 | 4.22 |
| 2MC10×41.1 | 24.2 | 60.0 | 13.9 | 1.58 | 26.4 | 70.7 | 15.7 | 1.71 | 30.9 | 83.1 | 17.7 | 1.85 | 35.5 | 3.61 |
| ×33.6 | 19.7 | 49.5 | 12.1 | 1.58 | 21.5 | 58.2 | 13.6 | 1.72 | 25.2 | 68.3 | 15.3 | 1.86 | 28.9 | 3.75 |
| ×28.5 | 16.7 | 43.5 | 11.0 | 1.61 | 18.7 | 51.1 | 12.3 | 1.75 | 21.9 | 59.8 | 13.8 | 1.89 | 25.0 | 3.89 |
| 2MC10×25 | 14.7 | 27.8 | 8.18 | 1.38 | 14.0 | 33.6 | 9.36 | 1.51 | 16.8 | 40.4 | 10.7 | 1.66 | 19.5 | 3.87 |
| ×22 | 12.9 | 25.4 | 7.67 | 1.40 | 12.8 | 30.7 | 8.76 | 1.54 | 15.2 | 36.8 | 10.0 | 1.69 | 17.6 | 3.99 |
| 2MC10×8.4 ⁴ | 4.92 | 1.05 | 0.700 | 0.462 | 1.40 | 1.75 | 1.03 | 0.596 | 2.32 | 2.79 | 1.49 | 0.753 | 3.24 | 3.61 |
| ×6.5 ⁵ | 3.90 | 0.414 | 0.354 | 0.326 | 0.757 | 0.835 | 0.615 | 0.463 | 1.49 | 1.53 | 0.990 | 0.626 | 2.22 | 3.43 |
| 2MC9×25.4 | 14.9 | 29.2 | 8.34 | 1.40 | 14.5 | 35.2 | 9.53 | 1.53 | 17.3 | 42.2 | 10.9 | 1.68 | 20.1 | 3.43 |
| ×23.9 | 14.0 | 27.8 | 8.05 | 1.41 | 13.8 | 33.4 | 9.19 | 1.54 | 16.4 | 40.1 | 10.5 | 1.69 | 19.0 | 3.48 |
| 2MC8×22.8 | 13.4 | 27.7 | 7.91 | 1.44 | 13.5 | 33.2 | 9.01 | 1.58 | 16.0 | 39.7 | 10.2 | 1.72 | 18.6 | 3.09 |
| ×21.4 | 12.6 | 26.3 | 7.63 | 1.45 | 12.8 | 31.6 | 8.68 | 1.59 | 15.2 | 37.7 | 9.86 | 1.73 | 17.5 | 3.13 |
| 2MC8×20 | 11.7 | 17.1 | 5.66 | 1.21 | 9.88 | 21.2 | 6.61 | 1.34 | 12.1 | 26.2 | 7.70 | 1.49 | 14.3 | 3.04 |
| ×18.7 | 11.0 | 16.2 | 5.45 | 1.21 | 9.34 | 20.1 | 6.35 | 1.35 | 11.4 | 24.8 | 7.39 | 1.50 | 13.5 | 3.09 |
| 2MC8×8.5 | 5.00 | 2.16 | 1.15 | 0.658 | 2.14 | 3.14 | 1.52 | 0.793 | 3.08 | 4.47 | 1.99 | 0.946 | 4.02 | 3.05 |
| 2MC7×22.7 | 13.3 | 29.0 | 8.06 | 1.47 | 13.9 | 34.7 | 9.16 | 1.61 | 16.4 | 41.3 | 10.4 | 1.76 | 18.9 | 2.67 |
| ×19.1 | 11.2 | 25.1 | 7.27 | 1.50 | 12.1 | 30.0 | 8.25 | 1.64 | 14.2 | 35.7 | 9.34 | 1.78 | 16.3 | 2.77 |

⁶ Shape is slender for compression with $F_y = 36$ ksi.

AMERICAN INSTITUTE OF STEEL CONSTRUCTION

Fig. B-16 Wale Channels

Handout 12. Recommended Thickness of Wood Lagging

| Recommended thickness of Wood Lagging when Soil Arching will be developed | | | | | | | | | | | | | | | |
|--|-------------------------|------------|---|----|----|----|----|-----|------------|----|----|----|----|----|----|
| Soil Classification | Unified | Depth | Recommended Thickness of Lagging for clear spans of | | | | | | | | | | | | |
| | | | 5' | 6' | 7' | 8' | 9' | 10' | | | | | | | |
| Competent Soils | | | | | | | | | | | | | | | |
| Silts or fine sand and silt above water table | ML, SM – ML | 0' to 25' | 2" | 3" | 3" | 3" | 4" | 4" | | | | | | | |
| Sands and gravels (Medium dense to dense) | GW, GP,GM,GC, SW, SP,SM | | | | | | | | | | | | | | |
| Clays (Stiff to very stiff); non-fissured | CL, CH | | | | | | | | 25' to 60' | 3" | 3" | 3" | 4" | 4" | 5" |
| Clays, medium consistency | CL, CH | | | | | | | | | | | | | | |
| Difficult Soils | | | | | | | | | | | | | | | |
| Sands and silty sands (loose). | SW, SP, SM | 0' to 25' | 3" | 3" | 3" | 4" | 4" | 5" | | | | | | | |
| Clayey sands (medium dense to dense) below water table. | SC | | | | | | | | | | | | | | |
| Clays, heavily overconsolidated fissured | CL, CH | 25' to 60' | 3" | 3" | 4" | 4" | 5" | 5" | | | | | | | |
| Cohesionless silt or fine sand and silt below water table. | ML; SM – ML | | | | | | | | | | | | | | |
| Potentially Dangerous Soils | | | | | | | | | | | | | | | |
| Soft clays | CL, CH | 0' to 15' | 3" | 3" | 4" | 5" | | | | | | | | | |
| Slightly plastic silts below water table. | ML | 15' to 25' | 3" | 4" | 5" | 6" | | | | | | | | | |
| Clayey sands (loose), below water table | SC | 25' to 35' | 4" | 5" | 6" | | | | | | | | | | |
| Adapted from (Trenching and Shoring Manual, California department of transportation, 2011) | | | | | | | | | | | | | | | |

Fig. B-17 Wale Channels

Handout 13: Analysis of Basal Heave

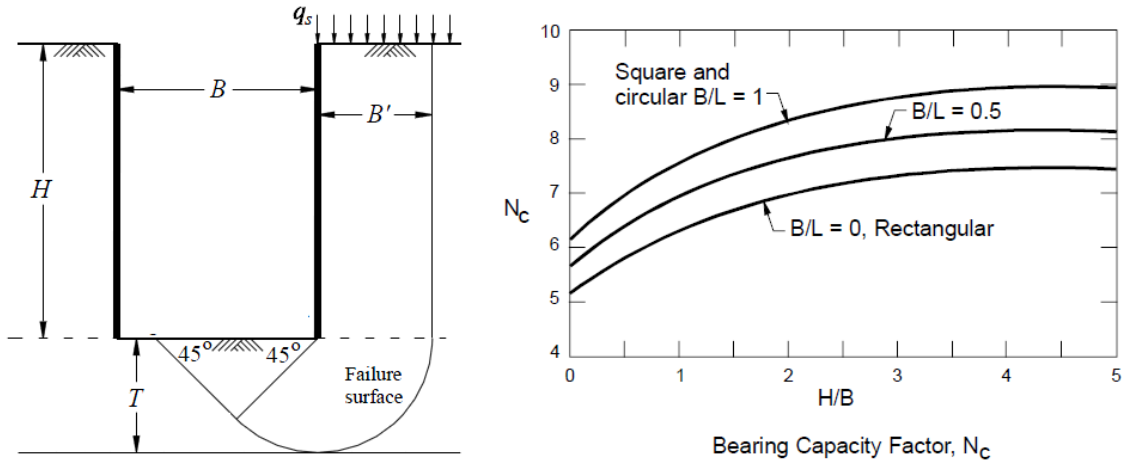


Fig. B-18 Analysis of basal heave in soft to medium clays

$$FS = \frac{S_u \cdot N_c}{(\gamma_s + q_s/H - S_u/B) \cdot H}$$

Where:

$B' = \text{minimum of } B/\sqrt{2} \text{ or } T$

$B = \text{Width of the excavation}$

$T = \text{Thickness of clay below the excavation}$

$q_s = \text{Surcharge loading}$

$\gamma_s = \text{Unit weight of the soil}$

$N_c = \text{Bearing capacity factor}$

$S_u = \text{Undrained shear strength}$

$H = \text{Excavation depth}$

Handout 14 Anchor Testing

| Loading | Applied Load | Record and Plot Total Movement (δ_{ti}) | Record and Plot Residual Movement (δ_{ri}) | Calculate Elastic Movement (δ_{ei}) |
|---------|------------------|--|---|--|
| Cycle 1 | <i>Al</i> | --- | --- | $\delta_{t1} - \delta_{r1}$ |
| | <i>0.25 DL</i> | δ_{t1} | --- | |
| | <i>Al</i> | --- | δ_{r1} | |
| Cycle 2 | <i>0.25 DL</i> | δ_2 | --- | $\delta_{t2} - \delta_{r2}$ |
| | <i>0.50 DL</i> | δ_{t2} | --- | |
| | <i>Al</i> | --- | δ_{r2} | |
| Cycle 3 | <i>0.25 DL</i> | δ_3 | --- | $\delta_{t3} - \delta_{r3}$ |
| | <i>0.50 DL</i> | δ_3 | --- | |
| | <i>0.75 DL</i> | δ_{t3} | --- | |
| | <i>Al</i> | --- | δ_{r3} | |
| Cycle 4 | <i>0.25 DL</i> | δ_4 | --- | $\delta_{t4} - \delta_{r4}$ |
| | <i>0.50 DL</i> | δ_4 | --- | |
| | <i>0.75 DL</i> | δ_4 | --- | |
| | <i>1.0 DL</i> | δ_{t4} | --- | |
| | <i>Al</i> | --- | δ_{r4} | |
| Cycle 5 | <i>0.25 DL</i> | δ_5 | --- | $\delta_{t5} - \delta_{r5}$ |
| | <i>0.50 DL</i> | δ_5 | --- | |
| | <i>0.75 DL</i> | δ_5 | --- | |
| | <i>1.0 DL</i> | δ_5 | --- | |
| | <i>1.2 DL</i> | δ_{t5} | --- | |
| | <i>Al</i> | --- | δ_{r5} | |
| Cycle 6 | <i>0.25 DL</i> | δ_6 | --- | $\delta_{t6} - \delta_{r6}$ |
| | <i>0.50 DL</i> | δ_6 | --- | |
| | <i>0.75 DL</i> | δ_6 | --- | |
| | <i>1.0 DL</i> | δ_6 | --- | |
| | <i>1.2 DL</i> | δ_6 | --- | |
| | <i>1.33 DL *</i> | δ_{t6} | --- | |
| | <i>Al</i> | --- | δ_{r6} | |

* This load is held for 10 minutes. If movements between 1 and 10 minutes exceeds the specified maximum creep movement; the load is maintained for an additional 50 minutes and total movement is recorded. If the results that creep the anchor may be incorporated into the structure at a reduced load, may be replaced, or, may be regouted in the case of postgroutable anchors. This portion of the performance test is referred to as a creep test

Fig. B-19 Typical record of a Performance Test

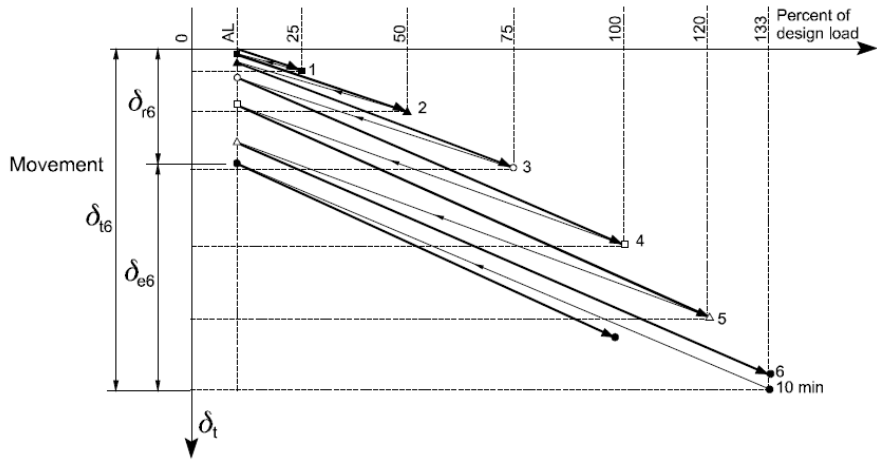


Fig. B-20 Typical plotting of a performance test

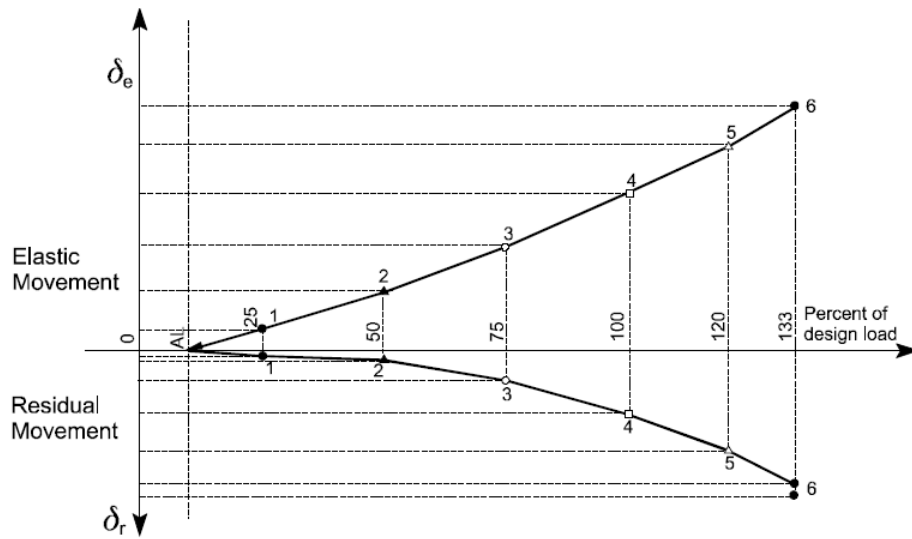


Fig. B-21 Elastic and residual moments in a performance test

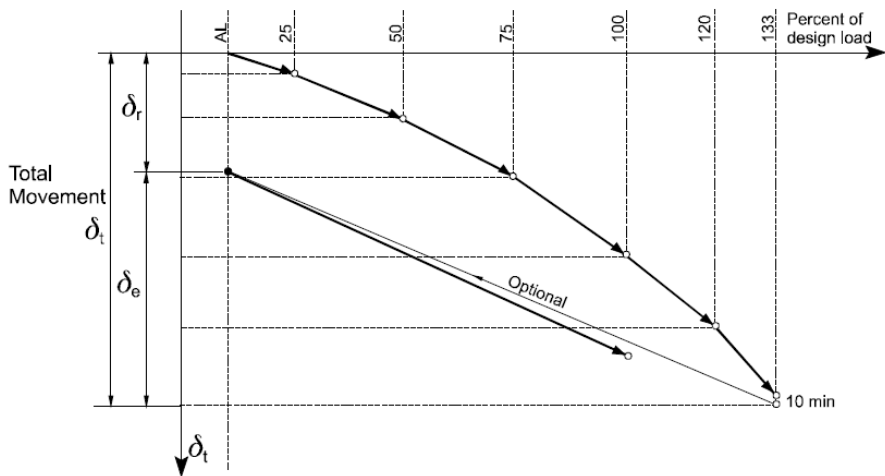


Fig. B-22 Typical plotting of a proof test

| Loading | Maximum Cycle Load | Total observation Period (min) | Movements measured at following times (min) |
|----------------|---------------------------|---------------------------------------|--|
| <i>Cycle 1</i> | <i>0.25 DL</i> | <i>10</i> | <i>1, 2, 3, 4, 5, 6, 10</i> |
| <i>Cycle 2</i> | <i>0.50 DL</i> | <i>30</i> | <i>1, 2, 3, 4, 5, 6, 10, 15, 20, 25, 30</i> |
| <i>Cycle 3</i> | <i>0.75 DL</i> | <i>30</i> | <i>1, 2, 3, 4, 5, 6, 10, 15, 20, 25, 30</i> |
| <i>Cycle 4</i> | <i>1.0 DL</i> | <i>45</i> | <i>1, 2, 3, 4, 5, 6, 10, 15, 20, 25, 30, 45</i> |
| <i>Cycle 5</i> | <i>1.2 DL</i> | <i>60</i> | <i>1, 2, 3, 4, 5, 6, 10, 15, 20, 25, 30, 45, 60</i> |
| <i>Cycle 6</i> | <i>1.33 DL</i> | <i>300</i> | <i>1, 2, 3, 4, 5, 6, 10, 15, 20, 25, 30, 45, 60, 300</i> |

Fig. B-23 Load schedule for and extended creep test

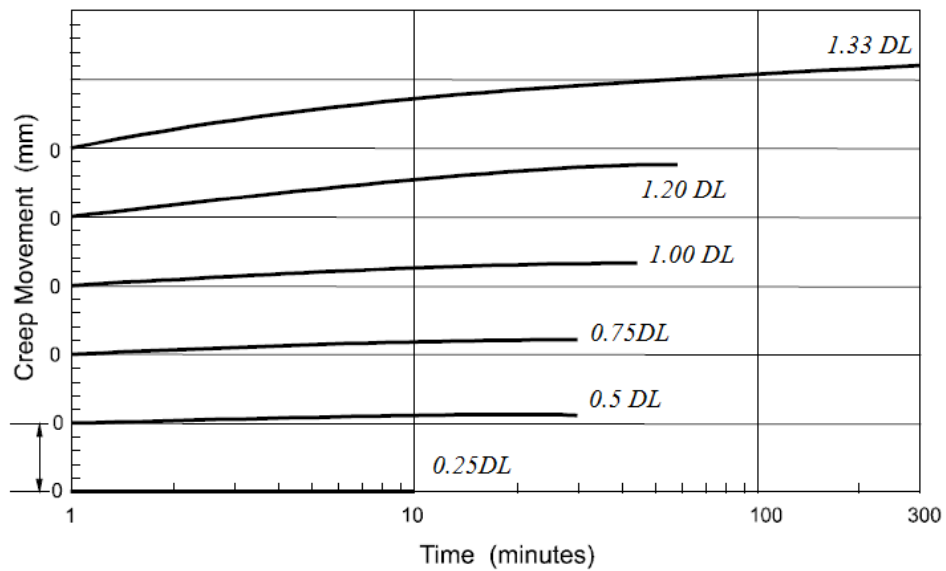


Fig. B-24 Load schedule for and extended creep test

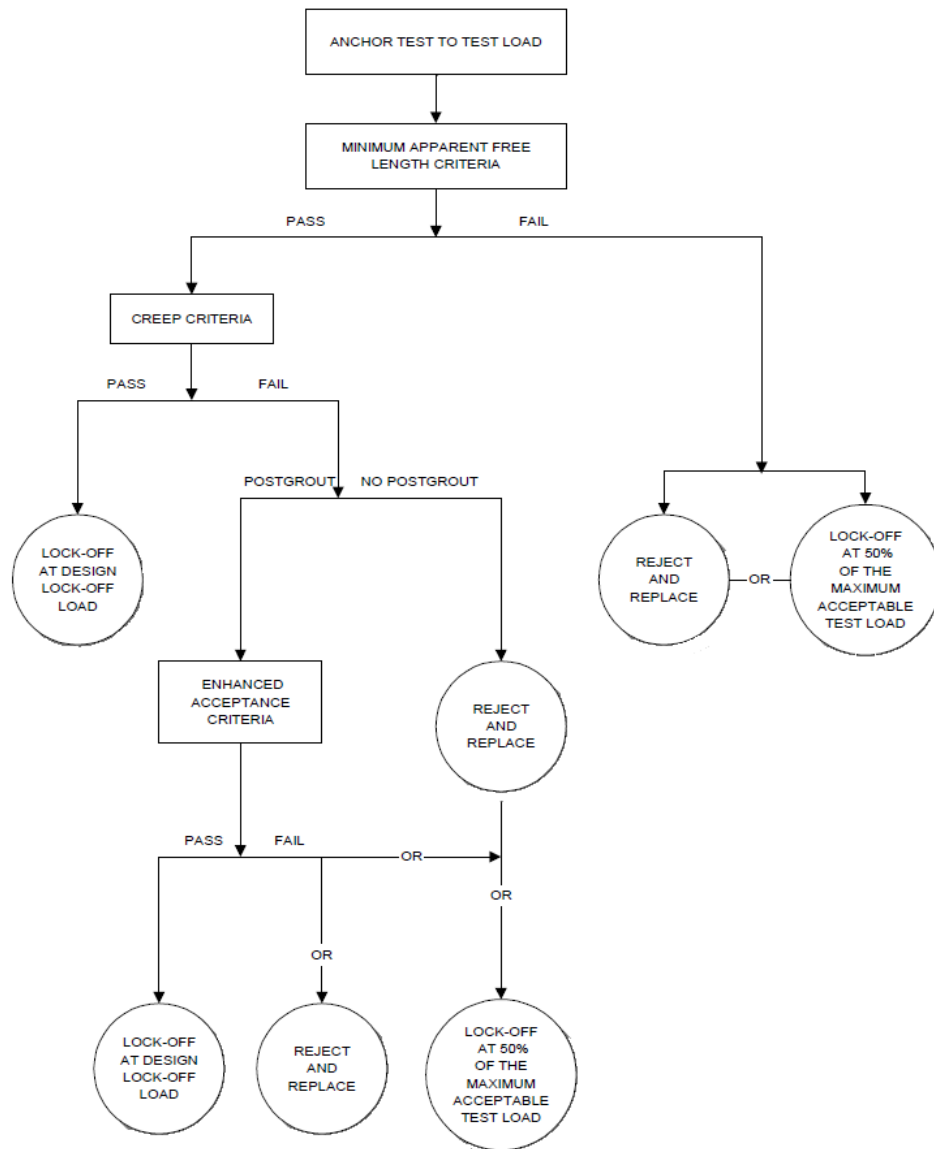


Fig. B-25 Load schedule for and extended creep test

Appendix C

Matlab Code for the Numerical Procedure


```

% tz approach ground anchors
clearvars
% Anchor properties
% number of functions
nf=1;
% Length of the anchor (bonded length) (m)
L=;
% Number of segments (m)
n=;
% length of each segment (m)
for k=1:n
    dl(k)=L/n;
end
% Anchors Diameter (m)
d=;
% Area of the anchor m2
Ap=;
% Modulus of elasticity of the pile (kN*m^2)
Ep=;
% Area of the strand m2
As=;
% Modulus of strand (kN*m^2)
Es=;
% Given values
zbottom=0.01/1000:0.05/1000:0.45/1000;%m
Fbottom=zeros(1,length(zbottom));%kN 10
% t=@(z);
wu=;
tu=;
% model 1
a=((bta-1+sqrt*(1-bta))/2*bta)*(wu/tu);

```

```

b=((1-sqrt*(1-bta))/2*bta)*(1/tu);
c=((2-bta-2*sqrt*(1-bta))/4*bta)*(1/tu);
tz=@(zm)z*(a+c*zm)/((a+b*zm)^2);
% model 2
n=;
tz=@(zm)tu(((n+1)*(zm/wu)^(n/(n+1)))-(n*zm/wu));
ZB=zeros(n,length(zbottom),nf);
ZM=zeros(n,length(zbottom),nf);
ZH=zeros(n,length(zbottom),nf);
FB=zeros(n,length(zbottom),nf);
FM=zeros(n,length(zbottom),nf);
FH=zeros(n,length(zbottom),nf);
tz=zeros(n,length(zbottom),nf);
%tolerance for the computation
tol=10^-8;
nfi=1;
wu=;
fmaxi(1:n)=;%kPa
nfi=1;
for k=1:length(zbottom)
    for j=1:n
        if j==1
            ZB(j,k,nfi)=zbottom(k);%m
            FB(j,k,nfi)=Fbottom(k);
        else
            ZB(j,k,nfi)=ZH(j-1,k,nfi);
            FB(j,k,nfi)=FH(j-1,k,nfi);
        end
        ZM(j,k,nfi)=2*ZB(j,k,nfi);
        zaux=ZM(j,k,nfi);
    end
end

```

```

    fun=@(zm)zm-ZB(j,k,nfi)-
(FB(j,k,nfi)+(1./2).*((dl(j).*d.*pi/2).*((zm<=0).*0+(zm>0).*(tz(zm))).*(1./(Ep.*Ap)).*(
dl(j)./2)-tol;
    ZM(j,k,nfi)=fzero(fun,zaux);
    %load transfer function
    tzcurve=@(zm)(((zm<=0).*0+((zm>0)).*tz(zm)));% <----- tz curve
    FM(j,k,nfi)=FB(j,k,nfi)+(dl(j).*d.*pi/2)*tzcurve(ZM(j,k,nfi));
    FH(j,k,nfi)= FB(j,k,nfi)+2*(FM(j,k,nfi)-FB(j,k,nfi));
    ZH(j,k,nfi)=ZB(j,k,nfi)+(FM(j,k,nfi)*dl(j)/(Ep*Ap));
    tz(j,k,nfi)=tzcurve(ZM(j,k,nfi));
    % plotting load transfer function
    xi=0:0.1/1000:3/1000;
    yi=tzcurve(xi);
    plot(xi*1000,yi)
end
end
% Elongation
de=(FH(n,:)*L)/(As*Es);
dtotal=de+ZH(1,:);
x1=[0;dtotal(:,nfi)'];
y1=[0;FH(n,1:end,nfi)'];
plot(x1*1000,y1,'or')
figure
plot(y1,x1*1000,'rs',y1,x1*1000,'b')
yi=[zeros(1,length(zbottom));FH];
xi=[0:L/n:L]';
plot(xi,yi,xi,yi,'s')

```


References

- Adekunte, A., Madsen, D., Margetson, N., and Quinn, L. (2007). "Predicted and Observed Performance of an Anchored Retaining Wall in Granite." *Ground Anchorages and Anchored Structures in Service 2007*, 427-437.
- Barley, A. D. (2005). "Discussion of "Performance of Tension and Compression Anchors in Weathered Soil" by Nak-Kyung Kim." *Journal of Geotechnical and Geoenvironmental Engineering*, 131(5), 671-672.
- Benmokrane, B., and Ballivy, G. (1991). "Five-year monitoring of load losses on prestressed cement-grouted rock anchors." *Canadian Geotechnical Journal*, 28(5), 668-677.
- Benmokrane, B., Chekired, M., and Xu, H. (1995). "Monitoring Behavior of Grouted Anchors Using Vibrating-Wire Gauges." *Journal of Geotechnical Engineering*, 121(6), 466-475.
- Blanco, M. L. (2012). "Theoretical and experimental study of fully grouted rockbolts and cablebolts under axial loads." Doctoral thesis, Paris School of Mines, Paris, France.
- Briaud, J.-L., Griffin, R., Yeung, A., Soto, A., Suroor, A., and Park, H. (1998). "Long-Term Behavior of Ground Anchors And Tieback Walls." *FHWNTX-99/1391-1*, Federal Highway Administration, Austin, TX.
- Briaud, J.-L., Griffin Richard, Yeung Albert, Soto Alfonso, Abdul Suroor, and Heemun, P. (1998). "Long-Term Behavior of Ground Anchors and Tieback Walls." Texas Department of Transportation, Austin, Texas.
- Briaud, J.-L., III, W. F. P., and Weatherby, D. E. (1998). "Should Grouted Anchors Have Short Tendon Bond Length?" *Journal of Geotechnical and Geoenvironmental Engineering*, 124(2), 110-119.
- Briaud, J. L., and Lim, Y. (1999). "Tieback Walls in Sand: Numerical Simulation and Design Implications." *Journal of Geotechnical and Geoenvironmental Engineering*, 125(2), 101.
- Bryson, L. S., and Zapata-Medina, D. G. (2012). "Method for Estimating System Stiffness for Excavation Support Walls." *Journal of Geotechnical and Geoenvironmental Engineering*, 138(9), 1104-1115.
- Cai, F., and Ugai, K. (2003). "Response of flexible piles under laterally linear movement of the sliding layer in landslides." *Canadian Geotechnical Journal*, 40(1), 46-53.
- CALTRANS (2011). "Trenching and Shoring Manual."
- Carlà, T., Macciotta, R., Hendry, M., Martin, D., Edwards, T., Evans, T., Farina, P., Intrieri, E., and Casagli, N. (2018). "Displacement of a landslide retaining wall and application of an enhanced failure forecasting approach." *Landslides*, 15(3), 489-505.
- Chung, M., and Briaud, J.-L. (1993). "Behavior of a full scale tieback wall in sand." *Rep. to Schnabel Foundation and the Federal Highway Administration*, Department of Civil Engineering, Texas A&M University, College Station, TX.
- Clough, G. W., and O'Rourke, T. D. (1990). "Construction induced movements of in situ walls." *Proc., Design and Performance of Earth Retaining Structures*, ASCE, New York, 439-470.
- Clough, G. W., Smith, E. M., and Bryan P. Sweeney (1989). "Movement Control of Excavation Support Systems by Iterative Design." *Proc., ASCE Foundation Engineering: Current Principles and Practice*, ASCE, New York, NY, 869-884.

- Coyle, H. M., and Reese, L. (1966). "Load transfer for axially loaded piles in clay." *Journal of the Soil Mechanics and Foundations Division*, Vol. 92(2), 1-26.
- Ehrlich, M., and Silva, R. C. (2015). "Behavior of a 31m high excavation supported by anchoring and nailing in residual soil of gneiss." *Engineering Geology*, 191, 48-60.
- Finno, R. J., Blackburn, J. T., and Roboski, J. F. (2007). "Three-Dimensional Effects for Supported Excavations in Clay." *Journal of Geotechnical and Geoenvironmental Engineering*, 133(1), 30-36.
- Gorsevski, P. V., Brown, M. K., Panter, K., Onasch, C. M., Simic, A., and Snyder, J. (2016). "Landslide detection and susceptibility mapping using LiDAR and an artificial neural network approach: a case study in the Cuyahoga Valley National Park, Ohio." *Landslides*, 13(3), 467-484.
- Grant, W. P. (1985). "Performance of Columbia Centre shoring wall." *Proc., 11th Int. Conf. Soil Mech. Found. Engrg.* Balkema, Rotterdam, The Netherlands, 2079–2082.
- Han, J.-Y., Zhao, W., Chen, Y., Jia, P.-J., and Guan, Y.-P. (2017). "Design Analysis and Observed Performance of a Tieback Anchored Pile Wall in Sand." *Mathematical Problems in Engineering*, 2017, 23.
- Hansen, M. C. (1995). "Landslides in Ohio." *Geofacts, Ohio Department of Natural Resources, Division of Geological Survey*, Vol 8.
- Hegazy, Y. A. (2003). "Reliability of Estimated Anchor Pullout Resistance." *Third International Conference on Grouting and Ground Treatment*, ASCE, New Orleans, LA, 772 - 779.
- Houghton, R. C., and Dietz, D. L. (1990). "Design and performance of a deep excavation support system in Boston, Massachusetts." *Proc., ASCE Conf. on Des. and Perf. of Earth Retaining Struct., Geotech. Spec. Publ. No. 25*, ASCE, New York, NY, 795–816.
- Hsieh, P.-G., and Ou, C.-Y. (1998). "Shape of ground surface settlement profiles caused by excavation." *Canadian Geotechnical Journal*, 35(6), 1004-1017.
- Hsu, S.-C., and Chang, C.-M. (2007). "Pullout performance of vertical anchors in gravel formation." *Engineering Geology*, 90(1-2), 17-29.
- Kim, N.-K. (2003). "Performance of Tension and Compression Anchors in Weathered Soil." *Journal of Geotechnical and Geoenvironmental Engineering*, 129(12), 1138-1150.
- Kim, N.-K., Park, J.-S., and Kim, S.-K. (2007). "Numerical simulation of ground anchors." *Computers and Geotechnics*, 34(6), 498-507.
- Knellwolf, C., Peron, H., and Laloui, L. (2011). "Geotechnical Analysis of Heat Exchanger Piles." *Journal of Geotechnical and Geoenvironmental Engineering*, 137(10), 890-902.
- Kung, G. T., Juang, C. H., Hsiao, E. C., and Hashash, Y. M. (2007). "Simplified Model for Wall Deflection and Ground-Surface Settlement Caused by Braced Excavation in Clays." *Journal of Geotechnical and Geoenvironmental Engineering*, 133(6), 731-747.
- Lambe, T. W., Wolfskill, L. A., and Wong, I. H. (1970). "Measured performance of braced excavation." *Journal of the Soil Mechanics and Foundations Division*, 96(3), 817-836.

- Lee, C.-J., Wei, Y.-C., Chen, H.-T., Chang, Y.-Y., Lin, Y.-C., and Huang, W.-S. (2011). "Stability analysis of cantilever double soldier-piled walls in sandy soil." *Journal of the Chinese Institute of Engineers*, 34(4), 449-465.
- Liang, R. Y. (2000). "Instrumentation and Monitoring of Tieback Wall on Sum 82 at Brecksville." FHWA/OH-2000/015, ed.Columbus, OH.
- Liao, H. J., and Hsieh, P. G. (2002). "Tied-Back Excavations in Alluvial Soil of Taipei." *Journal of Geotechnical and Geoenvironmental Engineering*, 128(5), 435-441.
- Littlejohn, G. S. (1997). "Ground Anchorages and Anchored Structures: Proceedings of the International Conference Organized by the Institution of Civil Engineers ", Thomas Telford, London, UK.
- Liu, X., Wang, J., Huang, J., and Jiang, H. (2017). "Full-scale pullout tests and analyses of ground anchors in rocks under ultimate load conditions." *Engineering Geology*, 228, 1-10.
- Long, M. (2001). "Database for Retaining Wall and Ground Movements due to Deep Excavations." *Journal of Geotechnical and Geoenvironmental Engineering*, 127(3), 203-224.
- Ludwig, H. (1984). "Short-Term and Long-Term Behavior of Tiebacks Anchored in Clay." PhD Thesis, McGill University, Montreal, Quebec, Canada.
- Ma, J. Q., Berggren, B. S., Bengtsson, P. E., Stille, H., and Hintze, S. (2010). "Behavior of anchored walls in soils overlying rock in Stockholm " *International Journal of Geoenvironment Case Histories*, Vol. 2(1), 1–24.
- Macciotta, R., Rodriguez, J., and Hendry, M. (2017). "The 10-mile Slide north of Lillooet, British Columbia—history, characteristics and monitoring." *3rd North American Symposium on Landslides* Roanoke, VA.
- Mana, A. I., and Clough, G. W. (1981). "Prediction of movements for braced cuts in clay." *Journal of Geotechnical and Geoenvironmental Engineering*, 107(ASCE 16312 Proceeding).
- Mueller, C. G. (2000). "Load and Deformation Response of Tieback walls." PhD dissertation, University of Illinois at Urbana-Champaign, Urbana, IL.
- Mueller, C. G., Long, J. H., Weatherby, D. E., Cording, E. J., Powers III, W. F., and Briaud, J.-L. (1998). "Summary Report of Research on Permanent Ground Anchor Walls, Volume III: Model-Scale Wall Tests and Ground Anchor Tests." Federal Highway Administration, McLean, Virginia.
- Nandi, A., and Shakoor, A. (2008). "Application of logistic regression model for slope instability prediction in Cuyahoga River Watershed, Ohio, USA." *Georisk: Assessment and Management of Risk for Engineered Systems and Geohazards*, 2(1), 16-27.
- Ni, P., Song, L., Mei, G., and Zhao, Y. (2017). "Generalized Nonlinear Softening Load-Transfer Model for Axially Loaded Piles." *International Journal of Geomechanics*, 17(8), 04017019.
- Oda, H., Zhang, M., and Skimayanma, M. (1997). "Study on load-dispersive anchorage and shear stress in surrounding soils." *Proc., proceedings of International conference on Application and Development of Rock-soil Anchoring Technology*. Liuzhou, China, 237-244.
- Ooi, P. S. K., and Ramsey, T. L. (2003). "Curvature and Bending Moments from Inclinator Data." *International Journal of Geomechanics*, 3(1), 64-74.

- Ostermayer, H., and Scheele, F. (1978). "Research on ground anchors in non-cohesive soils." *Revue Française de Géotechnique*(3), 92-97.
- Peck, R. B. (1969). "Deep excavations and tunneling in soft ground." *Proc., 7th Int. Conf. Soil Mech. Found. Engrg.*, ISSMGE, Mexico City, Mexico, 225–281.
- Post-Tensioning Institute (PTI) (2014). "Recommendations for Prestressed Rock and Soil Anchors."
- Ren, F. F., Yang, Z. J., Chen, J. F., and Chen, W. W. (2010). "An analytical analysis of the full-range behaviour of grouted rockbolts based on a tri-linear bond-slip model." *Construction and Building Materials*, 24(3), 361-370.
- Rowe, P. W. (1957). "SHEET-PILE WALLS IN CLAY." *Proceedings of the Institution of Civil Engineers*, 7(3), 629-654.
- Sabatini, P. J., Pass, D. G., and Bachus, R. C. (1999). "Ground Anchors and Anchored Systems." *Rep. FHWA-IF-99-015*, Federal Highway Administration, Washington D.C.
- Sáez, E., Pardo, G. S., and Ledezma, C. (2015). "Seismic response of a pile-supported excavation on Santiago gravel." *Soil Dynamics and Earthquake Engineering*, 76, 2-12.
- Seo, D.-H., Chang, B.-S., Jeong, S.-S., and Kim, S.-I. (1999). "Evaluation of the sequential behavior of tieback wall in sand by small scale model tests." *Journal of the Korean Geotechnical Society*, 15(3), 113-129.
- Smethurst, J. A., and Powrie, W. (2007). "Monitoring and analysis of the bending behaviour of discrete piles used to stabilise a railway embankment." *Géotechnique*, 57(8), 663-677.
- Tan, Y., and Li, M. (2011). "Measured performance of a 26 m deep top-down excavation in downtown Shanghai." *Canadian Geotechnical Journal*, 48(5), 704-719.
- Tan, Y., Li, X., Kang, Z., Liu, J., and Zhu, Y. (2015). "Zoned Excavation of an Oversized Pit Close to an Existing Metro Line in Stiff Clay: Case Study." *Journal of Performance of Constructed Facilities*, 29(6), 04014158.
- Tan, Y., and Wang, D. (2013). "Characteristics of a Large-Scale Deep Foundation Pit Excavated by the Central-Island Technique in Shanghai Soft Clay. I: Bottom-Up Construction of the Central Cylindrical Shaft." *Journal of Geotechnical and Geoenvironmental Engineering*, 139(11), 1875-1893.
- Tan, Y., and Wang, D. (2013). "Characteristics of a Large-Scale Deep Foundation Pit Excavated by the Central-Island Technique in Shanghai Soft Clay. II: Top-Down Construction of the Peripheral Rectangular Pit." *Journal of Geotechnical and Geoenvironmental Engineering*, 139(11), 1894-1910.
- Terzaghi, K., and Peck, R. B. (1967). *Soil Mechanics in Engineering Practice*, John Wiley & Sons, Inc, New York, NY.
- Tschebotarioff, G. P. (1973). *Foundations, Retaining, and Earth Structures*, McGraw-Hill, New York, NY
- Urbański, A., and Michalski, Ł. (2016). "Finite element analysis of lateral earth pressure on a lagging in soldier pile walls." *Czasopismo Techniczne*.
- Weatherby, D. E. (2010). "Behavior of Tiedback H-Beam Walls and Recommendations for Their Design." *Earth Retention Conference 3*.
- Weatherby, D. E., Chung, M., Kim, N.-K., and Briaud, J.-L. (1998). "Summary Report of Research on Permanent Ground Anchor Walls, Volume II: Full-Scale Wall Tests

- and a Soil-Structure Interaction Model." Federal Highway Administration, McLean,VA.
- Wei, Z., Yin, G., Wang, J. G., Wan, L., and Jin, L. (2012). "Stability analysis and supporting system design of a high-steep cut soil slope on an ancient landslide during highway construction of Tehran–Chalus." *Environmental Earth Sciences*, 67(6), 1651-1662.
- Xanthakos, P. P. (1991). *Ground Anchors and Anchored Structures*, John Wiley & Sons, Inc., New York, N.Y.
- Xu, D.-S., and Yin, J.-H. (2016). "Analysis of excavation induced stress distributions of GFRP anchors in a soil slope using distributed fiber optic sensors." *Engineering Geology*, 213, 55-63.
- Xu, H.-Y., Chen, L.-Z., and Deng, J.-L. (2014). "Uplift tests of jet mixing anchor pile." *Soils and Foundations*, 54(2), 168-175.
- Yoo, C. (2001). "Behavior of Braced and Anchored Walls in Soils Overlying Rock." *Journal of Geotechnical and Geoenvironmental Engineering*, 127(3), 225-233.
- Zapata-Medina, D. G. (2007). "Semi-Empirical Method for Designing Excavation Support Systems Based on Deformation Control." MS Thesis, University of Kentucky, Lexington,KY.
- Zhang, Q.-Q., and Zhang, Z.-M. (2012). "A simplified nonlinear approach for single pile settlement analysis." *Canadian Geotechnical Journal*, 49(11), 1256-1266.
- Zhang, W., Goh, A. T. C., and Xuan, F. (2015). "A simple prediction model for wall deflection caused by braced excavation in clays." *Computers and Geotechnics*, 63, 67-72.

Vita

Jorge Octavio Romana Giraldo was born in Apartado-Colombia. He graduated from National University of Colombia at Medellin. He worked for an engineering company in Colombia before moving to Kentucky to attend the Master of Science program.

Publications:

- Bryson, L. S., Zapata-Medina, D. G., and Romana-Giraldo, J. (2018). "Empirical Method to Estimate Lateral Wall Deformation Profiles and Bending Moment in Excavation Retaining Walls." IFCEE 2018 Orlando, Florida.
- Huff, J., Bryson, L. S., and Giraldo, J. R. (2018). "Economy and Design of Augered Cast-In-Place Piles at the Fargo WTP." IFCEE 2018, ASCE, Orlando, Florida.